

University of Mississippi

eGrove

---

Electronic Theses and Dissertations

Graduate School

---

1-1-2021

# APPLICATION OF PASSIVE AIR SAMPLERS FOR ATMOSPHERIC RESEARCH, AND DETERMINATION OF METALS IN TREE RINGS AND MARINE SAPROPEL BY ICP-MS

Byunggwon Jeon  
*University of Mississippi*

Follow this and additional works at: <https://egrove.olemiss.edu/etd>



Part of the [Chemistry Commons](#)

---

## Recommended Citation

Jeon, Byunggwon, "APPLICATION OF PASSIVE AIR SAMPLERS FOR ATMOSPHERIC RESEARCH, AND DETERMINATION OF METALS IN TREE RINGS AND MARINE SAPROPEL BY ICP-MS" (2021). *Electronic Theses and Dissertations*. 2107.

<https://egrove.olemiss.edu/etd/2107>

This Dissertation is brought to you for free and open access by the Graduate School at eGrove. It has been accepted for inclusion in Electronic Theses and Dissertations by an authorized administrator of eGrove. For more information, please contact [egrove@olemiss.edu](mailto:egrove@olemiss.edu).

**APPLICATION OF PASSIVE AIR SAMPLERS FOR ATMOSPHERIC RESEARCH,  
AND DETERMINATION OF METALS IN TREE RINGS AND MARINE SAPROPEL  
BY ICP-MS**

A Dissertation  
presented in partial fulfillment of the requirements  
for the degree of Doctor of Philosophy  
in the Department of Chemistry & Biochemistry  
The University of Mississippi

by

Byungwon Jeon

August 2021

Copyright Byungwon Jeon 2021  
ALL RIGHTS RESERVED

## ABSTRACT

This research focuses on studies of atmospheric mercury (Hg) using passive air samplers (PAS) and studies of trace elements in tree cores and sediment using inductively coupled plasma mass spectrometry (ICP-MS). Mercury is a toxic element that is dispersed globally through the atmosphere. Accurately measuring airborne Hg concentrations aids understanding of the pollutant's sources, distribution, cycling, and trends. Mercury PAS are designed to capture gaseous elemental mercury (GEM) at a known rate. Compared to active air sampling the low-cost of PAS allows for greater spatial coverage. I used a commercially available Hg PAS (MerPAS®) and observed differences in GEM between landscapes, seasons, and elevations. Nearest to the surface, GEM levels were lowest in the wetland, where there was dense vegetation, and highest in an open grass field. GEM levels increased with the height above ground, except for the forest. We conclude that the PAS are capable of measuring GEM gradients between landscapes, elevations, and seasons, if given sufficient collection time, good analytical precision, and low blank levels.

We also deployed the PAS along the northern Gulf of Mexico. We observed higher GEM levels ( $p < 0.05$ ) in the winter compared to other seasons at all sites; with the general pattern being: winter > spring > summer  $\approx$  fall. Mean GEM levels were highest at Bay St. Louis, the western-most site nearest the New Orleans metropolitan area, and lowest at Cedar Point, a coastal marsh with extensive vegetation that can uptake GEM. Both the passive and active sampling methods showed the same seasonal trends and the difference between them was <15%, acceptable for

evaluating larger spatial and temporal trends. Overall, we demonstrate that PASs can provide insight into GEM levels and the factors affecting them along coastal regions.

In a separate study, we developed an analytical method to measure trace metals, including Hg, in tree rings. Trees can incorporate certain pollutants into wood providing a historical pattern of deposition. We determined Hg in tree bole wood using a direct mercury analyzer (DMA), and then analyzed the ash for metals left behind after combustion using ICP-MS. The ash was digested using nitric and hydrofluoric acids. The method was optimized and validated, and then applied to trees in the Tallahatchie Experimental Forest in the Holly Spring National Forest to examine differences between species and to obtain background data for future studies of pollution point sources such as coal-fired power plants.

We also determined the historical deposition of metals in a marine sapropel from Mangrove Lake, Bermuda. Sapropel is an organic-rich sediment formed under conditions that can result in trace metal enrichment. We determined the concentration of total-mercury (Hg) and 17 other trace metals (Al, Ba, Ca, Cd, Cr, Cs, Cu, Fe, Li, Mn, Ni, Pb, Sr, Tl, U, V, Zn) in a sapropel core that dated back nearly two millennia. We established historical patterns of metal deposition associated with pollution from industrialization, leaded gasoline, and possibly, volcanic activity, seawater intrusion, and local ship building on this remote island in the middle of the Atlantic Ocean, and used isotope ratios to assess possible pollution sources.

## LIST OF ABBREVIATIONS AND SYMBOLS

GEM	Gaseous Elemental Mercury
GOM	Gaseous Oxidized Mercury
PBM	Particulate-Bound Mercury
TGM	Total Gaseous Mercury
THg	Total Mercury
DMA	Direct Mercury Analyzer
USEPA	United States Environmental Protection Agency
CVAFS	Cold Vapor Atomic Fluorescence Spectrometry
NOAA	National Oceanic and Atmospheric Administration
TGM	Total Gaseous Mercury
LOI	Loss-On-Ignition
AAS	Atomic Absorption Spectrometry
TD	Thermal Desorption
NERR	National Estuarine Research Reserve
ICP	Inductively Coupled Plasma
MS	Mass Spectrometry/ Mass Spectrometer

## ACKNOWLEDGMENTS

I would like to thank my graduate advisor, Dr. James V. Cizdziel, for all his guidance and assistance throughout the project and research. His knowledge, wisdom, and commitment inspired and motivated me a lot. It would not have been possible to finish my doctoral degree without his guidance and expertise in environmental and analytical chemistry. I also like to thank our group members, Dr. Beau Black, Dr. Austin Scircle, Zhiqiang Gao, Kendall Wontor and all undergraduate researchers for their assistance. I would like to show my appreciation to my committee members, Dr. Murrell Godfrey, Dr. Amala Dass, Dr. Walter Cleland, and Dr. Stephen Brewer for their helpful guidance and critiques of my research. I would like to thank Dr. Winston T. Luke and Dr. Mark D. Cohen for their help for my research. I would like to thank staff working at the University Mississippi Biological Field Station for their help in meteorological data. Last, I would like to thank my family for their love and support during this long education.

## TABLE OF CONTENTS

Abstract .....	ii
List of Abbreviations .....	iv
Acknowledgements .....	v
Table of Contents .....	vii
List of table .....	viii
List of Figures .....	viii
Introductionto the dissertation .....	1
Chapter 1: Application of Passive Air Samplers for Atmospheric Hg Research .....	2
Chapter 2: Gaseous Elemental Mercury concentrations along the Northern Gulf of Mexico Using Passive Air Sampling, with a Comparison to Active Sampling .....	21
Chater 3: Determination of Metals in Tree Rings by ICP-MS using Ash from a Direct Mercury Analyzer .....	48
Chapter 4: Historical deposition of trace metals in a marine sapropel from Mangrove Lake, Bermuda with emphasis on mercury, lead, and their isotopic composition .....	67
List of References .....	95
Curriculum Vitae .....	111



## LIST OF TABLES

1. Weather conditions near the study site during sampling .....	11
2. Gaseous elemental mercury concentrations ( $\text{ng m}^{-3}$ ) at three different heights at.....	16
3. Coordinates for sampling sites and nearest weather stations, along with sampling .....	43
4. Amount of Hg (ng) collected on each PAS and GEM concentrations based on .....	44
5. Summary statistics for GEM concentrations at Grand Bay NERR by active and .....	45
6. Direct mercury analyzer (DMA) and ICP-MS instrumental settings .....	56
7. Comparison of the new method (with DMA ashing) with a standard method .....	59
8. Recoveries for reference materials determined by ICP-MS after microwave digestion .....	60
9. Concentration of elements in tree cores from the Tallahatchie Experimental Forest.....	65
10. ICP-MS instrumental settings and parameters.....	91
11. Hg isotopic composition (‰) for sapropel sediment from Mangrove Lake, Bermuda .....	92

## LIST OF FIGURES

1. Aerial view of study site at University of Mississippi’s Biological Field Station.....	2
2. A map showing the proximity of the sampling locations (red stars) at the adjacent .....	7
3. Photos showing the Hg passive air sampler (MerPAS) with a White Radiello.....	9
4. Deployment of Hg passive air sampler at the University of Mississippi Field .....	10
5. Mean concentrations ( $\text{ng m}^{-3} \pm 1\text{S.E.}$ ) of GEM determined with passive air .....	14
6. Grand Bay National Estuarine Research Reserve along the Northern Gulf of.....	21
7. Maps of the study site (A) close up showing the six sampling locations as green .....	28
8. Photos showing the MerPAS® configuration with cover on (A), with the cover.....	29
9. Views of the six sampling sites along the northern Gulf of Mexico showing .....	30
10. GEM concentrations determined using passive air samplers (PASs) deployed at .....	36
11. Wind roses showing the relationship between GEM levels and wind direction.....	39
12. GEM concentrations determined using passive and active sampling at Grand Bay.....	41
13. Wind roses showing the relationship between speed and wind direction for each.....	46
14. Hourly GEM concentrations determined at the Grand Bay NERR site using active .....	47
15. Tree core sampling using a hammer type borer .....	48
16. Location of the Tallahatchie Experimental Forest (TEF) in Holly Springs National .....	53
17. Example of tree cores collected with a 5.15-mm increment borer .....	54
18. Mean mercury concentration in tree rings from the Tallahatchie Experimental Forest .....	63
19. Mean concentrations of elements in bole wood tree rings from the Tallahatchie .....	64

20. Early work on sapropel from Mangrove Lake, Bermuda (circa 1991). .....	67
21. Map showing the location of Bermuda in the Atlantic Ocean (left inset), ~25 km .....	72
22. Mercury distribution in Mangrove Lake sapropel by deposition year, .....	80
23. Down core profiles for productivity and redox sensitive trace elements (Cu, Zn, Ni, .....	84
24. Down core profiles of Al, Fe, Mn, Ca, Sr, Li, Cs, and Tl in Mangrove Lake .....	85
25. Pb concentration and $^{206}\text{Pb}/^{207}\text{Pb}$ ratio of Mangrove Lake sediments by deposition .....	87
26. A three-isotope plot showing the isotopic composition of Pb in Mangrove Lake .....	87
27. Variation (‰) in mass dependent ( $\delta^{202}\text{Hg}$ ) and mass independent ( $\Delta^{199}\text{Hg}$ ) stable .....	89

## **INTRODUCTION TO THE DISSERTATION**

This dissertation is divided into four independent chapters, each published in peer-reviewed scientific journals. The first two chapters involve application of passive air samplers for atmospheric mercury studies. Mercury is a persistent and widespread toxic environmental pollutant that is dispersed globally through atmospheric pathways. It deposits to terrestrial and aquatic systems through wet and dry depositions where it can undergo biotic and abiotic transformation to mono-methylmercury, which readily bioaccumulates and concentrates in food webs. In Chapter 1 we examine the feasibility of a commercially available passive air sampler to discriminate between landscape, elevation, and seasonal effects on atmospheric mercury. In Chapter 2, we then apply the samplers along the Mississippi and Alabama Gulf Coast providing new insight into GEM levels and the factors affecting them along coastal regions. In Chapter 3, we shift gears to develop, validate, and apply a novel analytical method that measures Hg in tree cores with a direct mercury analyzer and measures additional elements in that same sample using an ICP-MS. In Chapter 4, we measure the historical deposition of trace elements in a sediment core from Mangrove Lake located in Bermuda. The study emphasizes Hg, Pb, and their isotopic distribution to provide insight into the pollution sources. Finally, additional research was conducted that did not make it into this document, but some of which is planned to be published later in journal articles. It includes atmospheric mercury isotope analyses, GEM measurements at Sardis, Enid and Grenada Lakes in north Mississippi, changes in mercury in a lake from dredging, and mercury emissions from controlled burning in national forests.

## CHAPTER ONE

### Application of Passive Air Samplers for Atmospheric Hg Research: Landscape, Seasonal, and Elevation Effects



Figure 1. Aerial view of study site at University of Mississippi's Biological Field Station.

Jeon, B., Cizdziel, J.V. *Atmosphere* **2020**, 10, 617. DOI: 10.3390/atmos10100617

## ABSTRACT

Accurately measuring gaseous elemental mercury (GEM) concentrations in the atmosphere is important to understand its sources, cycling, distribution, and temporal trends. The MerPAS passive air sampler from Tekran Inc. (Toronto, ON, Canada) captures GEM on sulfur-impregnated activated carbon after it passes through a Radiello diffusive barrier. Because they are small, relatively low in cost, and require no power, they can be deployed at multiple locations, yielding a much greater spatial resolution, albeit at coarser temporal resolution, compared to active sampling. In this study, we used the MerPAS to measure GEM concentration gradients at a mixed hardwood forest, wetland, pond, and a mowed field, all within close proximity (<500m) to each other. Vertical profiles were (0.5, 3.0, 5.5 m) assessed during summer and winter. The sorbent was analyzed using a direct mercury analyzer. The samplers were captured between 0.90 to 2.2 ng over 2 weeks, well above the mean blank of 0.14 ng. We observed differences between the landscapes, elevation, and seasons. Nearest to the surface, GEM concentrations were lowest in the wetland (both seasons), where there was dense vegetation, and highest in the mowed field (both seasons). Generally, GEM levels increased with the elevation above the ground, except for the forest where the trend was slightly reversed. This suggests a possible net GEM deposition from the atmosphere to surfaces for three of the four landscapes. GEM concentrations were slightly higher in the winter than the summer at 5.5 m height where air masses were unimpeded by vegetation. Overall, we conclude that the MerPAS is indeed capable of measuring GEM gradients between landscapes, elevations, and seasons, if given sufficient collection time, good analytical precision, and low blank levels.

## INTRODUCTION

Mercury (Hg) is a widespread global contaminant that is distributed primarily through the atmosphere, where it exists in three common forms: GEM, GOM, and PBM (Schroeder et al 1998, Valente et al 2007). GEM is the predominant form of Hg in the atmosphere, typically comprising >95% of TGM, often defined as GEM+GOM (Schroeder et al 1998). GEM has a relatively long residence time in the air (estimated from months to years), and thus it plays an important role in the global transport of Hg (Skov et al 2004, Gustin 2010). GEM is slowly converted by photochemical and other reactions to GOM, which, because of its solubility and particle-reactivity, has a relatively short lifespan in the atmosphere (estimated from days to weeks) depending on atmospheric conditions (Gustin 2010). Likewise, PBM is scavenged from the atmosphere at shorter time-scales depending on particle size and weather (Keller et al 1995). Each category of gaseous Hg can be deposited to terrestrial and aquatic surface through wet and dry deposition mechanisms. Once deposited, inorganic Hg can be methylated by certain microorganisms to form methyl Hg, a neurotoxin that can accumulate in biological tissues and concentrate up food chains (Driscoll et al 2013, Lin et al 1999).

To better describe the global biogeochemical cycling of Hg and to evaluate the effectiveness of the recent Minamata Convention, a global treaty to reduce Hg pollution and produce accurate measurements of Hg in the atmosphere are essential. However, reliably determining atmospheric Hg concentrations at ambient levels in the boundary layer is challenging because of its low background, which is on the order of 1-2 ng m<sup>-3</sup> (Lin et al 1999). Most methods to measure airborne Hg rely on active sampling, drawing air at a known rate over a sorbent designed specifically to trap gaseous Hg species, typically using gold coated quartz (Pandey et al 2011). The traps are subsequently heated, and the desorbed Hg is carried by argon gas into an

atomic fluorescence instrument for analysis. Recently, an eddy covariance flux method was validated for direct  $\text{Hg}^0$  flux measurements (Osterwalder et al 2019). Such setups are costly, require calibrated pumps, electrical power, trained operators, and have other constraints that limits their application (Gustin et al 2011, Landis et al 2002).

An alternative approach to measure GEM uses PASs, where gaseous Hg enters the sampler and diffuses at a known rate into a chamber where it is trapped on a sorbent. Compared to active sampling, the low-cost of passive sampling allows for a much larger number of samplers and thus a greater area coverage and spatial resolution, albeit at a coarser temporal resolution (Brumbaugh et al 2000). PASs can be deployed for extended periods without any need to revisit the site until they are removed for analysis, as long as the Hg sorbent capacity is not reached (Landis et al 2002, Brumbaugh et al 2000, Peterson et al 2012). One PAS designed for Hg uses sulfur-impregnated activated carbon as the sorbent, a Radiello diffusive barrier to constrain the sampling rate, and a protective shield for outdoors (McLagan et al 2016). The amount of GEM taken up by this type of PAS, determined by a direct mercury analyzer (DMA), was shown to increase linearly with time, yielding outdoor sampling rates of  $\sim 0.135 \text{m}^3 \text{day}^{-1}$  and a replicate precision of  $2 \pm 1.3\%$  (McLagan et al 2017). Gaseous Hg concentrations are calculated by dividing the mass of sorbed Hg by the deployment time and the sampling rate. A critical review of passive air sampling of gaseous Hg revealed some shortcomings in the methodology (e.g., sampling rates that vary due to meteorological factors and manufacturing inconsistencies) but also discussed potential routes to overcome these difficulties (McLagan et al 2016).

Because GEM recycles between environmental compartments, it is necessary to quantify fluxes between the atmosphere and both terrestrial and aquatic surfaces (Sommar et al 2013). However, GEM fluxes from the natural landscapes are relatively poorly characterized compared



with many point sources of Hg, even though they can play a large role in influencing airborne Hg concentrations on local, regional, and global scales (Gustin 2010, Gustin et al 2008). A variety of factors have been shown to influence GEM fluxes from natural surfaces, including the substrate's Hg concentration, sunlight, temperature, atmospheric turbulence, relative humidity, rain events, and vegetation cover (Gustin et al 2008, Choi et al 2009). Another important factor is reduction of oxidized divalent mercury ( $\text{Hg}^{2+}$ ) to  $\text{Hg}^0$  in both soil and aquatic environments, a process which is catalyzed by solar radiation (Gustin et al 2008, Poissant et al 1998).

Gradient fluxes of GEM from natural surfaces are typically measured using either enclosure (e.g., dynamic flux chamber (DFC)) or micrometeorological methods (McLagan et al 2018) but can also be estimated from vertical profiles of gaseous Hg determined by PASs (Feigis et al 2018). Currently, Hg PASs are being used by the same University of Toronto research group that developed them to observe long term seasonal trends, the impact of wind speed, which can vary at different heights above the ground, at different sampling rates, and based on differences within and above the canopy. However, we are not aware of any studies comparing Hg concentrations between multiple landscapes in close proximity to each other, which is advantageous because weather and GEM carried by air masses entering the area are better constrained compared to landscapes separated by greater distances. It is worth noting that, while GEM fluxes vary diurnally, these fluctuations cannot be resolved by PASs due to the relatively long deployment times that they require (days to weeks, depending on concentrations).

We have previously examined GEM fluxes from different landscapes in Mississippi, USA using a dynamic flux chamber with active sampling (Cizdziel et al 2019). The main goal of the current study was to test the feasibility of the MerPAS to measure GEM concentration gradients between some of these same landscapes, as well as by elevation (vertical profiles) and season. To

address these goals, we deployed samplers in a mixed hardwood forest, wetland, pond and a mowed field, all within close proximity (~500 m) of each other. Vertical profiles (0.5, 3.0, 5.5m) were assessed during both summer and winter. We report trends in our observed data based on the context of what is known from the literature; fully quantifying the factors that affect the GEM concentrations and GEM fluxes is beyond the scope of this feasibility study.

## MATERIAL AND METHODS

### Study Site

The University of Mississippi Field Station (UMFS) is a 3 km<sup>2</sup> research and educational facility located 18 km northeast of the main campus of the University of Mississippi, USA. It consists of mixed hardwood forest, wetlands, former pasture land, and 220 experimental ponds, with each type of landscape in close proximity (~500 m) of each other (Fig. 2). The site lies within the Eocene Hills of the interior coastal plain of the southeastern U.S. and is characterized by sandy and sandy-loam soils. The area was row crops prior to 1947. The depth of the pond was ~1m.

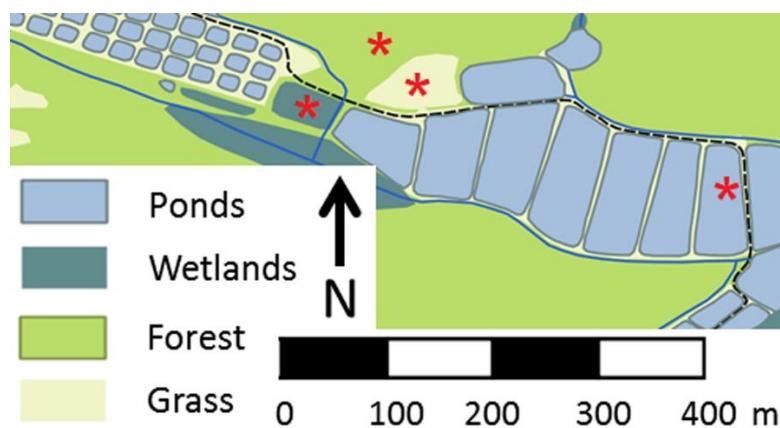


**Figure 2. A map showing the proximity of the sampling locations (red stars) at the adjacent landscapes at the University of Mississippi Field Station.**

## Hg Passive Air Sampler

We used a commercially available Hg PAS called “MerPAS” (Tekran Inc., Toronto, ON, Canada) (Fig. 3). The MerPAS is based on a design developed by researchers at the University of Toronto that has been described in detail in several papers (McLagan et al 2016, 2017). Briefly, sulfur-impregnated activated carbon powder (HGR-AC, Calgon Carbon Corp., Pittsburg, PA, USA) housed in a stainless-steel mesh cylinder was inserted into a porous polyethylene diffusive barrier (White Radiello<sup>®</sup>, Sigma Aldrich, St. Louis, Mo, USA) that controls the rate of diffusion from the air to the sorbent. This diffusive barrier was then attached to the inside of a plastic (polyethylene terephthalate) protective shield to minimize and control the effects of wind, solar radiation, and precipitation on the rate of Hg uptake from the air (McLagan 2016). The MerPAS is considered to be GEM sampler because the diffusive barrier has been shown to prevent reactive gaseous mercury species (GOM) from passing through (Stupple et al 2019). It is also worth recalling that GEM generally makes up >95% of the TGM at most locations not impacted by point sources.



**Figure 3. Photos showing the Hg passive air sampler (MerPAS) with a White Radiello diffusive body inside a protective shield and the mesh cover in the background (left), as well as a close up of the diffusive body, stainless-steel mesh screen, and sulfur-impregnated activated carbon sorbent (right).**

In the present study, MerPAS samplers were loaded the day before deployment with freshly crushed and sieved HGR-AC (particles ranged in size between 250 and 1000  $\mu\text{m}$ ). The stainless-steel mesh cylinder held  $0.60 \pm 0.02\text{g}$  of the sorbent, with sufficient capacity to collect ambient levels of outdoor Hg for at least a year. Prior to loading the stainless-steel cylinders, the sorbent was analyzed to assure that it met the low-blank criteria ( $<0.2\text{ Hg ng/sampler}$ ). Diffusive barriers were re-used after inspection to make sure they were not visibly dirty; the mean rate of gaseous Hg uptake did not differ between new and previously used barriers if they remained clean (McLagan 2016, 2017, 2018).

### **Deployment of PAS**

We deployed the PASs at the UMFS at three heights (0.5, 3.0, and 5.5m) above a forest floor, a wetland, a mowed field, and a pond during the summer and winter of 2019 (Fig. 4). Each site was within a 400 m of each other. The samplers were mounted on a metal bracket attached to long wood (oak) boards purchased from a local hardware store (Fig. 4). This sampling configuration was selected in part because there was a limited number of PASs to deploy at each site and other logistics. For instance, 5.5 m was the maximum height achievable by coupling two of the longest boards available from a local hardware store with a metal bracket; 0.5 m was selected as the lowest height to minimize water entering the samplers from splashing during rain events; and a middle height was selected to have three heights to assess vertical profiles.

To simplify sampler deployment and retrieval, a metal fence pole was driven into the ground such that the boards with samplers attached could readily be inserted for vertical deployment, and later lifted out and laid on the ground to remove or replace the samplers. During

the winter, we deployed 4 samplers at each height for a total of 48 samplers, while in the summer we deployed 3 samplers at each height for a total of 36 samplers, followed by a second summer sampling campaign targeting the pond and mowed field. The samplers were deployed concurrently at each location for 2 weeks, then retrieved, placed in zip-lock bags, and transported to the laboratory, where they were stored in a clean room until analyses (within two days).



**Figure 4. Deployment of Hg passive air sampler at the University of Mississippi Field Station during winter 2019.**

Mean weather conditions at the nearest operational weather station (located 7 km to the southwest) during sampler deployment are reported in the appendix (Table 1).

**Table 1. Weather conditions near the study site during sampling.**

Parameter	Winter	Summer
Mean Temperature (°C)	11.9	25.7
Mean Wind Speed (m/s)	0.16	0.08
Accumulated Precipitation (mm)	1.1	6.9

## **Determination of Hg on the Sorbent and in the Soil and Sediment using a Direct Mercury Analyzer**

Total-Hg in the samples was determined with a Direct Mercury Analyzer (DMA-80; Milestone Inc., Shelton CT) following US EPA method 7473, with some modifications for the activated carbon (MerPAS) samples. The method is based on thermal decomposition-atomic absorption spectrometry, which has been widely used to measure Hg in a variety of complex matrices, including fish, sediment and coal (Lopez-Anton et al 2010, Cizdziel et al 2002, Chen et al 2015). Here, we focus on the procedure for analyzing the PASs. After retrieving them from the field, the stainless-steel cartridge containing the sorbent was removed in the laboratory and about half of its contents were carefully transferred into a pre-heated (blanked) quartz sample boat and recorded its weight. Then ~0.2 g of  $\text{Na}_2\text{CO}_3$  was added directly on top of the sorbent. This process was repeated using a second boat because the amount of sorbent exceeded the capacity of a single boat. Adding  $\text{Na}_2\text{CO}_3$  has been shown to greatly increase the lifetime of the DMA catalyst by minimizing the  $\text{SO}_2$  that reaches the catalyst (McLagan et al 2017). When the sulfur-impregnated carbon sorbent is combusted it produces  $\text{SO}_2$  gas which can poison the catalyst.  $\text{Na}_2\text{CO}_3$  reacts with  $\text{SO}_2$  to make  $\text{Na}_2\text{SO}_3$  (s) along with  $\text{CO}_2$ . We also amended the catalyst tube itself with 5 g of  $\text{Na}_2\text{CO}_3$  powder.

The quartz boats with the PAS sorbent were loaded onto the auto-sampler which sequentially inserts the boats into the decomposition furnace. There, samples are thermally decomposed at  $750^\circ\text{C}$  and the Hg released is carried by oxygen to the catalyst, where Hg species are reduced to gaseous elemental vapor ( $\text{Hg}^0$ ). As other combustion gases are flushed from the system, Hg is trapped by amalgamation with gold. The trap is subsequently heated to  $900^\circ\text{C}$  and Hg is released and carried through an absorption cell, where it is quantitatively measured at 253.7

nm. The instrument was set to collect the Hg from two quartz boats representing one PAS before heating the amalgamator to obtain one measurement per PAS.

The DMA instrument was calibrated using a series of standard Hg solutions prepared from a stock Hg standard solution from Spex Certiprep (Netuchen, NJ). For quality control, coal fly ash standard reference material (NIST 1633C) was analyzed before the samplers and every ~20 boats thereafter. Recovery of the CRM was  $97.5 \pm 5.6\%$  (mean  $\pm$  SD). Sample boats were pre-heated to remove Hg and boat blanks were analyzed to assure there was negligible contribution of Hg. The limit of detection (3 sigma criterion) was 0.014 ng of Hg.

### **Calculation of Atmospheric Hg Concentration**

Concentrations of GEM were calculated by dividing the mass of sorbed Hg (ng) by the deployment time (days) and the sampling rate ( $\text{m}^3 \text{ day}^{-1}$ ). The blank subtracted uptake (mass loading) of Hg from the atmosphere to the samplers ranged from 0.90 to 2.2 ng. Carbon blanks were <15% of this amount. We used a sampling rate of  $0.111 \text{ m}^3 \text{ day}^{-1}$ , modified slightly to reflect mean temperature and wind speeds for each season. The  $0.111 \text{ m}^3 \text{ day}^{-1}$  base sampling rate was recommended by Tekran Inc. who has done a variety of inter-comparison studies to assess the MerPAS sampling rate (E. Prestbo, Tekran Inc., personal comm.). Our adjusted sampling rates were  $0.115 \text{ m}^3 \text{ day}^{-1}$  in the summer and  $0.103 \text{ m}^3 \text{ day}^{-1}$  in the winter. Whereas these are slightly lower than  $0.135 \text{ m}^3 \text{ day}^{-1}$  determined by McLagan et al. who deployed similar samplers worldwide, the Tekran MerPAS was reconfigured slightly from that earlier version for mass production, and it includes a screen that has slightly less open surface area than the earlier model (E. Prestbo, Tekran Inc., personal comm.). In any case, here we are primarily concerned with the relative differences between landscapes, heights, and seasons, not the absolute concentrations. We

conducted the research of comparing the MerPAS with active sampling for Hg at the Grand Bay, Mississippi.

### **Statistical analysis**

Data was analyzed using SPSS Version 25. Analysis of variance (ANOVA) was used to examine differences in GEM between landscapes by season and GEM between heights for each landscape. Tukey's tests were used to provide pairwise differences in means among landscapes and heights. Differences were deemed significant at the  $p < 0.05$  level.

## **RESULTS AND DISCUSSION**

### **Summary Statistics and Overall Trends**

GEM concentrations by landscape, elevation, and season are shown Figure 4, with exact values in Table 8. The levels are at or below those generally accepted as North American background ( $1-2 \text{ ng m}^{-3}$ ), but within the range we have previously measured using active sampling in the area (Cizdziel et al 2019). These relatively low concentrations indicate that there are no Hg point sources in the local area to affect the results. Total-Hg concentrations ( $\text{ng g}^{-1} \pm \text{Standard Error}$ ) in the bulk soil and sediment (substrate) were forest ( $74.8 \pm 2.8$ ) > wetland ( $45.5 \pm 1.9$ ) > mowed field ( $21.2 \pm 0.6$ ) (Table 2). We observed several statistically significant differences ( $p < 0.05$ ) between certain landscapes, between the 0.5 and 5.5 m elevations (within certain landscapes), and between seasons (for certain landscapes). Together, these data and observations (described below) suggest that the MerPAS is indeed capable of discriminating the effects that landscapes, elevation, and seasons have on atmospheric Hg, provided the sampler is given sufficient collection time, there is good analytical precision, and blank levels are low.



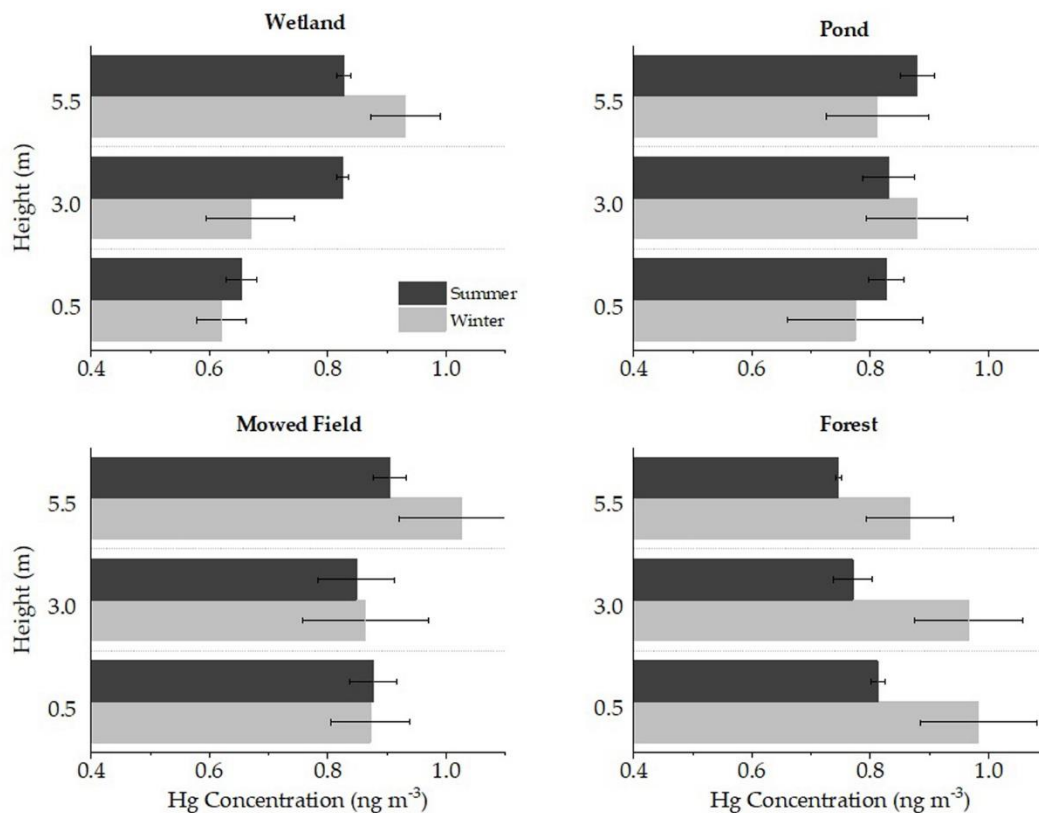


**Figure 5. Mean concentrations ( $\text{ng m}^{-3} \pm 1 \text{ S.E.}$ ) of GEM determined with passive air samplers deployed at four adjacent landscapes in north-central Mississippi.**

GEM concentrations ( $\text{ng m}^{-3} \pm 1 \text{ Standard Error}$ ) nearest to the surface (0.5 m) ranged from  $0.62 \pm 0.04$  at the wetland during the winter to  $0.98 \pm 0.10$  at the forest during the winter. At the highest elevation (5.5 m) concentrations ranged from  $0.75 \pm 0.01$  at the forest during the summer to  $1.03 \pm 0.11$  at the mowed field during the winter. At the 0.5 m height, we observed statistically lower concentrations at the wetland ( $0.65 \pm 0.03$ ) compared with both the mowed field ( $0.88 \pm 0.04$ ) and the pond ( $0.83 \pm 0.03$ ) in the summer. Also, in the summer, the forest (5.5 m) had lower concentrations ( $0.75 \pm 0.01$ ) than both the mowed field ( $0.91 \pm 0.03$ ) and pond ( $0.88 \pm 0.03$ ). There were also statistical differences between elevations. During both the summer and winter,

concentrations at the wetland were lower ( $p < 0.01$ ) at the 0.5 m height compared to the 5.5 m height (Fig. 5).

Seasonally, higher mean GEM concentrations were observed at the 5.5 m height in the winter compared to the summer at three of the landscapes, with the pond the exception (Figure 10). GEM concentrations in air masses have also been reported to be higher in the winter compared to the summer primarily due to uptake of Hg by plants (Schroeder et al 1998). However, in the summer there can be higher evasion fluxes from soil and other surfaces due to both higher temperatures and more intense solar radiation (Lindberg et al 2002, Gustin et al 2005). In our study, GEM concentrations in the forest were slightly lower in the summer, though not statistically different. Forests influence gaseous Hg differently in part because of large changes in foliage and due to shade from the canopy which influence Hg uptake and penetration of solar radiation (Kuiken et al 2008).

Trends for GEM concentrations with elevation above the surface were also evident. Concentrations were significantly greater with elevation for the wetland, and to lesser extent the mowed field, suggesting Hg deposition from the atmosphere to surface (Fig. 5). These landscapes have plants near and around the lower sampling height which may be stripping some Hg from the atmosphere. Plants are known to be a sink for atmospheric Hg, and it has been hypothesized that Hg can migrate into leaf pores and in some cases transversing the cuticle until oxidized with organic acids and immobilized (Stamenkovic et al 2009). There was no apparent trend with height at the pond where air masses go unimpeded above the surface; however, there were relatively large uncertainties in data for the samplers above the water. At the forest, the trend with height was opposite with mean concentrations decreasing slightly (statistically insignificant) with elevation from the forest floor. As noted, the samplers were deployed below the canopy, so unlike the other

sites where air masses could impinge on the top samplers unimpeded, the forest trees and foliage disrupt the flow of air at all sampling heights as well as minimizing solar radiation reaching the soil. It should be mentioned that Hg PAS sampling rates can vary with temperature and wind speed, so measuring these variables and including them in the calculations can improve accuracy.

**Table 2. Gaseous elemental mercury concentrations ( $\text{ng m}^{-3}$ ) at three different heights at adjacent landscapes in Mississippi, USA**

Landscape	Hg in soil or sediment ( $\text{ng g}^{-1}$ , dry weight, n=6)	Height (m)	Summer		Winter	
			Mean (n=4)	Standard Error	Mean (n=3)	Standard Error
Wetland	45.5 ± 1.9	5.5	0.83	0.01	0.93	0.06
		3.0	0.83	0.01	0.67	0.07
		0.5	0.65	0.03	0.62	0.04
Pond	-	5.5	0.88 (n=10)	0.03	0.81	0.09
		3.0	0.83 (n=6)	0.04	0.88	0.09
		0.5	0.83 (n=8)	0.03	0.77	0.11
Mowed Field	21.2 ± 0.6	5.5	0.91	0.03	1.03	0.10
		3.0	0.85 (n=7)	0.06	0.86	0.10
		0.5	0.88 (n=6)	0.04	0.87	0.07
Forest	74.8 ± 2.8	5.5	0.75	0.01	0.87	0.07
		3.0	0.77	0.03	0.97	0.09
		0.5	0.81	0.01	0.98	0.10

However, we did not have the capability to deploy weather stations at each site and it was beyond the scope of our feasibility study. A single weather station near the study site showed differences in temperature, wind speed, and precipitation between the summer and winter (Table 1). Rain, while impacting gaseous oxidized Hg and particle-bound Hg, affects GEM to a much less extent because GEM, which comprises >95% of the GEM, is not particularly soluble in water (Lin et al 1999). From the observed trends and statistical differences discussed above, we are confident that the MerPAS is capable of being used to differentiate patterns in GEM with seasons, landscapes

and in some cases by height, but we acknowledge that there is room for improved precision. Some approaches to improve precision may be to deploy samplers for longer times (>2 weeks) to capture more Hg, increase the number of samplers at each position, thoroughly assess blank contributions, and measure wind speed and other meteorological parameters at each location and at two or more heights. Below we present some further results for each landscape separately.

### **Wetland**

The mean GEM concentration at the wetland was significantly higher at 5.5 m compared to 3.0 m and 0.5 m during both the summer and winter (Table 2). As noted, the wetland had dense plant growth in the summer that surrounded the lower sampling height. This maze of plants can impede air flow and influence airborne Hg concentrations through uptake by plants. GEM concentrations at the lower two heights were slightly different between seasons, possibly reflecting differences in plant density and evasion fluxes. In contrast, GEM concentrations at the top (5.5 m) elevation, where there are no plants surfaces, were nearly the same in summer and winter.

### **Pond**

At the pond, where there was no vegetation around the samplers, there was little difference between the different sampling heights and by season. Others have shown that dissolved gaseous Hg correlates with incident radiation due to photo-induced reduction in the water (Amyot et al 1994). Because gaseous Hg is not particularly soluble in water and because solar intensity is highest during the summer higher evasion fluxes can be expected in the summer. Another factor that promotes reduction of dissolved metal ions like  $\text{Hg}^{+2}$  in natural waters is dissolved organic

carbon (DOC); DOC can serve to absorb light and transfer energy to an electron acceptor, and thus enhance  $\text{Hg}^{+2}$  reduction and subsequent GEM emission in natural waters containing high DOC levels (Zhu et al 2013, Nrigau et al 1994). At the UMFS, there is high biological productivity and DOC levels in the ponds during the summer. However, the pond is also covered in lily pads which block much of the light from penetrating into the water. Also, unlike the other landscapes there are no plants extending into the air to hinder air flow or filter GEM above the water. If the pond was a significant source of Hg to the air, one might expect to see a concentration gradient with diminishing concentrations by elevation over the water. We did not observe this gradient, but it could have been masked by the relatively large uncertainty in some of the pond data.

### **Mowed Field**

Mean GEM concentrations generally increased height, with the greatest concentration at the highest elevation in both the summer and winter. Although the differences were not statistically significant, the trend is indicative of net emissions from the surface. We have previously measured GEM fluxes over a mowed field at the UMFS using a dynamic flux chamber, observing a net emission (mean  $4.52 \pm 4.8 \text{ ng m}^{-2} \text{ h}^{-1}$ ), however, that data was limited to a couple of days during an earlier summer (Cizdziel et al 2019). Others have observed relatively high GEM fluxes over grass, even at night (Ericksen et al 2006). Here, concentrations at the mowed field were statistically higher than the wetland during the summer ( $p=0.01$ ) at the 0.5 m height.

### **Forest**

As previously discussed, there were some different trends observed at the forest site. Some of these differences may be attributed to the canopy, which can moderate temperatures and sunlight,

influencing Hg fluxes (Gustin et al 2004, Feng et al 2005, Mazur et al 2014); all our measurements were taken below the canopy. Moreover, the forest topography was different, with the samplers being situated on the side of a hill instead of on the valley floor, so wind and other meteorological conditions may vary some. It is also known that leaves in the forest can uptake GEM, which can further influence local concentrations of GEM (Ericksen et al 2003, Gustin et al 2004). The forest soil, which is high in organic matter, had the highest concentration of total-Hg among the landscapes tested (Table 2). GEM concentrations in the forest generally decreased with the height, suggesting possible net emission from the soil surface. Forest GEM concentrations were also slightly higher in the winter than the summer. It has also been demonstrated that soil is a major contributor to atmospheric Hg and that solar radiation, which can reach the ground more during the winter due to decreased forest canopy, can impact emission fluxes (Gustin et al 2004, Feng et al 2005).

## **CONCLUSIONS**

The purpose of this research was to assess the feasibility of using the MerPAS to measure vertical concentration gradients of GEM at different landscapes and by season. We observed differences between certain landscapes, elevations, and to a lesser extent, seasons. Generally, we measured lower GEM concentrations near to the surface where vegetation was abundant and greater concentrations at higher elevations where air masses are unimpeded. We conclude that, given sufficient collection time, good analytical precision, and low blank levels, the MerPAS is indeed capable of measuring GEM gradients in the environment at ambient (background) levels. However, the approach used in this study could benefit from improved precision to better quantify

the factors affecting GEM concentrations and potentially to measure GEM fluxes. To that end, we recommend deploying the samplers for longer times (>2 weeks), increasing the number of samplers at each location, thoroughly assessing blank contributions, and measuring site-specific meteorological conditions including wind speeds at different heights. Because of their low cost and ease of deployment, PASs have the potential to open up research opportunities to improve understanding of the many factors that influence GEM concentrations and GEM fluxes at disparate and under-studied landscapes.

### **ACKNOWLEDGMENTS**

We are grateful to Scott Knight and staff at the University of Mississippi Field Station for access to the site and for local meteorological data. We also thank Eric Prestbo and Lucas Hawkins at Tekran Inc. and Frank Wania and David McLagan at the University of Toronto for helpful information and suggestions on many aspects of Hg PASs

## CHAPTER TWO

### Gaseous Elemental Mercury concentrations along the Northern Gulf of Mexico Using Passive Air Sampling, with a Comparison to Active Sampling



**Figure 6. Grand Bay National Estuarine Research Reserve along the northern Gulf of Mexico**

Jeon B., Cizdziel J., Brewer J.S., Luke W., Cohen M., Ren X. Kelley P. *Atmosphere* **2020**, 11, 1034. <https://doi.org/10.3390/atmos11101034>



## ABSTRACT

Mercury is a toxic element that is dispersed globally through the atmosphere. Accurately measuring airborne mercury concentrations aids understanding of the pollutant's sources, distribution, cycling, and trends. We deployed MerPAS® passive air samplers (PAS) for ~4 weeks during each season, from spring 2019 to winter 2020, to determine gaseous elemental mercury (GEM) levels at six locations along the northern Gulf of Mexico, where the pollutant is of particular concern due to high mercury wet deposition rates and high concentrations in local seafood. The objective was to (1) evaluate spatial and seasonal trends along the Mississippi and Alabama coast, and (2) compare active and passive sampling methods for GEM at Grand Bay National Estuarine Research Reserve, an Atmospheric Mercury Network site. We observed higher GEM levels ( $p < 0.05$ ) in the winter ( $1.53 \pm 0.03 \text{ ng m}^{-3}$ ) compared to other seasons at all sites; with the general pattern being: - winter > spring > summer  $\approx$  fall. Average GEM levels (all deployment combined) were highest at Bay St. Louis ( $1.36 \pm 0.05 \text{ ng m}^{-3}$ ), the western-most site nearest the New Orleans metropolitan area, and lowest at Cedar Point ( $1.07 \pm 0.09 \text{ ng m}^{-3}$ ), a coastal marsh with extensive vegetation that can uptake GEM. The MerPAS units compared reasonably well with the established active monitoring system, but gave slightly lower concentrations, except in the winter when the two methods were statistically similar. Both the passive and active sampling methods showed the same seasonal trends and the difference between them for each season was <15%, acceptable for evaluating larger spatial and temporal trends. Overall, this work demonstrates that PASs can provide insight into GEM levels and the factors affecting them along coastal regions.

## INTRODUCTION

Mercury is a persistent and toxic pollutant with a complex biogeochemical cycle, where the atmosphere plays an important role, including transport of the contaminant on local, regional, and global scales (Fitzgerald et al 1998). The understanding of atmospheric Hg has greatly advanced with the capability to measure gaseous elemental mercury (GEM), gaseous oxidized mercury (GOM), and particle bound mercury (PBM), the three main classes of airborne Hg species. There are challenges in accurately measuring these species and properly interpreting the results (Gustin et al 2010, 2015, Lyman et al 2020). GEM, the predominant form typically encompassing >95% of the total gaseous Hg, has relatively long residence time (~6 months or more) compared to GOM and PBM (~days to weeks) (Schroeder et al 1998). Levels of each Hg species vary depending on proximity to sources, meteorological conditions, season, and other factors, with GOM and PBM levels plummeting when they are scavenged by precipitation (Driscoll et al 2013, Lin et al 1999). GEM concentrations tend to be more stable, with background levels in the northern hemisphere about  $1.5 \text{ ng m}^{-3}$  (Sprovieri et al 2016). GEM levels are decreasing at many sites in North America and Europe, likely due to the phase-out of Hg from commercial products, and increased adoption of air pollution control technologies (Zhang et al 2016). GEM is slowly converted to PBM and highly soluble and particle-reactive GOM by photochemical and other reactions. GOM and PBM concentrations tend to be highest near anthropogenic point sources, especially combustion sources such as coal fired power plants or waste incinerators (Schroeder et al 1998, Driscoll et al 2013, Lin et al 1999). Once deposited to terrestrial and aquatic ecosystem, Hg can be re-emitted or, given the right biogeochemical conditions, converted by certain microorganisms to methyl-Hg, a neurotoxic form that can readily

accumulate in organisms and concentrate up the food chain to levels that can harm both wildlife and humans (Driscoll et al 2013, Choi et al 2008).

With abundant coastal wetlands that promote production and transfer of methyl-Hg into primary producers, the northern Gulf of Mexico (nGoM, a portion of the U.S. Gulf Coast extending from the Suwannee River, in the Florida panhandle, to the Sabine River, near the state line between Louisiana and Texas) is prone to Hg contaminated food webs (Hall et al 2007). Another factor contributing to high Hg levels along the nGoM is that the region consistently has some of the highest wet Hg deposition rates in the USA (Ren et al 2016, Engle et al 2007). So, it is not surprising that levels of methyl-Hg in seafood along the nGoM exceed other U.S. coastlines, and that there are widespread fish consumption advisories in the region. This is concerning because (1) nGoM residents tend to consume more seafood than other U.S. residents, with as much as 30% of the coastal population estimated to exceed the U.S. Environmental Protection Agency's reference dose for MeHg (Lincoln et al 2011), and (2) the economy of the region is intricately linked to commercial and recreational fishing. Moreover, we hypothesize that the GoM "dead-zone", a low oxygen area in the waters of the nGoM near the mouth of the Mississippi River and its spillways that occur each summer as a result of nutrient pollution from agriculture and developed land runoff in the Mississippi River watershed, may exacerbate the Hg problem by producing conditions that favor the production of MeHg, because organic matter and low oxygen fuel certain methylating-microbes (Merritt et al 2009). The periodic nature of the dead-zone (oxic-anoxic changes) may affect the speciation and bioavailability of Hg, which, in turn, may affect the net surface exchange of GEM with the atmosphere. Thus, it is important to measure atmospheric Hg at locations along the nGoM to help understand Hg sources, distribution, trends and cycling in that region.

There is a relatively long record of atmospheric Hg measurements at Grand Bay National Estuarine Research Reserve (NERR) located on the eastern portion of the Mississippi coastline (Ren et al 2020). In addition to long-term speciated-mercury measurements, collected with an automated instrument from Tekran Instruments Corporation (hereafter just Tekran) atop a 10m tower, along with trace gas and meteorological monitoring, research at the site has included intensive studies on atmospheric mercury speciation (Ren et al 2014) and Hg isotopic analysis (Rolison et al 2013). The data have provided a valuable insight on atmospheric Hg at the site, including impacts from both local and regional sources as well as large scale Hg cycling phenomena, species-specific isotopic compositions, and diurnal and seasonal variation in Hg species. As the instrument uses active sampling, the data are temporally rich, allowing correlation with other atmospheric constituents, such as ozone and sulfur dioxide (Pandey et al 2011). GEM depletion events have been observed in the early morning at the site, likely due to uptake by plants, and a slight GEM elevation during the day has generally been observed, likely due to downward mixing from higher concentrations aloft (Ren et al 2020). However, the research has been unable to directly address spatial variability in GEM concentrations because the Tekran instrument is stationary, costly, and requires power.

Passive air sampling is a low-cost no-power alternative approach to active sampling. In passive sampling the gaseous analyte enters a sampler and diffuses at a known rate through a barrier into a chamber where it is trapped on a sorbent. The sorbent is later analyzed to determine the amount of analyte present. The airborne concentration of the analyte is calculated by dividing the mass of sorbed analyte (ng) by the deployment time (days) and the sampling rate ( $\text{m}^3 \text{ day}^{-1}$ ). Passive air samplers (PAS) are increasingly being used for studies where spatially-resolved data are needed, or where active sampling is not possible due to cost, site restrictions, such as lack of

electrical power or trained operators, or other constraint (Gustin et al 2011, Skov et al 2007, Brumbaugh et al 2000, Peterson et al 2012). The main advantage is that a large number of samplers can be deployed to increase area coverage and improve spatial resolution. The main limitations are that the samplers require longer periods of time to collect the analyte, limiting temporal resolution, and, specifically for atmospheric Hg, that measurements of atmospheric mercury forms other than GEM (e.g., GOM and PBM) remain challenging, although some designs have had success (Lyman et al 2010).

The MerPAS<sup>®</sup> from Tekran is a commercially available mercury passive air sampler (PAS) that traps GEM on sulfur-impregnated activated carbon and uses a diffusive barrier to constrain the sampling rate (McLagan et al 2016). The device includes a protective shield for deployment outdoors, where it can be left to collect GEM for months without revisiting the site until it is removed for analysis. At the laboratory the sorbent is analyzed, typically with a direct mercury analyzer (DMA), and the concentrations of GEM are calculated as discussed earlier; details of the entire method and sampling rate calculations are described in Section 2.

Recent research has shown that the MerPAS sampler can not only measure GEM but also characterize and quantify atmospheric mercury sources, both with and without isotope tracing (Szponar et al 2020, McLagan et al 2019). We have recently shown that the MerPAS<sup>®</sup> sampler can also discriminate landscape, seasonal, and elevation effects on GEM if given sufficient collection time, adequate analytical precision, and low blank levels (Jeon et al 2019). In the present study, we used MerPAS<sup>®</sup> units to quantify GEM at six sites along the Mississippi and Alabama Gulf coast during four consecutive seasons, from spring 2019 to winter 2020. Herein, we report our results with emphasize on spatial and temporal trends in GEM, and a comparison between passive

and active sampling data co-collected at Grand Bay NERR, a National Atmospheric Deposition Program Atmospheric Mercury Network (AMNet) site.

## **MATERIAL AND METHODS**

### **Study Sites and Meteorological Measurements**

GEM was determined at five locations along the Mississippi Gulf Coast, including Bay St. Louis, Gulf Port, Gulf Coast Research Laboratory (GCRL) main campus near Ocean Springs, GCRL at Cedar Point, Grand Bay NERR near Moss Point, as well as at the Dauphin Island Sea Lab located to the southeast on a barrier island in Alabama (Fig. 7). Figure 7 also shows anthropogenic Hg point sources based on US Environmental Protection Agency 2018 toxic release inventory (TRI) data, the most recent TRI data available (USEPA 2020). Table 3 provides site coordinates, sampling periods, and mean temperature and wind speed during deployment. Meteorological data stems from the nearest weather stations, ranging from on-site at Grand Bay to 4.9 km away at Bay St. Louis. The samplers were deployed for ~4 weeks during 4 consecutive seasons, starting in spring 2019. The Grand Bay site has been described in detail elsewhere (Ren et al 2014). Briefly, the National Oceanic and Atmospheric Administration's (NOAA's) Air Resources Laboratory established Hg monitoring at the wetland site in 2006, and has been operating Tekran systems there as part of the National Atmospheric Deposition Program's AMNet. Long-term observations of atmospheric speciated Hg at the site have been published elsewhere (Ren et al 2020). The Cedar City site was also within a coastal wetland, whereas the other sites were at the immediate coastline with MerPAS® units deployed above open water.

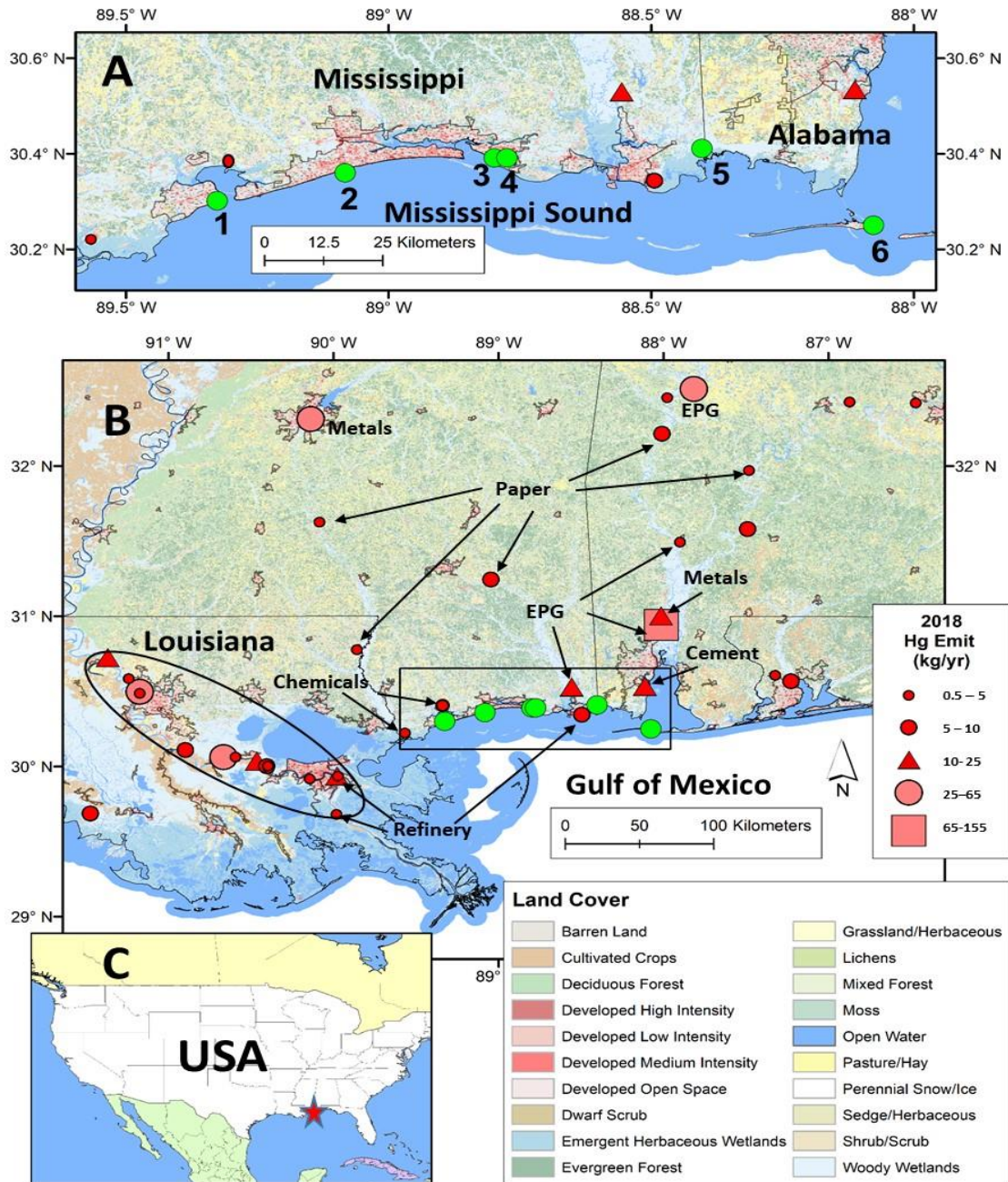


**Figure 7. Maps of the study site. (A) = close up showing the six sampling locations as green circles (1 = Bay St. Louis; 2 = Gulfport; 3 = Gulf Coast Research Laboratory (GCRL) Main; 4 = GCRL Cedar Point; 5 = Grand Bay National Estuarine Research Reserve; 6 = Dauphin Island). (B) = a regional view with the close-up domain indicated in the box. (C) = a general map showing the study site with star. The Hg air emission point sources are based on the most recent toxic release inventory data (2018), where the size and shape of the emissions symbols indicate the amounts of emissions (kg/year) and the color of the symbol indicates the source category: refineries and chemicals (red); electric power generation (pink); metals (gray); paper (blue); cement (yellow). Land cover categories are based on the 2011 National Land Cover Database. The New Orleans and Baton Rouge area (shown with an oval) has gaseous elemental mercury emission sources from multiple industries.**

## The MerPAS<sup>®</sup> and Its Preparation and Deployment in This Study

We used four to six MerPAS<sup>®</sup> units (Tekran Corp., Toronto, ON, Canada) to concurrently collect GEM at each site during each deployment (Fig. 8). The development and performance characteristics of the passive sampler have been described in detail elsewhere (McLagan et al 2016 2017, 2018). Briefly, sulfur-impregnated activated carbon serves as a sorbent, and is housed in a stainless-steel mesh cylinder at the center of the device (Fig. 8). The mesh is inserted into a microporous diffusive barrier (White Radiello<sup>®</sup>, Sigma Aldrich, St. Louis, MO, USA) which constrains the sampling rate. GEM diffuses through the barrier and is retained on the sorbent, but GOM and PBM do not appreciably pass the barrier (Stuppel et al 2019). The diffusive barrier itself is screwed into the center of a protective shield that permits outdoor deployment. The shield has an opening at the bottom that allows for air circulation but keeps precipitation out.

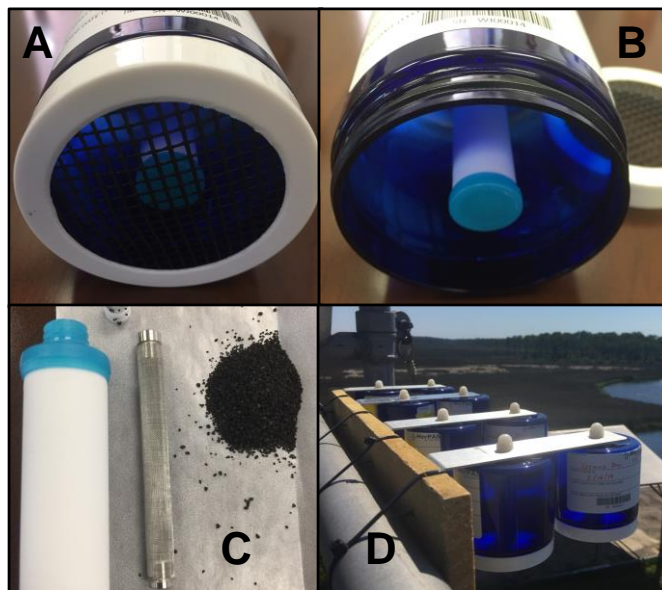


**Figure 8. Photos showing the MerPAS<sup>®</sup> configuration with cover on (A), with the cover off (B), and with diffusive body, stainless-steel mesh screen, and activated carbon sorbent (C), and deployment on the tower at Grand Bay (D)**



In this study, we loaded about 0.6g of freshly crushed sieved (250 – 1000  $\mu\text{m}$ ) sulfur-impregnated activated carbon sorbent (HGR-AC, Calgon Carbon Corp., Pittsburg, PA, USA) into the samplers <3 days prior to deployment. Before loading the samplers, the activated carbon was analyzed for Hg to ascertain the blank level; the sorbent was only used when it would contribute <0.15 ng of Hg per sampler, amounting to <4% of the Hg accumulated during sampling. Samplers were deployed at 1.5 to 3.0 m above the water surface to prevent water from splashing into the device, except at Grand Bay where they were deployed at the top of a 10m tower. We did not observe any salt inside the samplers and do not suspect water splashed into them. After each use, we cleaned diffusive barriers with a stream of nitrogen, and would only re-use them if they remained clean and undamaged; others have shown no significant difference in sampling rate between new and used barriers if the barriers are kept clean and in good condition (McLagan et al 2017).

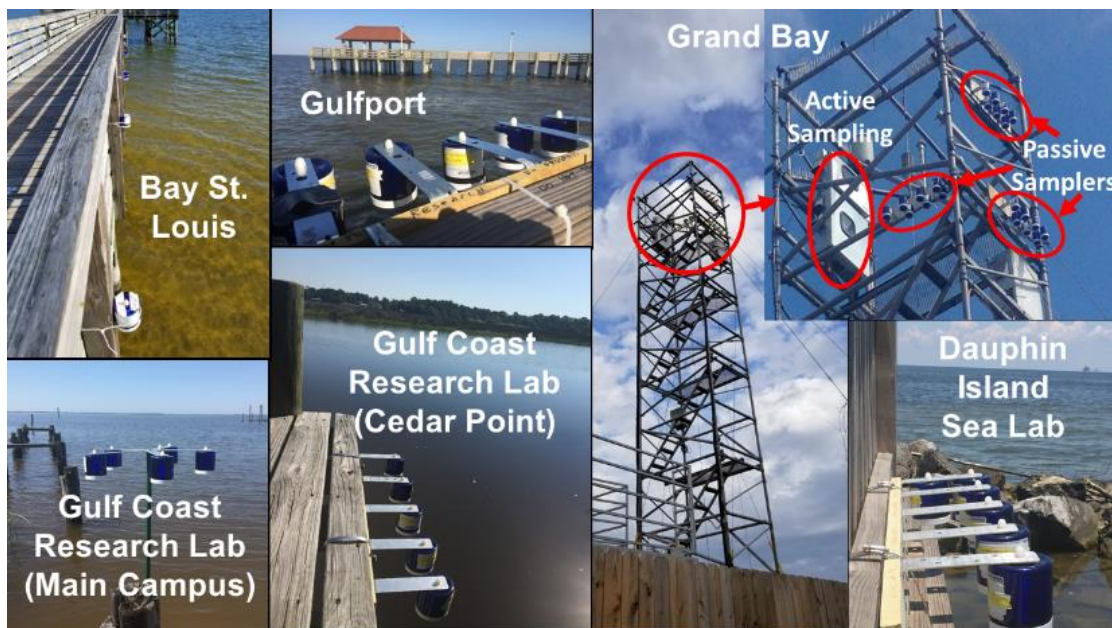


**Figure 9. Views of the six sampling sites along the northern Gulf of Mexico showing deployment of passive air samplers for GEM collection.**

## **Determination of Hg collected on the PAS sorbent and Calculation of Atmospheric Hg concentrations.**

Upon retrieval the PASs were capped, sealed with polytetrafluoroethylene tape, placed in Ziplock bags, transported to the laboratory, and stored in a clean room until analysis within 2 days of collection. Details of the analysis were described in a previous study (Jeon et al 2019). Briefly, total Hg collected on the sorbent was determined by a Direct Mercury Analyzer (DMA-80; Milestone Inc., Shelton, CT, USA), a technique which is based on thermal decomposition, gold amalgamation, and atomic absorption spectrometry. We followed U.S. Environmental Protection Agency (EPA) Method 7473, with some modifications for trapping the sulfur released from the sulfur-impregnated activate carbon with Na<sub>2</sub>CO<sub>3</sub> (McLagan et al 2017). Prior to analysis, quartz sample holders (boats) were pre-cleaned by soaking in 5% nitric acid overnight, rinsed with deionized water, and heated to 550 °C for several hours to remove any traces of Hg. Then the sorbent within the stainless-steel mesh cylinder was weighed into the boats and covered with ~0.2 g of Na<sub>2</sub>CO<sub>3</sub>. This process was repeated using a second boat because the capacity of a single boat was not enough for the amount of sorbent in a PAS. The boats were then loaded into the autosampler and analyzed by the DMA, with the Hg for the two boats being combined. The DMA instrument was calibrated using Hg solutions that were prepared from a 10 µg ml<sup>-1</sup> Hg stock solution (Spex Certiprep, Metuchen, NJ, USA). Coal fly ash standard reference material (SRM; NIST 1633C) was analyzed before beginning the sample analysis and every 20 boats thereafter. Recovery of SRM over the analyses was 94.6 ± 4.2% (mean ± SD, n = 16). The limit of detection was 0.014 ng of Hg.

Concentrations of GEM were calculated by dividing the mass of adsorbed Hg (ng) by the deployment time (days) and the sampling rate (m<sup>3</sup> day<sup>-1</sup>). Hg uptake (after blank subtraction)

ranged from 3.14 to 4.58 ng during ~4 weeks deployment period. We used a sampling rate of 0.111 m<sup>3</sup> day<sup>-1</sup> recommended by Tekran. The sampling rate was adjusted for local temperature and wind speed, factors which can influence the molecular diffusivity of GEM and the overall sampling rate, respectively. Meteorological data are given in Table 5. The adjusted sampling rate was calculated using Equation (1) (McLagan et al 2017) and ranged from 0.106 to 0.133 (m<sup>3</sup> day<sup>-1</sup>), depending on season and location.

$$\begin{aligned}
 SR_{\text{adj.}} = & SR_{\text{cal.}} + (T - 9.89 \text{ }^{\circ}\text{C}) \cdot 0.0009 \text{ m}^3 (\text{day} \cdot \text{ }^{\circ}\text{C})^{-1} \\
 & + (W - 3.41 \text{ m s}^{-1}) \cdot 0.003 \text{ m}^3 (\text{day } ^{\circ}\text{C})^{-1} \quad (1)
 \end{aligned}$$

### **Measurement of GEM at NOAA's Grand Bay Site Using Active Sampling**

Atmospheric speciated mercury (GEM, GOM, and PBM) was monitored at the Grand Bay using a Tekran speciation system, which has been described elsewhere (Ren et al 2016, 2020). Briefly, ambient air is sampled by the mercury detection system at approximately 10 L min<sup>-1</sup>. Large particles ( $d > 2.5 \mu\text{m}$ ) are removed at the inlet by an elutriator/impactor assembly, GOM is collected on a KCL-coated quartz annular denuder, and PBM ( $d < 2.5 \mu\text{m}$ ) is collected on a quartz regenerable particle filter (RPF). GEM passes through the glassware unimpeded and is sequentially collected on one of two gold traps at 5 min intervals. As one trap collects GEM, the other is heated to thermally desorb GEM into a flow of argon, and the liberated GEM is detected via cold vapor atomic fluorescence spectrometry. After one hour, sample collection ceases and the collected GOM on the denuder and PBM on the quartz filter are then sequentially thermally desorbed in a flow of mercury free zero air and quantitatively converted to GEM, which is then analyzed by the mercury detector. Thus, the speciation system operates on a 50% duty cycle, and reports GEM in

real time at 5min intervals during the sampling hour, and one-hour integrated concentrations of GOM and PBM during the subsequent desorption cycle. AMNet standard operating protocols (Gay et al 2013), were followed for mercury measurement and data reduction. Herein we focus on the GEM data for comparison with our PAS data.

### **Statistical Analysis**

Differences in passively sampled GEM concentrations among locations and seasons and the interaction between location and season were examined using univariate repeated measures analysis of variance (rmANOVA). Location was treated as a between-subjects effect, whereas season and its interaction with location were treated as within-subject effects. Given a significant main effect of location, Tukey's tests of honest significant differences (HSD tests) were used to examine pairwise differences in GEM means among locations. Pairwise differences among seasons were tested using t-tests and a Sidak  $p$ -value adjustment for multiple comparisons. The components of a significant season • location interaction were tested using planned orthogonal contrasts. Contrasts were chosen to test the hypothesis that GEM concentrations were greater outside the growing season (winter) than during other times of the year, and lower during the hottest growing season (summer) than in the spring and fall. Contrasts associated with the components of the season • location interaction included (1) the difference in GEM between winter and the remaining seasons depended on location ((winter v. rest) • location), (2) the difference in GEM between summer and the average of spring and fall depended on location ((summer v. spring/fall) • location), and (3) the difference in GEM between spring and fall depended on location ((spring v. summer) • location). Differences were deemed significant at a  $p < 0.05$  level.

Four one-sample t-tests (one for each season) were used to examine GEM concentration differences between active and passive sampling methods at Grand Bay NERR. Since the same active sampler was used to take hundreds of measurements in a given season, the measurements could not be considered independent observations. Hence, we averaged all actively sampled measurements in each season, assuming no replication and thus no within-season variation for the active sampler. We then compared the sample mean and standard error (SE, defined as the sample standard deviation (SD) divided by the  $\sqrt{n}$ ) of passively-sampled GEM concentrations for the deployment periods in each season to the average GEM concentration for the active sampler during the corresponding period. Although the one-sample t-tests assumed no statistical error, active samplers have an estimated 10% measurement error (Ren et al 2014, 2020). We therefore assumed that the seasonal average measurement of GEM by each active sampler represented the midpoint of this 10% measurement uncertainty interval. We corrected the  $p$ -values produced by each of the four one-sample t-tests using Sidak's multiplicative correction for multiple t-tests. Differences were deemed significant at a  $p < 0.05$  level. Data were analyzed using SYSTAT (version 13.0, San Jose, CA, USA).

## **RESULTS AND DISCUSSION**

Overall precision between the samplers deployed side-by-side averaged ~7% relative standard deviation, which is in the expected range for this method (McLagan et al 2018). Adjustment of the sampling rate using local meteorological data generally decreased the GEM levels from 0–8%, except during the cold fall and winter periods where GEM increased at a few sites by up to 6%, and during July 2019 when a windy summer tropical storm helped decrease

GEM levels by as much as 14% at Gulfport. Adjustments at Grand Bay were generally greater because it tended to be windier atop the 10 m tower.

### **Seasonal Trends of GEM Concentration along the nGoM Using PASs**

GEM concentrations ( $\text{ng m}^{-3}$ ) varied significantly among seasons (rmANOVA  $F_{\text{season } 3,75} = 107.58$ ; unadjusted and Greenhouse–Geisser  $p \ll 0.01$ ). Mean seasonal GEM concentrations ( $\text{ng m}^{-3} \pm 1 \text{ SE}$ ) at each of the six locations are shown in Figure 10, with specific values given in Table 4. Mean concentrations ranged from  $1.00 \pm 0.03 \text{ ng m}^{-3}$  in the summer at GCRL Cedar Point to  $1.77 \pm 0.03 \text{ ng m}^{-3}$  in the winter at Bay St. Louis. Differences among seasons averaged across locations revealed that GEM concentrations were significantly higher in the winter than in all other seasons across all sites ( $1.53 \pm 0.03$  (winter),  $1.18 \pm 0.03$  (fall),  $1.25 \pm 0.03$  (spring), and  $1.14 \pm 0.02$  (summer); Sidak-adjusted  $p < 0.05$ ; Figure 14). GEM concentrations were lower in the summer than in spring (Sidak  $p < 0.01$ ; Figure 14), but not significantly lower than in fall (Sidak-adjusted  $p = 0.12$ ). There was no significant difference in GEM concentration between spring and fall (Sidak-adjusted  $p = 0.29$ ; Figure 10).

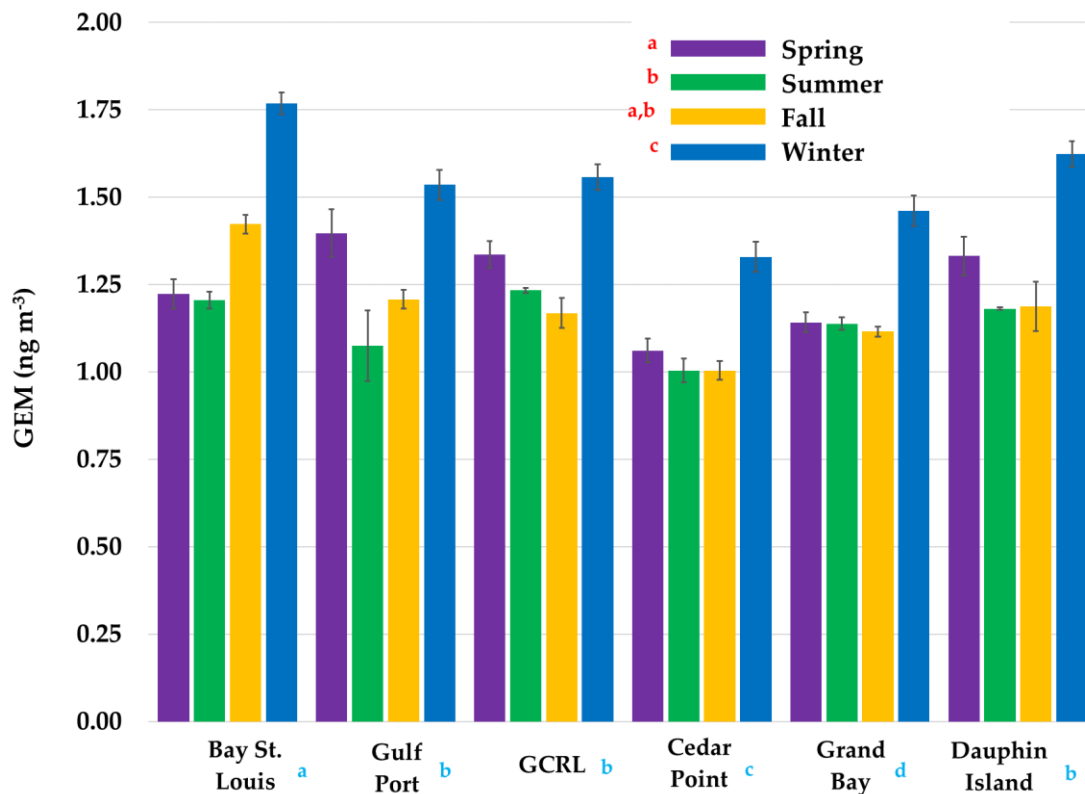


**Figure 10.** GEM concentrations determined using passive air samplers (PASs) deployed at six sites along the nGoM from May 2019 to February 2020. Sites are depicted west to east (from left to right) and error bars represent 1 standard error. Results for two sets of statistical analyses are shown: (1) pairwise means comparisons for the main effect of season (red letters), and (2) pairwise means comparisons for the main effect of location (blue letters). Seasons or locations that do not share letters are statistically different ( $p < 0.05$ ) as determined by Tukey’s honest significant difference tests. The season • location interaction is described in the text.

GEM levels tend to be higher in the winter due in part to the uptake of Hg by plants during the growing season which generally extends from spring through early fall (Schroeder et al 1998), but also due to shifts in prevailing winds which are generally from the south (arriving from the GoM) in the summer and from the north (over terrestrial areas with point sources) in the winter (Fig. 11) (Ren et al 2014, 2020). Other factors that can contribute to seasonal differences in atmospheric Hg species include greater sunlight intensity in the summer, which can increase

conversion of GEM to GOM by photochemical oxidation, and precipitation in the summer from convective thunderstorms that can strip GOM from the air, resulting in high levels of wet Hg deposition (Ren et al 2014, 2020, NADP/MDN). Seasonal trends of airborne Hg species in southeastern U.S. have now been studied using both active and passive sampling, and our data are consistent with previously reported trends (Nair et al 2012, Gustin et al 2012).

The pattern of seasonal differences in GEM concentrations varied among locations, as indicated by a significant season • location interaction (rmANOVA  $F_{\text{season} \cdot \text{location}} (15,75) = 3.14$ ; unadjusted and Greenhouse–Geisser  $p < 0.01$ ). The difference in GEM between fall and spring varied among locations (Contrast  $F_{\text{fall v. spring} \cdot \text{location}} (5,25) = 3.14$ ;  $p = 0.03$ ). Whereas GEM in the fall was greater than GEM in the spring at Bay St. Louis, the same was not true at other locations (Fig. 10). The difference in GEM between summer and the average of spring and fall varied significantly among locations (Contrast  $F_{\text{summer v. spring/fall} \cdot \text{location}} (5,25) = 4.12$ ;  $p < 0.01$ ). Whereas GEM was lower in the summer than the average for spring or fall at Bay St. Louis and Gulfport, this difference was lower at Dauphin Island, Cedar Point, and GCRL, and absent at Grand Bay (Fig. 10). Spatial differences are examined further below.

### **Spatial Trends of GEM Concentration along the nGoM Using PASs**

Previous studies have shown that coastal sites can be influenced by both polluted air from urban environments and cleaner Gulf of Mexico marine air (Griggs et al 2009). In our study, GEM concentrations varied significantly among locations (rmANOVA  $F_{\text{location}} (5,25) = 38.60$ ;  $p \ll 0.01$ ). Averaged across seasons, Tukey’s HSD tests revealed that GEM at Bay St. Louis was higher than at all other sites ( $p < 0.05$ ) (Fig. 10). As the western-most site, Bay St. Louis is closest to New Orleans (<100 km), by far the largest population center in the area with a number of Hg sources



from various industries. For the New Orleans and Baton Rouge area, Hg emissions in 2018 amounted to ~206 kg, more than double the amount emitted from all the sites in Mississippi shown in Figure 7. In addition, there is a close-in point source ~6 km to the north of the Bay St. Louis site (Fig. 7). Generally, there are higher GEM concentrations from the north and northeast during the winter and from the southwest during the summer for active sampling at the Grand Bay site (Fig. 12). Detailed air mass back-trajectory and source-receptor modelling at each site is beyond the scope of this work. Additional study is needed to determine the persistence and cause of the higher GEM concentrations found at Bay St. Louis.

We also observed the lowest GEM concentrations at the Cedar Point coastal marsh site (Fig. 10). The site is located away from the coastal beach area in a sheltered Bayou and was in proximity to the most surrounding vegetation, a known sink for airborne Hg. The Grand Bay site is also within a wetland, but we sampled there from the top of the 10 m tower, likely capturing air masses relatively unimpeded by vegetation, which may have moderated the wetland effect. Tukey's HSD tests revealed no statistical differences among the other open water coastal sites (Gulfport, GCRL Main Campus, and Dauphin Island;  $p > 0.83$ ). However, there are certainly additional complexities in this sub-tropical coastal environment that passive air samplers are unable to resolve given their long deployment times. For example, although GOM data is not included herein, GOM concentrations at coastal sites can be influenced not only by regional point sources (Ren et al 2020), but by conversion of GEM to GOM through photochemical oxidation associated with halogen species, such as BrO and BrCl, derived from marine aerosols (Sigler et al 2009, Coburn et al 2016, Hedgecock et al 2004).

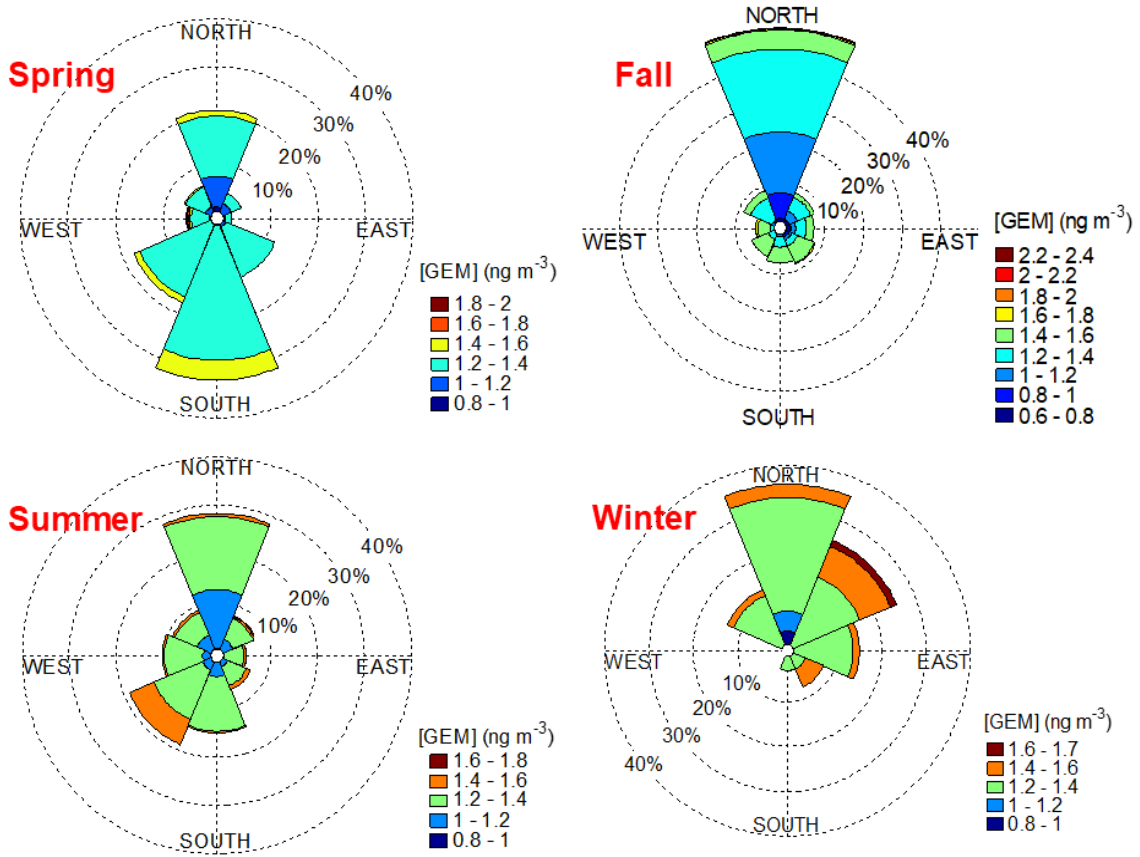


**Figure 11. Wind roses showing the relationship between GEM levels and wind direction for each sampling period at Grand Bay.**

## Comparison of GEM Determined by Active and Passive Sampling at Grand Bay

Compared to passive sampling, active sampling provides high temporal resolution with many more data points. At Grand Bay, we observed diurnal variations, seasonal trends, unknown plume events, and other complexity (Fig. 12). Detailed analysis of Hg species fluctuations is beyond the scope of this study, but others have reported on this in the region (Griggs et al 2020, Yi et al 2013). Here, we focus on preliminary data comparing GEM concentrations between passive and active sampling techniques for data co-collected at the AMNet Grand Bay NERR site. It is worth mentioning that GEM levels have been declining at the Grand Bay site at a rate of  $-0.009 \text{ ng m}^{-3} \text{ y}^{-1}$  from 2007–2018, which may be partly explained by a concurrent decrease in anthropogenic Hg emissions in the region, especially for the electric power generating industry (Ren et al 2020, USEPA 2020).

Summary statistics for GEM concentrations determined at Grand Bay are given in Table 5. We observed similar seasonal trends in GEM concentration with highest concentrations in winter by both active and passive sampling methods. However, active sampling gave slightly higher mean GEM concentrations in the spring, summer, and fall, but not in the winter (one-sample  $t_{(\text{passive-active})} = -5.16, -7.13, -10.66, \text{ and } 1.43$  for spring, summer, fall, and winter, respectively, with  $df = 5, 5, 11, \text{ and } 5$ ; Fig. 12). The trend is also depicted in Figure 14. It is unclear why passive sampling gave slightly lower average concentrations compared to active sampling for the spring, summer, and fall, and why winter was the exception. The re-use of the passive samplers may have caused a small bias or the activated carbon stock may have changed in some way over time, although it was still analyzed prior to analyses for blank subtraction. Nevertheless, the  $<15\%$  difference between the averages of the two methods, operated by two different groups, may be considered acceptable, especially when evaluating larger spatial and temporal trends.

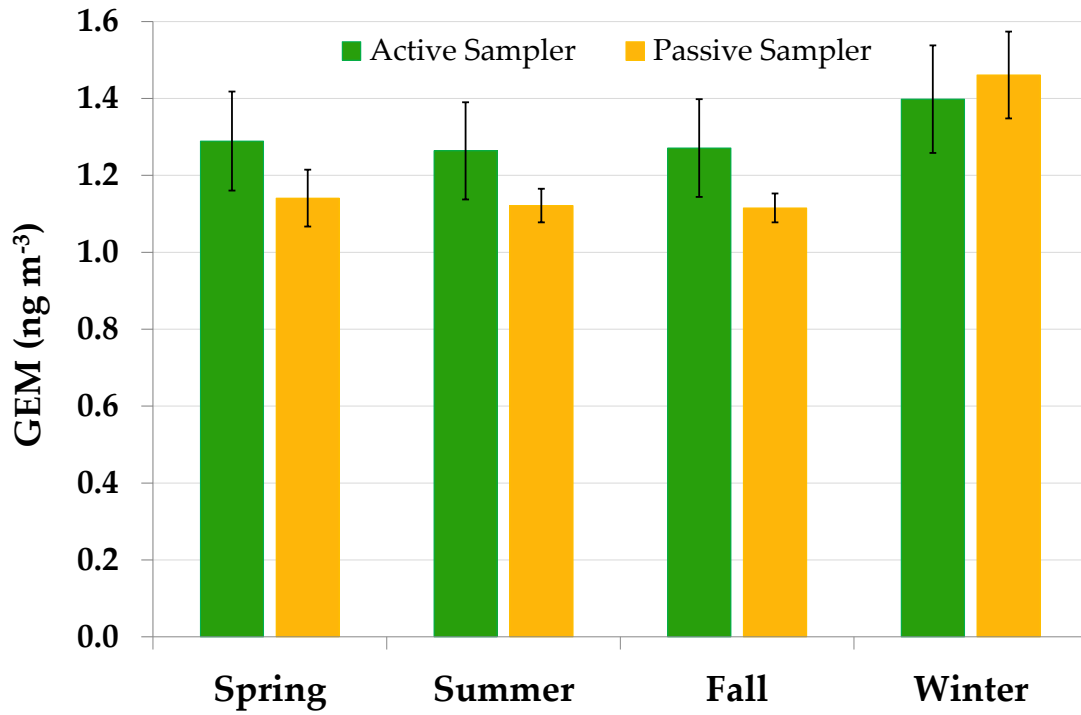


**Figure 12. GEM concentrations determined using passive and active sampling at Grand Bay NERR. Error bars for passive sampler data represent 95% confidence intervals. Bars for the active sampler data represent 10% measurement error.**

## **CONCLUSIONS**

We deployed MerPAS<sup>®</sup> passive air samplers to determine GEM at multiple sites along the nGoM over the course of a year. We observed higher GEM levels in the winter compared to other seasons across the sites. Spatially, mean GEM levels were highest at Bay St. Louise, the westernmost site nearest New Orleans at Cedar Point, a coastal marsh site with extensive vegetation. MerPAS<sup>®</sup> units were also deployed at Grand Bay near a Tekran air Hg speciation system that is based on active sampling. The passive air samplers gave slightly lower concentrations to the active sampling method, except in the winter. Despite the difference, the MerPAS<sup>®</sup> passive air samplers were capable of discriminating both seasonal and spatial differences, providing further insight into the sources and factors that influence GEM along the nGoM.

## **ACKNOWLEDGMENTS**

We thank those who gave us permission to deploy our PASs at our sampling sites. We are particularly grateful to Mike Archer at the Grand Bay NERR for access to the AMNet tower and help with sampling. We are also thankful to Eric Prestbo, Lucas Hawkins, Diana Babi, and others at Tekran Corp. for their continued advice and support. This research was funded by seed grants from the Mississippi Space Grant Consortium and RII Track-2 FEC: Emergent Polymer Sensing Technologies for Gulf Coast Water Quality Monitoring, which was part of NSF Award #1632825.

**Table 3. Coordinates for sampling sites and nearest weather stations, along with sampling periods and mean temperature and wind speed during deployment.**

	<b>Bay St. Louis</b>		<b>Gulf Port</b>		<b>GCRL (Main Campus)</b>		<b>GCRL (Cedar Point)</b>		<b>Grand Bay</b>		<b>Dauphin Island</b>	
Deployment Sites:	30.302°N, 89.327°W		30.361°N, 89.083°W		30.392°N, 88.799°W		30.392°N, 88.775°W		30.412°N, 88.404°W		30.251°N, 88.077°W	
Weather Stations:	30.287°N, 89.376°W		30.364°N, 89.086°W		30.401°N, 88.808°W		30.401°N, 88.773°W		30.412°N, 88.404°W		30.254°N, 88.103°W	
Sampling Period	Temp. (°C)	Wind (m/s)	Temp. (°C)	Wind (m/s)	Temp. (°C)	Wind (m/s)	Temp. (°C)	Wind (m/s)	Temp. (°C)	Wind (m/s)	Temp. (°C)	Wind (m/s)
5.16.2019– 6.13.2019	27.0	1.6	27.0	5.7	27.2	0.3	26.4	0.9	26.7	3.0	27.2	1.0
6.13.2019– 7.11.2019	28.1	1.4	28.5	4.7	28.7	0.3	27.9	0.9	27.9	2.9	28.7	1.2
7.11.2019– 8.8.2019	26.8	1.3	26.4	4.9	27.4	0.3	26.8	0.8	26.7	2.2	28.3	1.1
8.8.2019– 9.5.2019	27.4	0.8	28.4	3.5	27.5	0.2	27.1	0.4	27.4	1.8	28.5	0.9
11.1.2019– 12.3.2019	12.8	1.0	13.7	3.6	13.0	0.5	13.0	0.5	13.4	2.3	14.9	2.1
1.27.2020– 2.18.2020	13.7	1.3	14.3	4.6	14.3	0.7	14.3	1.1	14.8	4.9	14.6	2.1

**Table 4. Amount of Hg (ng) collected on each PAS and GEM concentrations based on those amounts (n=6, unless otherwise noted).**

Sampling Period	Amount of Hg Collected and GEM Level	Bay St. Louis		Gulf Port		GCRL Main Campus		GCRL Cedar Point		Grand Bay		Dauphin Island		All Locations	
		Mean	SE	Mean	SE	Mean	SE	Mean	SE	Mean	SE	Mean	SE	Mean	SE
16/5/2019–13/6/2019	Hg (ng)	4.12 <sup>a</sup>	0.14	4.60	0.22	4.54	0.13	3.64	0.12	4.00	0.11	4.48	0.19	4.23	0.15
	Conc. (ng m <sup>-3</sup> )	1.22	0.04	1.40	0.07	1.34	0.04	1.06	0.03	1.14	0.03	1.33	0.06	1.25	0.03
13/6/2019–11/7/2019	Hg (ng)	3.77 <sup>b</sup>	0.09	3.90	0.08	3.95	0.17	3.45 <sup>a</sup>	0.13	3.77	0.12	3.85	0.06	3.78	0.07
	Conc. (ng m <sup>-3</sup> )	1.15	0.03	1.10	0.02	1.24	0.05	1.06	0.04	1.11	0.04	1.18	0.02	1.14	0.02
11/7/2019–8/8/2019	Hg (ng)	Lost in tropical storm		3.36	0.21	4.07	0.11	3.14 <sup>a</sup>	0.06	4.00	0.16	3.98 <sup>a</sup>	0.12	3.71	0.70
	Conc. (ng m <sup>-3</sup> )	Lost in tropical storm		0.89	0.05	1.24	0.03	0.95	0.02	1.17	0.05	1.18	0.04	1.09	0.05
8/8/2019–5/9/2019	Hg (ng)	4.19 <sup>a</sup>	0.07	4.29	0.06	3.95	0.10	3.25	0.21	3.98	0.07	4.11	0.02	3.96	0.15
	Conc. (ng m <sup>-3</sup> )	1.26	0.02	1.24	0.02	1.22	0.03	1.00	0.06	1.13	0.02	1.19	0.01	1.17	0.02
1/11/2019–3/12/2019	Hg (ng)	4.36 <sup>a</sup>	0.08	4.43 <sup>a</sup>	0.10	3.92 <sup>a</sup>	0.14	3.37 <sup>a</sup>	0.09	3.96	0.05	4.26	0.25	4.05	0.16
	Conc. (ng m <sup>-3</sup> )	1.42	0.03	1.21	0.03	1.17	0.04	1.00	0.03	1.12	0.01	1.19	0.07	1.18	0.03
27/1/2020–18/2/2020	Hg (ng)	4.58 <sup>b</sup>	0.08	4.35	0.12	4.17	0.10	3.60	0.12	4.42	0.13	4.50	0.10	4.27	0.15
	Conc. (ng m <sup>-3</sup> )	1.77	0.03	1.54	0.04	1.56	0.04	1.33	0.04	1.46	0.04	1.62	0.04	1.53	0.03
All Seasons	Hg (ng)	4.21	0.07	4.15	0.09	4.10	0.06	3.42	0.06	4.02	0.05	4.20	0.07		
	Conc. (ng m <sup>-3</sup> )	1.36	0.05	1.23	0.04	1.29	0.03	1.07	0.09	1.19	0.02	1.28	0.03		

**Table 5. Summary statistics for GEM concentrations at Grand Bay NERR by active and passive sampling along with meteorological data used to obtain the adjusted sampling rate for each PAS.**

Season	Mean Temperature (°C)	Mean Wind Speed (m/s)	Statistical Parameter	Active Sampler (ng m <sup>-3</sup> )	Passive Sampler (ng m <sup>-3</sup> )
Spring 2019	26.7	3.0	n	324	6
			Range	0.90–1.81	1.07–1.27
			Mean	1.29	1.14
			Median	1.30	1.14
			SD	0.10	0.07
Summer 2019	27.3	2.5	n	550	18
			Range	0.98–1.64	1.03–1.38
			Mean	1.26	1.14
			Median	1.26	1.12
			SD	0.10	0.09
Fall 2019	13.4	2.3	n	371	6
			Range	0.71–1.68	1.06–1.15
			Mean	1.27	1.12
			Median	1.30	1.12
			SD	0.20	0.04
Winter 2020	14.8	4.9	n	256	6
			Range	0.89–1.66	1.35–1.64
			Mean	1.40	1.46
			Median	1.39	1.43
			SD	0.14	0.11



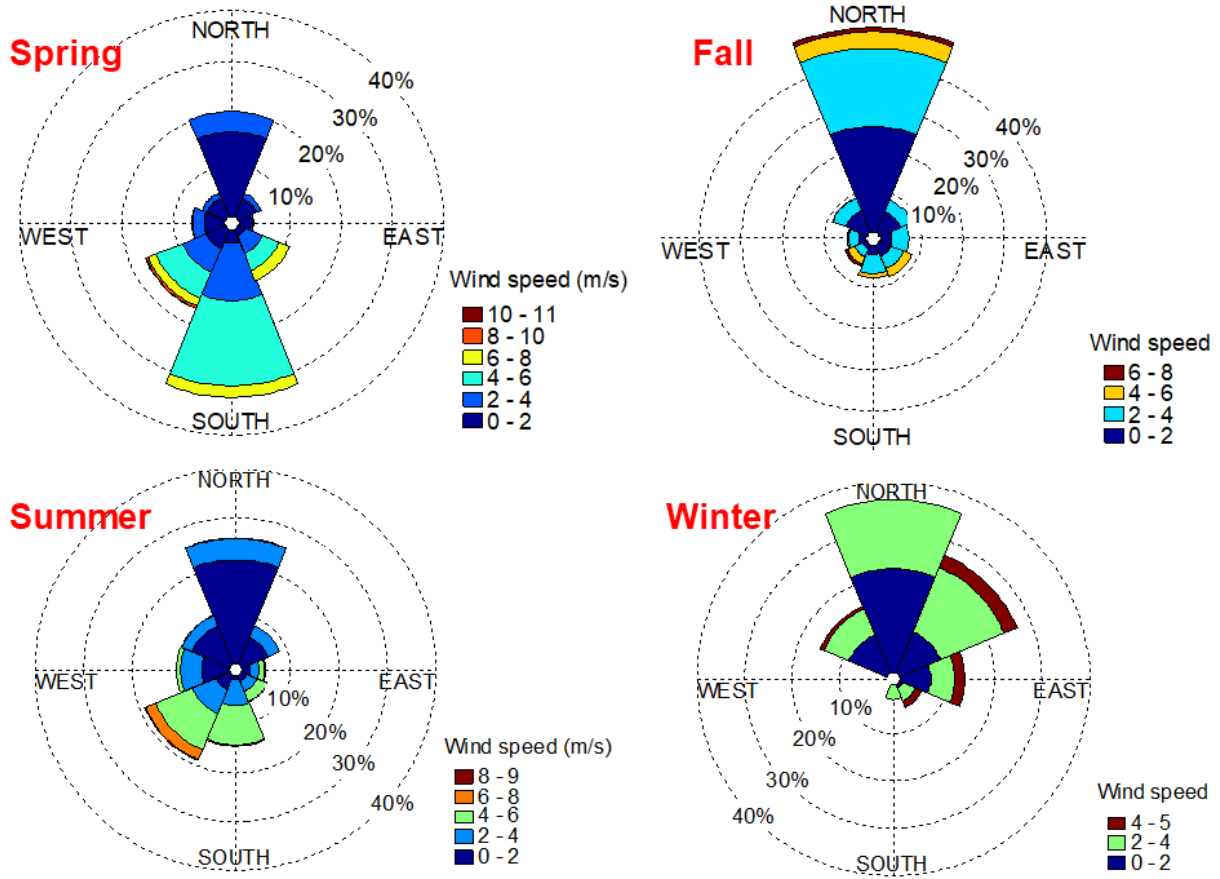


**Figure 13. Wind roses showing the relationship between speed and wind direction for each sampling period at Grand Bay.**

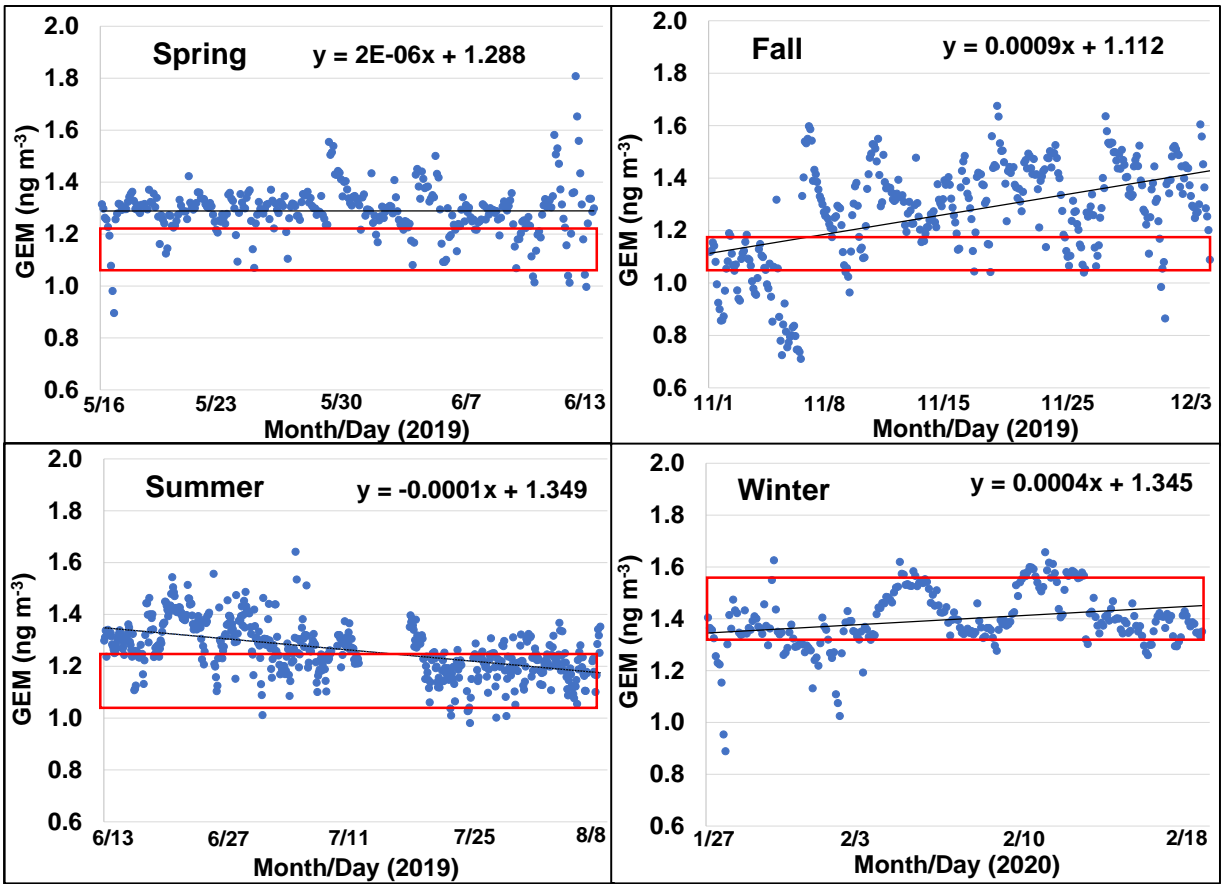


**Figure 14. Hourly GEM concentrations determined at the Grand Bay NERR site using active sampling. The red box encompasses the passive sampler data (average ± 1SD) obtained for the same period. The equation is for the linear regression of the data with the trend line in black.**

## CHAPTER THREE

### Determination of Metals in Tree Rings by ICP-MS using Ash from a Direct Mercury Analyzer



**Figure 15. Tree core sampling using a hammer type borer**

Jeon B., Cizdziel J. *Molecules* **2020**, *25*, 2126. [doi.org/10.3390/molecules25092126](https://doi.org/10.3390/molecules25092126)

## ABSTRACT

Elemental profiles in cores of tree trunks (bole wood) have been used for environmental monitoring and reconstruction of metal pollution history. Mercury (Hg) is a global pollutant that can be accurately measure in tree rings in a simple and pragmatic fashion using a direct mercury analyzer (DMA) that is based on thermal decomposition, amalgamation, and atomic absorption spectrophotometry. In this feasibility study, we demonstrate that the ash remaining after the DMA analyses can be used to quantify a wide range of other non-volatile elements (Ba, Be, Co, Cr, Cu, Fe, Ga, Mg, Mn, Ni, Pb, Sr, Th, and U) in that same sample of wood by inductively coupled plasma mass spectrometry (ICP-MS) after microwave-assisted acid digestion. Other elements (Ag, Cd, Cs, Rb, Tl, and V) exhibited poor recoveries, possibly due to losses during sample preparation. We assessed the accuracy with reference materials, spikes, and by comparison with EPA Method 3052 (Microwave Assisted Digestion of Siliceous and Organically Based Matrices). For the first group of elements (deemed suitable for the method), recoveries ranged between 80% and 120% and the relative standard deviation was generally  $< 15\%$ , indicating acceptable precision. We applied the method to five species of trees: eastern red cedar (*Juniperus virginiana*), loblolly pine (*Pinus taeda*), shortleaf pine (*Pinus echinata*), white oak (*Quercus alba*), and tulip poplar (*Liriodendron tulipifera*) from Holly Springs National Forest in north Mississippi, USA. Mercury concentrations ( $\text{ng/g} \pm \text{SE}$ ) were highest in the cedar ( $1.8 \pm 0.3$ ;  $n = 5$ ), followed by loblolly pine ( $1.6 \pm 0.3$ ,  $n = 3$ ), shortleaf pine ( $1.2 \pm 0.2$ ;  $n = 3$ ), oak ( $1.1 \pm 0.2$ ;  $n = 5$ ), and poplar ( $0.5 \pm 0.1$ ;  $n = 5$ ). Concentrations of other elements were generally  $\text{Fe} > \text{Mg} > \text{Ba} \approx \text{Sr} \approx \text{Mn} > \text{Cr} \approx \text{Cu} > \text{Ni} \approx \text{Rb} > \text{Co} > \text{Ga} \approx \text{Ag}$ , with the other elements generally below the method detection limit (MDL). Overall, we showed that the DMA can be used to not only determine total Hg in segments of tree core, but can

serve as the ashing step in the preparation of wood for ICP-MS analysis, thus allowing the determination of non-volatile elements along with Hg in the very same sample.

## INTRODUCTION

Profiles of trace elements, including Hg and other toxic metals, in tree rings have been used in a variety of studies worldwide for environmental monitoring and the reconstruction of pollution history (Watmough et al 1996, Bindler et al 2004, Cheng et al 2007, Hojdová et al 2011). These dendrochemical investigations rely on the preservation of a chemical record of metal deposition from the local environment incorporated into the annual growth increments of trees (Cutter et al 1993). In some cases, when there are overlapping features from living and dead trees that have preserved timber, annually resolved chronologies can stretch back hundreds of years (McCarroll et al 2004). However, using tree rings as records of environmental pollution requires caution due to potential differences in both the mobility of elements in wood and in physiological mechanisms of uptake of elements among species (Monticelli et al 2009). Whereas analysis of an individual tree-ring may not pinpoint a specific year of environmental change, trees can record long-term patterns and serve as biomonitors of macro-environmental trends (Padilla et al 2002). Thus, there continues to be interest in rapid and pragmatic analytical methods for dendroanalysis, especially for methods capable of determining multiple elements, including Hg.

Mercury is a global pollutant transported through the atmosphere that is incorporated into tree tissues primarily through atmospheric deposition (Schroeder et al, Yang et al 2018). Monitoring Hg in the environment is essential for evaluating the effectiveness of the recent (2017) Minamata convention, a global regulatory mechanism to decrease environmental Hg loadings (Gustin et al 2016). While some studies have shown that tree cores can serve as temporal total-Hg

biomonitors, recording changes in Hg deposition with pollution history (Yang et al 2018, Becnel et al 2004), others have not (Siwik et al 2010), suggesting that the cycling of Hg in individual species of trees needs to be further investigated. In any case, quantifying Hg in tree wood and other tissues is also important to understanding the pools and fluxes of Hg in forest ecosystems (Yang et al 2018). However, measuring Hg in trees, especially wood, is difficult due to its low concentration, which is often below method detection limits (Yang et al 2017). Despite its low concentration, the Hg content of wood often comprises the largest pool of Hg in forests, except for the soil, due to its relatively high biomass (Obrist et al 2012). Moreover, wildfires are a poorly characterized but potentially important source of Hg to the atmosphere, and a lack of data on Hg in wood leading to uncertainty in ecosystem Hg budget (Yang et al 2017, 2018).

Recently, Yang et al. showed that a direct mercury analyzer (DMA), based on thermal decomposition, catalytic conversion, amalgamation, and atomic absorption spectrophotometry, can reliably measure Hg in wood. The method is popular because compared to inductively coupled plasma mass spectrometry (ICP-MS), it is much less costly, requires virtually no sample preparation, is rapid (<6 min/sample), and can be run by students after minimal training. Moreover, whereas Hg can be effectively determined by ICP-MS, the analyst must be keenly aware of a number of pitfalls, including potential carryover as Hg is prone to “memory” effects (e.g., sorption/desorption from pump tubing). Mercury also has a relatively high ionization potential (~10.4 eV) and its signal is spread out over its seven stable isotopes. Thus, Hg in bole wood is increasingly being determined with DMAs. However, the ash that remains after the Hg analysis is typically discarded, despite containing non-volatile elements whose concentration can also be determined for pollution and other dendrochemistry-related studies.

The purpose of the current study was to develop and validate an analytical method for the analysis of bole wood tree rings which combines the determination of total-Hg using the DMA with multi-elemental analysis using ICP-MS. Effectively, we used the DMA as a sample-ashing step before microwave-assisted acid digestion and ICP-MS analysis of the diluted bole wood digests. As we have not seen this approach documented in the scientific literature, and because others are now routinely measuring Hg in tree wood using DMAs as it has become apparent that wood is, by mass, the most important reservoir of Hg in forests after soil (Navrátil et al 2017, Wright et al 2014), we carefully evaluate and optimize the method. Here, we report on the methodology and its application to trees from Holly Springs National Forest in Mississippi, which will serve as a background site for future dendrochemical studies tracing the pollution history of coal-fired power plants and other potential point sources of airborne metal pollution in the region. We focused on the outer (most recent) tree rings; fully quantifying the distribution and trends of Hg and other elements in the full tree cores is beyond the scope of this method feasibility study.

## **MATERIAL AND METHODS**

### **Site Description and collection of Tree Cores**

Tree cores were collected from five species of tree—eastern red cedar (*Juniperus virginiana*), loblolly pine (*Pinus taeda*), shortleaf pine (*Pinus echinata*), white oak (*Quercus alba*), and tulip poplar (*Liriodendron tulipifera*)—from Tallahatchie Experimental Forest (TEF), which is part of the Holly Springs National Forest located in the north central hills of Mississippi (Figure 18). The forest encompasses 629 km<sup>2</sup> and was established in 1936 after loblolly pine was planted in the area to convert rapidly eroding abandoned agricultural land to forest. The TEF, located near

Oxford, Mississippi, was created in 1950 to study relationships between mixed pine and hardwood forests, flooding, and soil erosion.

Trees were identified using bark and leaves, and cores were collected at about 1 m above the ground using a 5.15-mm diameter increment borer made from hardened steel with a PTFE coating (Haglöf, Sweden) or an increment hammer, also made of steel (Fig. 17). The extractor is stainless steel. All tools were cleaned and rinsed with deionized water and methanol before sampling. The tools were inspected between uses to make sure no material was transferred between samples. Given the Teflon coating and hardened materials used, we do not expect any impact on metal concentration in the wood. Extracted cores were inserted in an increment core holder, which was placed into Ziploc bags for transport. The cores were air-dried in a laminar flow hood in a clean room for ~1 week before being stored in a desiccator. This was found to be sufficient for complete desiccation before analysis.

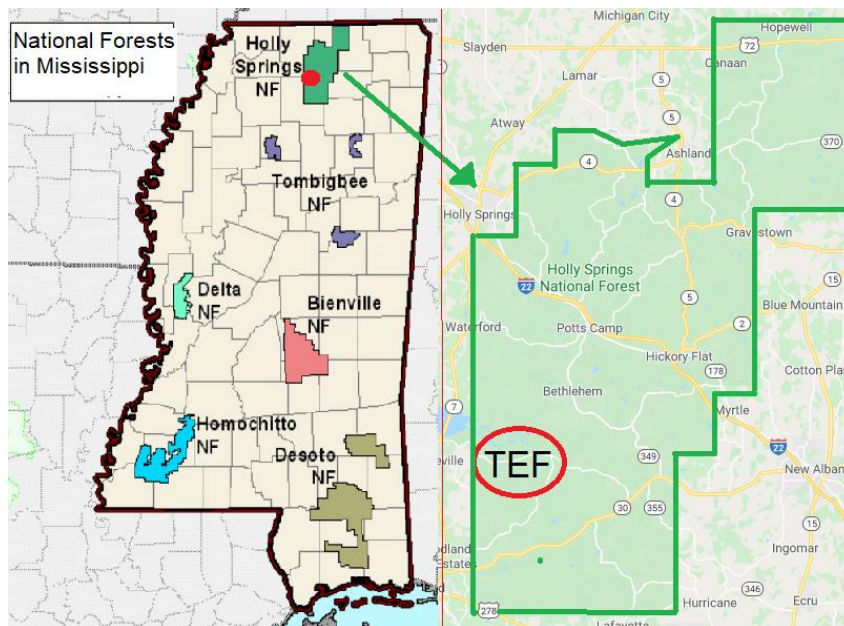


**Figure 16. Location of the Tallahatchie Experimental Forest (TEF) in Holly Springs National Forest (NF) in north central Mississippi, USA.**





**Figure 17. Example of tree cores collected with a 5.15-mm increment borer.**

### **Direct Mercury Analysis**

Total Hg was determined in ~1 cm (~ 0.1 g) segments of tree core using a DMA-80 (Milestone Inc., Shelton, CT, USA) following EPA Method 7473 with slight modifications. Briefly, the bole wood was weighed into quartz boats and the boats placed in the instrument's autosampler. The boats were sequentially inserted into the unit's combustion tube where the sample was thermally decomposed (combusted) at 650 °C with air serving as the carrier gas (200 mL/min). Instrument parameters are given in Table 1. The total analysis time was < 5 min per sample. The instrument was calibrated from 0.05 to 100 ng of Hg using six standards prepared from 10 µg/mL Hg standard solution (Spex Certiprep, Metuchen, NJ, USA). The system was checked for accuracy at the beginning and end of each run using SRM1633C (Coal Fly Ash). Recoveries were between 90% and 115%. Ash residue was carefully weighed into micro-sampling inserts for microwave digestion.

### **Microwave-assisted Acid Digestion of Trace Core Ash**

A general scheme showing the analytical process is given in the graphical abstract. The ash remaining after DMA analysis of the dried tree core segments (~10 mg) was digested with 1.5 mL of HNO<sub>3</sub> and 50 µL of HF (both trace metal grade, Fisher Chemical, Pittsburgh, PA, USA) in acid-cleaned 6 ml TFM micro sampling inserts using a 1200 W Ethos microwave digestion system (Milestone Inc., Shelton, CT, USA). The temperature program consisted of a 15 min ramp to 200 °C and a 20 min hold at that temperature. The resulting digest was transferred to polyethylene tubes and diluted to 50 mL with ultrapure water (deionized and 0.2 µm-filtered with a Milli-Q system; Millipore, Burlington, MA, USA). An additional 1:5 dilution was carried out in 2% HNO<sub>3</sub>. Sc, Rh, and Bi were used as internal standards at a final concentration of 1 ng/mL. Note, further dilution may be needed for certain elements like Mg and Ba depending on instrument sensitivity and concentrations in the samples. Reagent blanks were run with every set of digestions. Two reference materials were used to validate the new method. AR1946 is a wood fuel biomass CRM (Alpha Resources LLC, Stevensville, MI, USA) and SRM1633C is a coal fly ash SRM (NIST; Gaithersburg, MD, USA). The digested solutions were analyzed using a sector field-ICP-MS.

### **Determination of Metals in Ash from the DMA by ICP-MS**

Concentrations of 20 elements were determined by sector field ICP-MS using a Thermo Fisher Element-XR. The instrument features resolving power ( $m/\Delta m$ ) settings of low (~300) and medium (~3000) to remove certain isobaric interferences. We measured Be, Rb, Sr, Ag, Cd, Cs, Ba, Tl, Pb, Th and U in low resolution and Mg, V, Cr, Mn, Fe, Co, Ni, Cu, and Ga in medium resolution. Data acquisition parameters are given Table 1. Samples were introduced using a PFA

**Table 6. Direct mercury analyzer (DMA) and ICP-MS instrumental settings.**

DMA	
Gas flow	200 mL/min
Drying	200 °C for 60 s
Decomposition	650 °C for 180 s
Purge	60 s
Amalgamator	900 °C for 12s
Record	60 s
Plasma Parameters	
Cool gas flow	14 L/min
Auxiliary gas	0.9 L/min
Sample gas flow	1.1 L/min
RF power	1280 W
ICP-MS Data Acquisition	
Isotopes in LR	<sup>9</sup> Be, <sup>85</sup> Rb, <sup>88</sup> Sr, <sup>107</sup> Ag, <sup>111</sup> Cd, <sup>133</sup> Cs, <sup>137</sup> Ba, <sup>205</sup> Tl, <sup>208</sup> Pb, <sup>232</sup> Th, <sup>238</sup> U
Isotopes in MR	<sup>24</sup> Mg, <sup>51</sup> V, <sup>52</sup> Cr, <sup>55</sup> Mn, <sup>56</sup> Fe, <sup>59</sup> Co, <sup>60</sup> Ni, <sup>63</sup> Cu, <sup>69</sup> Ga
Integration time	10 ms (LR); 50 ms (MR)
Mass window	20% for LR; 125% for MR
Points per peak	50 (LR); 20 (MR)
Runs/passess	3/3 (E-scan)

LR = Low Resolution; MR = Medium Resolution.

concentric nebulizer and a PFA cyclonic chamber (Elemental Scientific, USA). The system was optimized for sensitivity and stability, yielding ~0.8 million counts-per-second for 1 ng g<sup>-1</sup> of 115 in low resolution mode with < 3.5% relative standard deviation (RSD). The mass window was set to 20% with 50 points per peak for low resolution mode and to 125% with 20 points per peak for medium resolution mode. Elements were quantified using external calibration which consisted of a blank, 0.05, 0.1, 0.2, 0.5, 1, 5 ng g<sup>-1</sup> standards from a multi-element solution (Spex CertiPrep, Metuchen, NJ, USA). The calibration curve correlation coefficient (r<sup>2</sup>) values were > 0.994 for each element. To back-calculate the concentration of the metals in the wood, the solution concentration was multiplied by a dilution factor consisting of the mass of the solution (after digestion and dilution to 50 mL mark) divided by the original weight of sample multiplied by 5 to

account for the 1:5 dilution of the digest prior to analysis. Concentrations reported herein are based on dry-weight.

## RESULTS AND DISCUSSION

### Method Comparison, Figures-of-merit, and Recovery Tests

EPA method 3052 is a common microwave digestion method applicable to organic matrices that uses 9 ml of concentrated HNO<sub>3</sub> and 3 ml of concentrated HF. However, given our sample size (~0.1 g) and the low concentration of many elements in wood, we modified the method to reduce dilution while maintaining optimal digestion conditions. To compare the two methods, we prepared a homogenized mixture of pulverized bole wood from white oak (*Quercus alba*) by cryogenic grinding (Spex 6875 Freezer/Mill) of the wood from multiple tree cores. The material was analyzed directly by EPA method 3052 and by our method after ashing with a DMA. Our method, described earlier, uses three “micro-inserts” in each digestion vessel and only 1.5 ml HNO<sub>3</sub> and 50 μL of HF. The results show good agreement between the two approaches, except for Cd, Cs, and Tl (Table 7). Cadmium is known to be volatile and is likely lost during the DMA analyses; Cs can form a metal oxide that can attack silica, and Tl was near the MDL (Table 8).

To estimate the MDL and limit of quantitation (LOQ) ( $3\sigma$  and  $10\sigma$  criteria, respectively), multiple reagent blanks were included with each set of digestions. MDLs ranged from  $<5 \text{ ng g}^{-1}$  for Ag, Co, Cs, Ga, Th, Tl, U, V to  $2 \mu\text{g g}^{-1}$  for Mg (Table 7). All calibration curves were  $> 0.994$ . For those elements suitable for the method, the relative standard deviation for the reference material was generally  $<15\%$ , indicating acceptable precision.

To check the accuracy of the method, we also analyzed reference materials, including CRM AR 1946 (wood fuel biomass) and NIST SRM 1633C (coal fly ash), the latter with and without DMA analysis (ashing). In addition, because only three of the twenty elements determined were certified in the wood reference material (six others had reference values), we spiked the wood CRM with 10 $\mu$ L of a 10 $\mu$ g mL<sup>-1</sup> multi-element standard (to yield ~0.4 ng g<sup>-1</sup> in the final diluted solution) and analyzed the material both with and without DMA ashing using microwave digestion and ICP-MS. The results for these recovery tests are summarized in Table 8. Recoveries for the three certified elements, Mg, Fe, and Mn, in the wood reference material were 93, 99, and 110% respectively. Recoveries for Sr (97%), Ba (117%), and Cu (118%) were also acceptable.

Recoveries for Ni, Pb, and V were low (31% to 51%); however, these elements only had reference values and Ni and Pb performed much better with spikes of the wood CRM as well as the other reference material where their concentration was certified. Recoveries for V were mixed with some low values ~60%; thus, the element should be carefully monitored as it may not be suited for this method.

Recoveries for the coal fly ash ranged from 80% to 110% for Ba, Co, Cr, Cu, Mn, Ni, Pb, Sr, U, V, for both DMA-heated samples and samples that were analyzed directly without the DMA. Recoveries for Cd, Cs, Tl were poor, as was the case in our comparison with the EPA method 3052, suggesting that these elements are also not well-suited for this method.

**Table 7. Comparison of the new method (with DMA ashing) with a standard method (EPA 3052, without DMA ashing) for determination of metals in pulverized bole wood prepared by cryogenic milling. Figures-of-merit are for the new method. Starred values indicate a relative percent difference (RPD) exceeding 25%, suggesting that the element may not be suitable for this method.**

Element	Mean ( $\pm 1$ SD; $n = 5$ )		RPD	MDL	LOQ	Calib. Curve Linearity ( $r^2$ )
	EPA 3052	New Method				
Ag (ng/g)	11.5 $\pm$ 6.9	<MDL	-	5.1	17.2	0.9995
Ba ( $\mu$ g/g)	200 $\pm$ 8	192 $\pm$ 4	4.1	0.04	0.12	0.9990
Be (ng/g)	80 $\pm$ 10	82 $\pm$ 18	3.1	15.2	50.7	0.9996
Cd (ng/g)	250 $\pm$ 8	67 $\pm$ 12	73.3*	7.2	23.9	0.9999
Co (ng/g)	348 $\pm$ 24	353 $\pm$ 47	1.4	1.5	4.9	0.9999
Cr ( $\mu$ g/g)	34.5 $\pm$ 4.4	31.0 $\pm$ 1.5	10.4	0.05	0.18	0.9999
Cs (ng/g)	6.0 $\pm$ 0.3	10.1 $\pm$ 4.4	67.2*	2.1	7.1	0.9993
Cu ( $\mu$ g/g)	1.9 $\pm$ 1.0	1.7 $\pm$ 1.3	14.2	1.1	3.7	0.9999
Fe ( $\mu$ g/g)	156 $\pm$ 20	188 $\pm$ 56	20.8	0.81	2.72	0.9961
Ga (ng/g)	7.0 $\pm$ 2.5	8.6 $\pm$ 4.4	23.5	1.3	4.5	0.9999
Mg ( $\mu$ g/g)	1200 $\pm$ 48	1200 $\pm$ 71	1.6	1.2	3.9	0.9947
Mn ( $\mu$ g/g)	100.0 $\pm$ 4.6	96.3 $\pm$ 0.9	3.7	0.10	0.34	0.9986
Ni ( $\mu$ g/g)	13.4 $\pm$ 1.6	13.2 $\pm$ 0.5	1.4	0.05	0.17	0.9999
Pb ( $\mu$ g/g)	1.71 $\pm$ 0.07	1.72 $\pm$ 0.06	0.9	0.06	0.19	0.9998
Rb ( $\mu$ g/g)	4.52 $\pm$ 0.17	4.30 $\pm$ 0.06	4.8	0.02	0.08	0.9999
Sr ( $\mu$ g/g)	49.5 $\pm$ 2.1	47.0 $\pm$ 0.3	5.2	0.02	0.07	0.9999
Th (ng/g)	3.2 $\pm$ 4.3	<MDL	-	2.4	7.9	0.9994
Tl (ng/g)	4.7 $\pm$ 0.5	3.0 $\pm$ 0.7	36.4*	2.9	9.8	0.9994
U (ng/g)	4.4 $\pm$ 2.3	3.6 $\pm$ 1.5	19.5	1.7	5.6	0.9986
V (ng/g)	210 $\pm$ 30	220 $\pm$ 20	0.9	3.2	10.5	0.9999

Recoveries from the coal fly ash were also poor for Fe, Mg, Th, and Rb, but that was the case for both DMA and non-DMA samples and given good recoveries from the wood reference material (both with and without DMA-ashing), the effect is likely matrix-dependent and coal fly ash is substantially different from wood ash. Thus, we feel that the method is suitable to determine Fe, Mg, Th and Rb in tree cores.

**Table 8. Recoveries for reference materials determined by ICP-MS after microwave digestion with or without prior ashing by a direct mercury analyzer.**

Element (Unit)	CRM AR 1946 (Wood Fuel Biomass)					NIST SRM 1633C (Coal Fly Ash)									AR1946 spiked with multi-element standard			
	Certified or Reference Value		With DMA Ashing ( <i>n</i> = 3)			Certified or Reference Value		With DMA Ashing ( <i>n</i> = 8)			Without DMA Ashing ( <i>n</i> = 8)			With DMA Ashing ( <i>n</i> = 2)		Without DMA Ashing ( <i>n</i> = 3)		
	Mean	SD	Mean	SD	Rec. (%)	Mean	SD	Mean	SD	Rec. (%)	Mean	SD	Rec. (%)	Rec. (%)	RPD	Rec. (%)	SD	
Ag (ng/g)	-	-	14.0	6.0	-	-	-	<MD	0.1	-	<MD	0.0	-	96.3	10.6	123.4	7.4	
Ba (µg/g)	47	-	54.9	2.0	116.8	1126	33	1158	83.6	102.9	1243	70.3	110.4	96.8	5.7	91.9	11.8	
Be (ng/g)	-	-	<MD	4.0	-	-	-	<MD	-	-	<MD	-	-	86.6	12.1	114.5	7.5	
Cd (ng/g)	-	-	39.0	11.0	-	0.758	0.005	<MD	-	156.4	<MD	-	140.7	7.6	110.4	110.0	7.7	
Co (µg/g)	-	-	<MD	0.1	-	42.9	3.5	36.8	3.4	85.9	37.8	0.8	88.0	76.0	16.8	103.7	11.7	
Cr (µg/g)	-	-	2.2	0.2	-	258	6	207	18	80.2	217.8	2.1	84.4	98.2	4.9	123.0	18.1	
Cs (ng/g)	-	-	35.0	6.0	-	9.39	0.22	4.7	1.2	50.0	8.0	0.2	85.2	76.9	7.4	114.1	8.1	
Cu (µg/g)	4	-	4.7	3.0	118.3	173.7	6.4	154.8	12.0	89.1	159.3	3.4	91.7	-	-	100.1	14.9	
Fe (%)	0.110	0.020	0.109	0.017	99.4	10.49	0.39	1.48	0.12	14.1	1.51	0.04	14.4	86.6	0.3	85.6	9.1	
Ga (ng/g)	-	-	112.0	3.0	-	-	-	47.6	4.1	-	48.5	1.1	-	87.8	12.6	110.4	9.7	
Mg (µg/g)	480	10.0	445	8.6	92.7	4980	520	278	81.5	14.0	637.5	26.4	32.2	93.0	6.4	87.4	14.8	
Mn (µg/g)	110	10.0	121	3.7	109.8	240.2	3.4	204	21.7	84.8	207.7	3.5	86.5	94.2	8.2	90.0	14.1	
Ni (µg/g)	3	-	1.3	0.2	43.5	132.0	10.0	129	21.6	97.6	124.6	2.5	94.4	80.6	39.2	111.2	7.1	
Pb (µg/g)	4	-	1.2	0.3	31.1	95.2	2.5	95.1	5.3	100.1	91.0	1.4	95.6	97.4	100.2	111.1	0.8	
Rb (µg/g)	-	-	2.9	0.0	-	117.42	0.53	31.2	2.2	26.6	43.8	2.4	37.3	56.4	68.3	95.7	15.6	
Sr (µg/g)	33	-	32.1	0.4	97.2	901	56	730	65	81.0	858.2	10.8	95.3	97.5	9.5	96.7	7.1	
Th (ng/g)	-	-	82.0	13.0	-	23.0	0.4	<MD	-	7.4	3.8	0.1	16.5	83.9	9.8	109.1	18.8	
Tl (ng/g)	-	-	<MD	0.0	-	-	-	5.9	0.5	-	5.7	0.1	-	52.9	16.4	114.9	7.3	
U (ng/g)	-	-	30.0	7.0	-	9.25	0.45	8.4	0.6	90.8	8.0	0.1	86.5	85.1	13.8	117.0	8.3	
V (ng/g)	3	-	1.7	0.2	58.0	286.2	7.9	247	19	86.3	256.3	4.2	89.5	61.1	21.1	105.0	0.4	

In summaries, Ag, Cd, Cs, Rb, Tl, and V are problematic and probably should not be quantified using this method; the remaining elements (Ba, Be, Co, Cr, Cu, Fe, Ga, Hg, Mg, Mn, Ni, Pb, Sr, Th, and U) can be quantified if the concentration is above the MDL in the tree wood. In any case, we emphasize that it is important that each laboratory documents the reliability of their own data using appropriate quality assurance measures.

### **Analysis of Tree Cores Collected from the Holly Springs National Forest**

We applied the method to bole wood collected from five tree species in Holly Springs National Forest. Mercury concentrations ( $\text{ng g}^{-1} \pm 1 \text{ SE}$ ) were highest in the cedar ( $1.8 \pm 0.3$ ;  $n = 5$ ), followed by loblolly pine ( $1.6 \pm 0.3$ ,  $n = 3$ ), shortleaf pine ( $1.2 \pm 0.3$ ;  $n = 3$ ), white oak ( $1.1 \pm 0.2$ ;  $n = 5$ ), and tulip poplar ( $0.5 \pm 0.1$ ,  $n = 5$ ) (Fig. 18). These concentrations are similar to those reported in other studies of tree cores: for example, Hg concentrations in cores of deciduous trees cores from Ontario, Canada, including Eastern cottonwood (*Populus deltoides*), willow (*Salix x rubens*), and red oak (*Quercus rubra*) ranged from  $\sim 0.7$  to  $4.1 \text{ ng g}^{-1}$  (Siwik et al 2010), and in hardwoods and conifers from the northeast USA, American beech (*Fagus grandifolia*), yellow birch (*Betula alleghaniensis*), red maple (*Acer rubrum*), sugar maple (*Acer saccharum*), red spruce (*Picea rubens*), white ash (*Fraxinus americana*), white pine (*Pinus strobus*) and balsam fir (*Abies balsamea*) ranged from  $\sim 0.4$  to  $5 \text{ ng g}^{-1}$  (Yang et al 2018, Siwik et al 2010). It is important to note that recent work has shown the suitability of tree rings as archives of global and regional atmospheric Hg pollution (Peckham et al 2019), and has been used track atmospheric Hg pollution, including from past mining operations in Australia (Schneider et al 2019).

Concentrations of elements determined in the DMA-ash by ICP-MS were generally in the following order,  $\text{Fe} > \text{Mg} > \text{Ba} \approx \text{Sr} \approx \text{Mn} > \text{Cr} \approx \text{Cu} > \text{Ni} > \text{Co} > \text{Pb}$ , with several other elements



(Be, Th, Ga, U) routinely near or below the MDL regardless of species (Fig. 19, Table 9). In general, elemental concentrations were higher in the slow-growing oak and cedar, compared to the pine and tulip poplar. Most of the trace metal concentrations are comparable to measurements of tree rings from other studies conducted in relatively pristine areas, and lower than those from contaminated areas. (Cocozza et al 2016) measured relatively high concentrations of Co ( $> 50 \mu\text{g g}^{-1}$ ) in tree rings collected from downy oak (*Quercus pubescens*) near an incinerator in an industrial area. Our highest measurement of Co was  $0.41 \mu\text{g g}^{-1}$ . In another study, (Madejón et al 2004) measured  $63 \mu\text{g g}^{-1}$  of Pb in white poplar (*Populus alba*) in riparian forests contaminated from a mine waste spill. All but one of our measurements for Pb were  $< 1 \mu\text{g g}^{-1}$ .

## CONCLUSIONS

We demonstrate that DMAs based on combustion atomic absorption spectrophotometry can be used effectively as an ashing step in the preparation of tree cores for ICP-MS analysis for certain metals, which allows the quantitative determination of non-volatile elements (Ba, Be, Co, Cr, Cu, Fe, Ga, Mg, Mn, Ni, Pb, Sr, Th, and U) in that very same sample after microwave-assisted acid digestion. Other elements (Ag, Cd, Cs, Rb, Tl, and V) were showed in poor recoveries, possible due to losses during sample preparation. We assessed the accuracy of our new method with spikes, reference materials, and by comparison with EPA method 3052. Newly developed and optimized method was applied to five species of tree from Holly Springs National Forest in north Mississippi, USA, with including Hg analyses by DMA.

Finally, we note that continued advancements in ICP-MS, including collision/reaction or laser ablation-ICP-MS, may make the technique more suitable for direct multi-element analyses (including mercury) in wood samples.

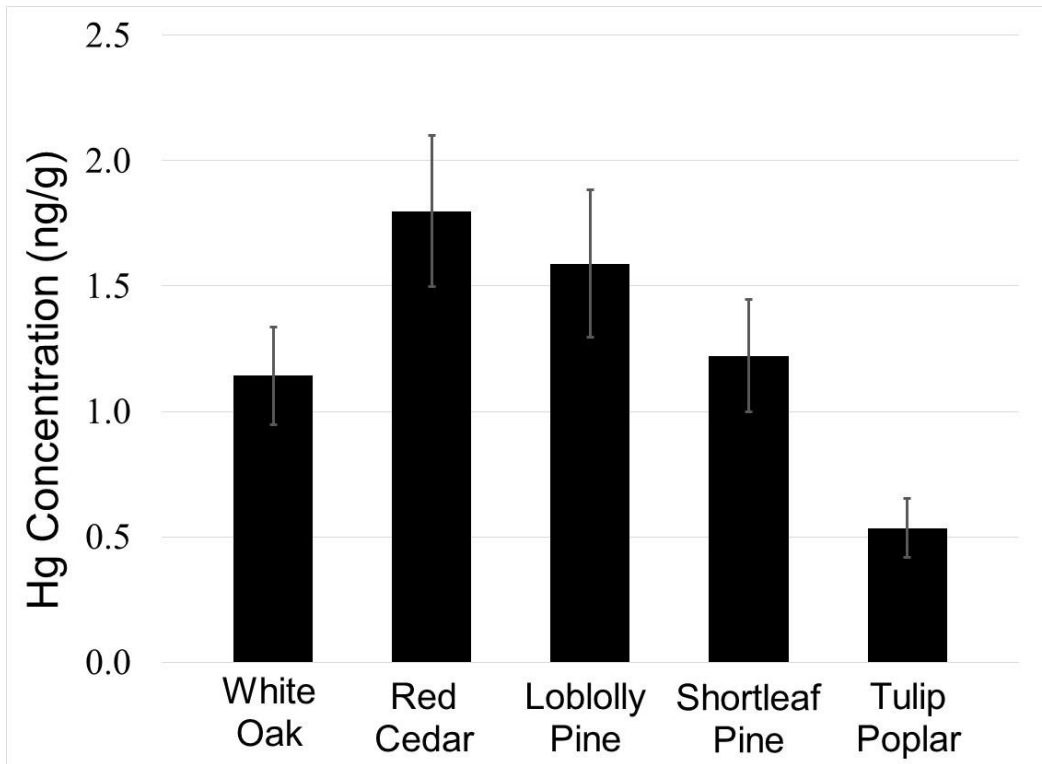


**Figure 18. Mean mercury concentration in tree rings from the Tallahatchie Experimental Forest in Holly Springs National Forest in north Mississippi determined with a direct mercury analyzer. Error bars are  $\pm 1$  standard error.**

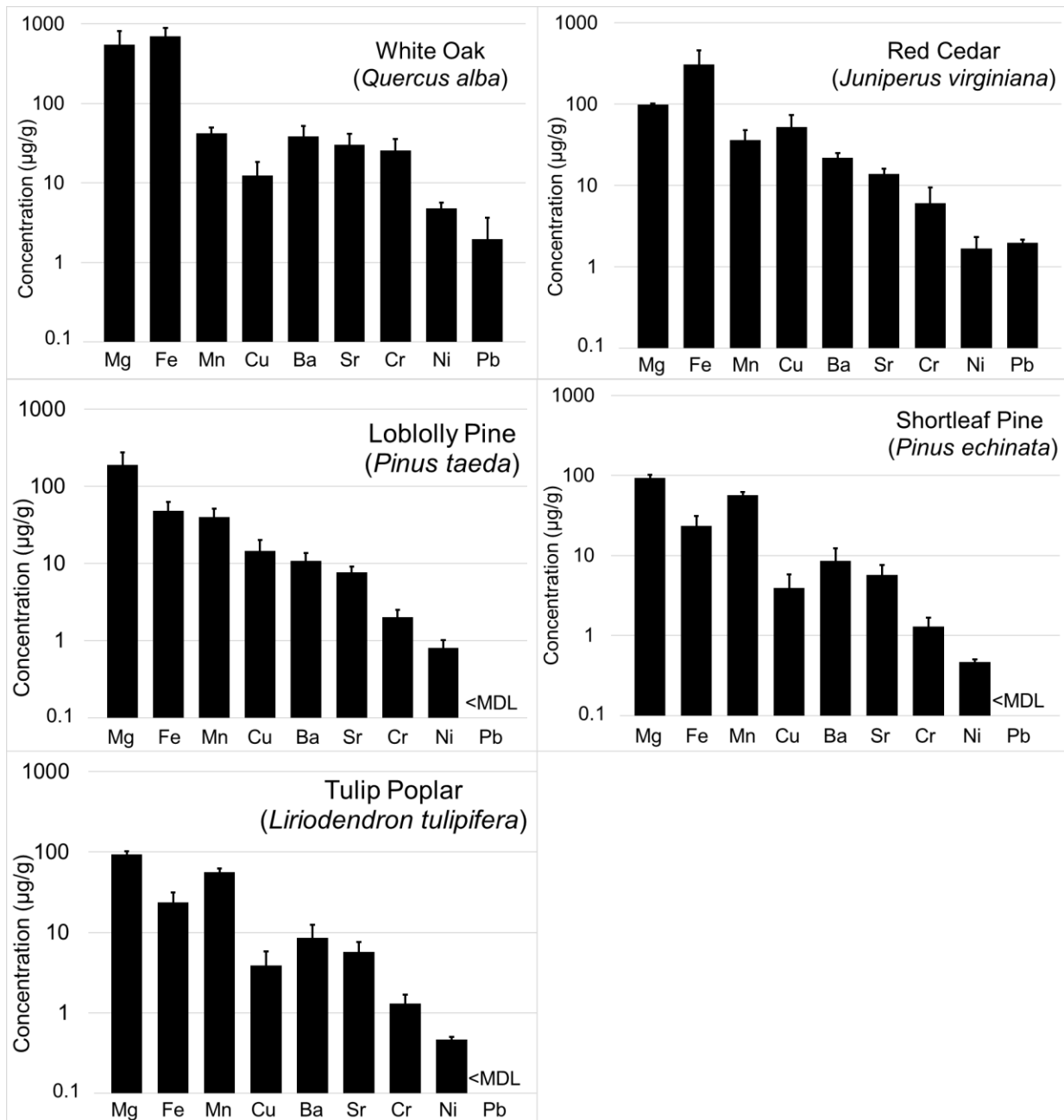


**Figure 19.** Mean concentrations of elements in bole wood tree rings from the Tallahatchie Experimental Forest in Holly Springs National Forest in north Mississippi determined by ICP-MS using ash from a direct mercury analyzer. Note: y-axis is on a logarithmic scale and error bars are  $\pm 1$  standard error.

**Table 9. Concentration of elements in tree cores from the Tallahatchie Experimental Forest in Holly Springs National Forest in north Mississippi determined by ICP-MS using ash from a direct mercury analyzer.**

Species:	<i>Quercus Alba</i>			<i>Juniperus Virginiana</i>			<i>Pinus Taeda</i>			<i>Pinus Echinata</i>			<i>Liriodendron Tulipifera</i>		
	Tree 1	Tree 2	Tree 3	Tree 1	Tree 2	Tree 3	Tree 1	Tree 2	Tree 3	Tree 1	Tree 2	Tree 3	Tree 1	Tree 2	Tree 3
Circumference (cm):	137	129	80	57	48	47	32	88	153	88	109	83	151	109	160
Ag (ng/g)	<MD	<MD	<MD	13.1	20.9	<MD	<MD	<MD	<MD	-	<MD	<MD	<MD	<MD	<MD
Ba (µg/g)	26.4	66.4	23.2	27.4	21.9	17.1	16.2	9.0	7.0	6.5	15.9	3.2	19.1	49.4	29.3
Be (ng/g)	<MD	41.3	<MD	<MD	<MD	<MD	<MD	<MD	<MD	<MD	<MD	<MD	<MD	<MD	<MD
Co (ng/g)	196	414	237	93.9	48.9	141	62.7	58.1	20.5	32.2	35.6	15.4	42.5	-	89.8
Cr (µg/g)	22.7	10.6	44.1	4.8	1.1	12.5	1.6	3.0	1.4	1.2	2.0	0.7	1.6	3.3	3.5
Cu (µg/g)	2.3	12.6	22.5	83.4	62.2	13.2	25.1	12.7	5.4	2.3	7.7	1.7	3.0	6.1	7.1
Fe (µg/g)	687	373	1041	321	33.8	567	48.7	72.1	24.1	20.3	38.0	12.3	22.4	76.7	71.1
Ga (ng/g)	36.0	22.7	19.8	37.2	37.4	43.3	42.9	<MD	<MD	<MD	<MD	0.3	0.1	1.6	2.5
Hg (ng/g)*	1.0	1.1	0.9	2.1	2.0	1.9	2.2	1.4	1.2	1.4	1.5	0.8	1.0	0.4	0.5
Trees 4 & 5:	1.9 (150 cm)	0.8 (77 cm)		2.4 (55 cm)	0.6 (52 cm)		-	-		-	-		0.3 (68 cm)	0.6 (77 cm)	
Mg (µg/g)	254	1079	321	95.9	104	98.2	359	122	86	105.6	74.2	98.2	122.4	319.8	179.3
Mn (µg/g)	55.1	42.1	29.4	18.0	59.6	30.7	53.0	49.7	17.6	45.3	59.7	64.4	37.8	74.7	71.6
Ni (µg/g)	3.3	6.3	4.9	1.9	0.43	2.7	0.71	1.2	0.5	0.5	0.5	0.4	0.7	5.0	1.2
Pb (µg/g)	0.48	5.3	0.17	0.53	0.07	0.67	<MD	<MD	<MD	<MD	<MD	<MD	<MD	<MD	<MD
Sr (µg/g)	52.6	20.4	17.9	18.1	11.1	12.6	10.4	6.7	6.0	5.7	8.9	2.6	44.6	18.2	29.6
Th (ng/g)	<MD	<MD	<MD	<MD	<MD	<MD	<MD	<MD	<MD	<MD	<MD	<MD	9.4	<MD	<MD
U (ng/g)	<MD	<MD	<MD	<MD	<MD	<MD	<MD	<MD	<MD	<MD	<MD	<MD	<MD	<MD	<MD

## **ACKNOWLEDGMENTS**

We are grateful to the US Forest Service personnel for support and guidance, especially Lorenzo Walton and James Schiller. Dr. Steve Brewer at the University of Mississippi Biology Department helped with identification of tree species.

## CHAPTER FOUR

### Historical deposition of trace metals in a marine sapropel from Mangrove Lake, Bermuda with emphasis on mercury, lead, and their isotopic composition



**Figure 20.** Early work on sapropel from Mangrove Lake, Bermuda (circa 1991). Al Mucci, Berni Boudreau, and Jens Gundersen deploying a microelectrode lander. Photo courtesy of B. Boudreau.

Jeon B., Scircle A., Cizdziel J., Chen J., Black O., Wallace D., Zhou Y., Lepak R., Hurley J., *J. Soils Sediments* **2020**, 20(4), 2266-2276. [doi.org/10.1007/s11368-020-02567-6](https://doi.org/10.1007/s11368-020-02567-6)

## ABSTRACT

Sapropel is an organic-rich sediment formed under conditions that can result in trace metal enrichment. We determined the concentration of total-mercury (Hg), lead (Pb), and 16 other metals (Al, Ba, Ca, Cd, Cr, Cs, Cu, Fe, Li, Mn, Ni, Sr, Tl, U, V, Zn) in a sapropel core from Mangrove Lake, Bermuda that dated back nearly two millennia. The purpose was to assess historical patterns of metal deposition on this geographically remote island in the North Atlantic Ocean. Two sediment cores were collected from Mangrove Lake using a modified piston corer. Cores were age-dated with a Bayesian statistical age-depth model using a multiproxy approach relying on  $^{210}\text{Pb}$  and radiocarbon dates. Total Hg was determined following US EPA Method 7473 using a direct mercury analyzer. Other metals were determined by sector field ICP-MS following a microwave-assisted strong-acid digestion. Stable isotope measurements of Hg and Pb were used to better track sources of these contaminants. Sapropel Hg concentrations were low ( $\sim 50 \text{ ng g}^{-1}$ ) from about 1000 AD to 1600 AD, followed by a slow rise in concentration until a high point of  $209 \text{ ng g}^{-1}$  in the early nineteenth century. Hg levels then returned to  $\sim 70 \text{ ng g}^{-1}$ , still elevated above baseline levels, before a final sharp rise in the mid-1900s to  $430 \text{ ng g}^{-1}$ . Pb, Zn, Cu, Cr, and Ba had similar patterns, with Pb isotope ratios showing early natural fluctuations followed by the greater influence of pollution sources. Mercury stable isotope data also show the influence of anthropogenic sources during the 1800s and suggest a mix of atmospheric, terrestrial, and possibly marine-derived Hg inputs to the lake. The vertical distribution of elements and isotopes reveals changes in deposition through time associated with pollution from industrialization, and, possibly, volcanic activity, seawater intrusion, intense hurricane events, and local pollution from ship and fortress building. Overall, this study demonstrates that organic-rich sapropel provides a good

historical record of metal contamination, and that Bermuda, despite its remote location, had metal deposition profiles much like the records of other sediment cores from around the world.

## INTRODUCTION

Mercury (Hg) and lead (Pb) are global threats to human and environmental health (Tchounwou et al. 2012). The heavy metal pollutants are emitted by both natural and anthropogenic sources, and are dispersed globally through the atmosphere over relatively short timescales ( $\leq 1$  year) (Gustin et al. 2015; Tchounwou et al. 2012). Since industrialization, metal concentrations have increased in terrestrial and aquatic ecosystems, and Hg, for example, has more than doubled in the atmosphere (Mason et al. 2012). In turn, Hg and Pb deposition rates have also increased over the last two centuries, as documented by lake sediment cores and other markers (Kang et al. 2016; Lindeberg et al. 2006; Yang et al. 2003). Other trace metal contaminants also accumulate and persist in sediments due in part to their particle reactivity (Park et al. 1997). Sediment organic matter, which can be found as surface coatings on inorganic materials or separate organic particles and debris, is another important parameter that affects the distribution of Hg, Pb and other trace elements in sediments (Sanei et al. 2006; Kainz et al. 2003). Pre-industrial concentrations of trace elements in sediments have been used as background concentrations in a number of studies (Engstrom et al. 1997; Yang et al. 2003).

Sapropels are organic carbon-rich sediments primarily composed of biogenic remains. They are generally formed when organic matter stemming from increased biological production, often associated with a high nutrient supply to the euphotic zone, is deposited and preserved under suboxic conditions (Stratford et al. 2000). The organic matter in sapropel is a significant sink for reduced sulfur species, such as sulfide and sulfur-containing amino acids that bind and retain Hg



species (Hartgers et al. 1997; Passier et al. 1999). Other trace metals emitted by anthropogenic sources, such as Pb, Cd, Ni, Cu and Zn, can also become enriched in sapropel, particularly during periods of high primary productivity (Birch et al. 1996; Gehrke et al. 2009; Angelidis et al. 2011). Thus sapropels can serve as sensitive archives for atmospheric pollution of anthropogenic metal contamination. However, investigations into the distribution of Hg, Pb and other trace heavy metals in well-dated marine sapropel cores are few. Gehrke et al. (2009) studied the geochemical behavior and isotopic composition of Hg in a mid-Pleistocene western Mediterranean sapropel, and Arnaboldi and Meyers (2007) examined trace element indicators of increased primary production during deposition of sapropels at five locations across the Mediterranean Sea.

Unlike the Mediterranean Sea which is close to many anthropogenic pollution sources, Bermuda is a geographically remote island located in the North Atlantic Ocean at 32°N and 62°W, over 900 km from the United States coastline. Remote islands, including Bermuda, have been used to study Hg fate and transport in the atmosphere and oceans (Gichuki et al. 2014). Recent estimates of Hg wet and dry deposition fluxes suggest that Bermuda is indeed impacted by anthropogenic sources, despite its remote location (Gichuki et al. 2014). Further, a mass balance for Hg across the air-sea interface around Bermuda indicates that the ocean is a net source to the region and likely reflects elevated deposition of Hg to the North Atlantic (Gichuki et al. 2014).

Presently, we determined Hg, Pb and other trace metals in two sapropel cores from Mangrove Lake, Bermuda. The lake occupies an inter-dune depression and contains sapropel sediments as deep as 14 m dating back about 10,000 years (Hatcher et al. 1982). We used sapropel cores previously collected for a paleotempestological study that assessed the frequency and magnitude of intense hurricanes over the past two millennia (Wallace et al. 2017). In the current study, we examined the vertical (temporal) distribution of Hg, other trace metals (Ba, Cd, Cr, Cs,

Cu, Li, Ni, Pb, U, Tl, V, Zn), and major elements (Fe, Al, Mn, Ca, Sr) in sapropel cores dating back two millennia. The purpose was to help reconstruct metal pollution history on Bermuda, where the atmosphere is likely the most important source of anthropogenic metal contaminants. Hg and Pb isotopic studies are also presented to further decipher possible sources of pollution of these heavy metals.

## MATERIAL AND METHODS

### Study Area

Mangrove Lake is located in Bermuda, a geographically remote island in the North Atlantic Ocean (Fig. 21). The lake is about 300 m × 400 m, has water depths of 2 m or less, and contains about 14 m of organic (sapropel) sediments (Hatcher et al. 1982). The lake itself exists in a depression situated between hills of Pleistocene-aged carbonate sands (Land et al. 1967), and the site been profoundly influenced by sea-level rise during the Holocene. Around 10,000 years before present (BP) sea level was lower than the base of the depression, and a freshwater reservoir formed where peats accumulated (Hatcher et al. 1982). As sea-level rose, so did the fresh water table, and eventually a marine invasion occurred ~4,000 yr BP which persists today (Hatcher et al. 1982). While Bermuda is the northern latitudinal limit for mangroves, the lake showed no evidence of mangroves (*Rhizophora mangle*) prior to ~3,000 yr BP (Watts et al. 1986, Ellison 1996). Canfield et al. (1998) investigated organic and inorganic carbon for the upper 60 cm of the lake sediment. The concentration of organic carbon in the lake sapropel is extremely high (~38 wt%), which is consistent with very low mineral content (10-15% of total dry weight) and further supported by elemental analysis (Canfield et al. 1998). Additionally, the sediments contain low inorganic carbon concentrations (<0.2 wt%) due to a lack of mineral sources to the lake (Canfield et al. 1998).

The only exception is some fine layers of coastal carbonate-rich sediment that are introduced during hurricanes; investigating these layers suggests that the frequency of intense hurricanes was significantly greater from about 1200 AD to 1800 AD (Wallace et al. 2017).

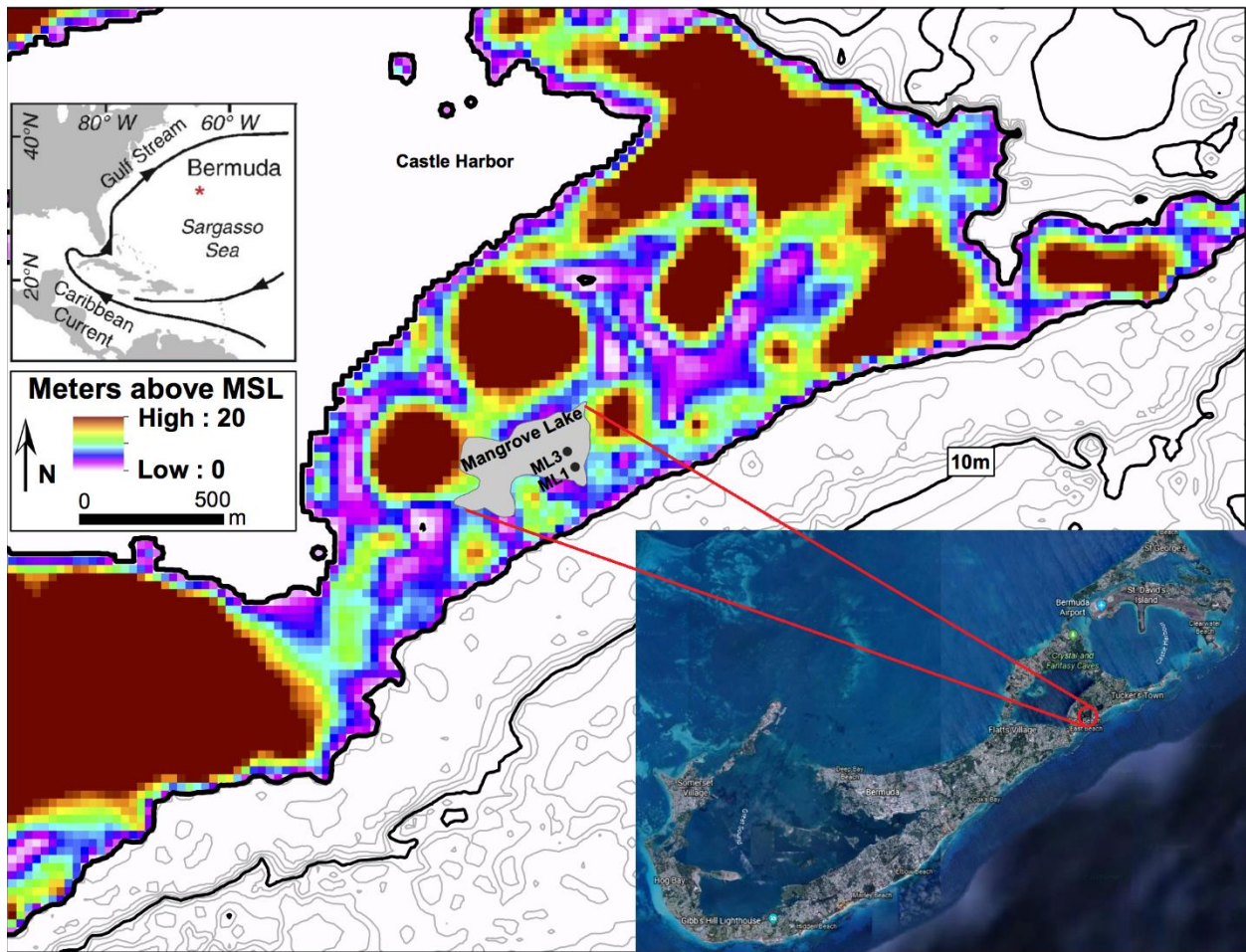


**Figure 21. Map showing the location of Bermuda in the Atlantic Ocean (left inset), ~25 km long-Bermuda Island (bottom right inset), the location of ~0.5 km-long Mangrove Lake on the Island, and the location of cores ML1 and ML3 within the lake. Bathymetric and elevation data are shown for the study area (data from NOAA, 2018)**

## Geochemistry in Mangrove Lake

Mangrove Lake has been the site of several geochemical studies (Hatcher et al., 1982; Orem et al. 1986; Knicker et al. 1996; Knicker and Hatcher 2001; Boudreau et al. 1992; Canfield et al. 1998). Organic geochemistry and pore water geochemistry of the sapropel, including measurements of sulfides, ammonia, methane, nitrogen gas, Ca, Mg, chloride, alkalinity, and pH were reported as far back as 1982 (Hatcher et al. 1982; Orem et al. 1986).  $^{13}\text{C}$  and  $^{15}\text{N}$  nuclear magnetic resonance was performed on the sapropel to examine nitrogen algal remains and investigate pathways of diagenesis (Knicker et al. 1996; Knicker and Hatcher 2001). Diagenetic processes have also been studied using a suite of indicator species, including  $\text{SO}_4^{2-}$ ,  $\text{H}_2\text{S}$ ,  $\text{CO}_2$ ,  $\text{NH}_4$ ,  $\text{PO}_4$ ,  $\text{Fe}^{2+}$ ,  $\text{Mn}^{2+}$  and sulfur addition to organic matter (Boudreau et al. 1992; Canfield et al. 1998). Briefly, the lake has normal seawater salinity (30-35 psu) and appears to be connected to the ocean by subsurface fissures on the south side of the lake; however, the tidal range is minimal (< 2 cm) indicating a strongly dampened system (Boudreau et al. 1992). The lake has relatively little freshwater input mainly from precipitation, as there is only limited groundwater input (Orem et al. 1986). The sapropel is primarily composed of dead plankton, with some shell detritus, chitin of insects and mangrove debris (Orem et al. 1986). It also has low mineral content with the  $\text{H}_2\text{S}$ -rich pore waters reflecting reducing conditions associated with decomposition of organic matter (Boudreau et al. 1992). Additional details of sediment pore water chemistry and chemical gradients developed from anoxic diagenesis are reported elsewhere (Hatcher et al. 1982; Orem et al. 1986; Canfield et al. 1998).

## **Coring method and sub-sampling**

Sediment cores were collected in Mangrove Lake using a modified Vohnout-Colinvaux piston corer (Woodruff et al. 2009, 2015). Cores ML1 and ML3 are about 85 meters and 150 meters from the edge of the lake, respectively (Fig. 21). Following collection, the cores were shipped to the University of Southern Mississippi and stored at 4°C. Cores were split vertically and investigated for a paleohurricane reconstruction study (Wallace et al. 2017). For the present study, sub-samples were removed from the cores and shipped to the University of Mississippi for trace metal analysis by ICPMS. For the ML1 core, we analyzed 70 samples consisting of 1-cm intervals collected for every 5 cm of depth starting near the surface and moving down core to a depth of 350 cm. For the ML3 core, we analyzed 21 samples collected every ~15 cm of depth.

## **Age dating of sediments**

Due to the proximity of ML1 and ML3, we used dates between cores interchangeably to construct a composite age/depth model. A gastropod in ML3 at 317.5 cm produced an age of  $2440 \pm 20$   $^{14}\text{C}$  yrs (Accession # OS-120885, conventional age), and a gastropod in ML1 at 214.5 cm produced an age of  $1730 \pm 100$   $^{14}\text{C}$  yrs (Wallace et al. 2014; Accession # OS-112048, gas bench age). Both ages were calibrated using Marine13 (Reimer et al. 2013) using a  $\Delta\text{R}$  of 375 (Wallace et al. 2017).  $^{210}\text{Pb}$  was previously performed on core ML1 (Wallace et al., 2017), and here we extract one age of ~65 years ago occurring at 54 cm using the constant rate of sedimentation model (Appleby 1998). A composite Bayesian statistical age-depth model (Blaauw et al. 2011, 2013) was produced relying on these  $^{210}\text{Pb}$  and radiocarbon dates. The resultant mean age-depth relationship was further supported by previously established chronology for Mangrove Lake (Hatcher et al. 1982; Watts et al. 1986). The maximum age uncertainties using this approach are  $\pm 350$  years (2

sigma). However, the majority of the age uncertainties are  $\pm 200$  years (2 sigma), with the lowest uncertainties in the upper meter of the core (last few centuries). Given the sampling interval and strategy presented in this study, the age dating is appropriate.

### **Sample drying**

Each sapropel sample was dried by lyophilization for 48 hours. Freeze-drying has been shown to preserve metal species in sediment and soils, and it improves homogeneity and reproducibility compared with analyses of fresh (wet-weight) samples (Muhaya et al. 1998; Hojdova et al. 2015). The moisture content averaged  $87\% \pm 3\%$  (1 SD, n=69).

### **Determination of mercury and loss-on-ignition**

Total-Hg was determined following US EPA Method 7473 using a direct mercury analyzer (DMA-80; Milestone Inc., Shelton, CT, USA). The method is based on thermal decomposition, amalgamation, and AAS, and has been used in multiple studies measuring Hg in aquatic sediments (Cizdziel et al. 2005; Chen et al. 2015; Rezende et al. 2018). Here, ~100 mg aliquots of dried sapropel were analyzed in nickel boats. Operating times for drying, combustion, and post-combustion flushing periods were 30, 180, and 45 s, respectively. The instrument was calibrated using a series of standard Hg solutions prepared from a stock Hg standard solution from Spex Certiprep. For quality control, a calibration check, duplicate, and blank were run about every 10 samples. Recoveries for MESS-3, marine sediment reference material (NRC Canada) were within 15% of the certified value. Relative percent difference for duplicates were also <15%. Blanks were negligible, yielding <0.10 ng of Hg. The limit of detection (3 sigma criteria) was estimated at ~0.02

ng, corresponding to  $0.2 \text{ ng g}^{-1}$  for a 100 mg sample. Concentrations are reported on a dry-weight basis.

A decomposition temperature ( $550^\circ\text{C}$ ) was chosen to match that of the conventional weight loss-on-ignition (LOI) method. LOI involves weighing the sample before and after an ashing treatment and has been used to estimate organic matter in soils and sediments (Bregy et al. 2018, De Vos et al. 2005, Heiri et al. 2001). We have previously shown that the DMA can be used in this manner to obtain reliable LOI data (Chen et al. 2015).

### **Determination of Trace Metals and Pb Isotopes**

Samples weighing 0.1 to 0.2 g were leached in acid-washed Teflon PFA vessels with 1 ml of HCl (optima grade, Fisher Chemical), 3 ml of  $\text{HNO}_3$  (trace metal grade, Fisher Chemical) and 6 ml of  $18.2 \text{ M}\Omega$  deionized water using a Milestone Ethos microwave digestion system. The microwave was operated at 1200 W and the temperature program consisted of a 30 min ramp to  $120^\circ\text{C}$ , followed by a 60 min ramp to  $180^\circ\text{C}$ , after which the temperature was held for an additional 20 min. This strong-acid digestion liberates metals that are “environmentally accessible” from organic matter, sulfides, and certain silicate minerals, but some quartz, feldspar and clay minerals may remain as insoluble residue (Gehrke et al. 2009). As the sapropel was mostly organic matter, there was very little residue after digestion. The resulting digests were diluted to 50 mL with  $18.2 \text{ M}\Omega$  deionized water. Before analysis each sample and standard was spiked with an internal standard solution yielding a solution containing  $\sim 1 \text{ ng g}^{-1}$  Rh in 2%  $\text{HNO}_3$ .

Concentrations of 17 metals (Al, Ba, Ca, Cd, Cr, Cs, Cu, Fe, Li, Mn, Ni, Pb, Sr, U, Tl, V, and Zn) were determined by sector field inductively coupled plasma mass spectrometry (SF-ICP-MS) using a Thermo Fisher Element-XR. The instrument features resolving power ( $m/\Delta m$ )

settings of low (~300), medium (~3000), and high (~10,000) to remove certain isobaric interferences. Samples were introduced using a glass concentric nebulizer with a cyclonic spray chamber. Data acquisition parameters are given in Table 10. The instrument was tuned prior to analysis for sensitivity and stability, yielding ~1 million counts-per-second for 1 ppb of <sup>115</sup>In in low resolution mode with <4% relative standard deviation (RSD). External calibration was used to quantify the elements. Mean recoveries for PACS-3 Marine Sediment Reference Material (NRC Canada) were within ±25% of certified or reference values, except for Ca and Sr, which were within ±40%. Precision of replicate samples were <15% relative percent difference.

### **Mercury Isotopic Composition Analysis**

Mercury isotopic analyses were carried out using methods described previously (Janssen et al. 2019). Briefly, samples and reference material (IAEA SL1 marine sediment) were digested in aqua regia and pre-concentrated with Hg reduction and gold trap amalgamation followed by thermal desorption and chemical trapping. The final solution was analyzed for precise Hg isotope ratios using a Neptune Plus MC-ICP-MS housed at the University of Wisconsin-Madison's State Laboratory of Hygiene. NIST 3133 was used as a bracketing reference and UM Almaden (NIST RM 8610) was used as a secondary standard.

Delta calculations followed the conventions set forth by others (Blum et al. 2007). Briefly, mass dependent fractionation (MDF) is expressed in  $\delta^{xxx}\text{Hg}$ , where  $\delta^{202}\text{Hg}$  is used to graphically signify MDF (Eq. (1)). The  $\delta$  notation is in units of permil (‰), referenced to the NIST-3133 Hg standard (analyzed before and after each sample):

$$\delta = \text{Hg}(\text{‰}) \left[ \left( \frac{^{xxx}\text{Hg}/^{198}\text{Hg}_{\text{sample}}}{^{xxx}\text{Hg}/^{198}\text{Hg}_{\text{NIST 3133}}} \right) - 1 \right] \times 1000 \quad (1)$$



Mass independent fractionation (MIF) is reported in  $\Delta$  notation ( $\Delta^{xxx}\text{Hg}$ ) and describes the deviation from mass dependency in ‰ (Eq. (2)). MIF is the difference between the measured  $\delta^{xxx}\text{Hg}$  and the theoretically predicted  $\delta^{xxx}\text{Hg}$  value using the following formula:

$$\Delta^{xxx}\text{Hg} \approx \delta^{xxx}\text{Hg} - (\delta^{202}\text{Hg} \times \beta) \quad (2)$$

Where,  $\beta$  is the independent isotope-specific scaling factor. Odd-MIF is described by  $\Delta^{199}\text{Hg}$  and even-MIF by  $\Delta^{200}\text{Hg}$ .

Data uncertainty reported in this study reflects the larger value of either the external precision of replication of UM-Almaden or the measurement uncertainty of standard reference materials. The mean value and uncertainty of 16 UM-Almadén measurements ( $\delta^{202}\text{Hg}$ :  $-0.56 \pm 0.03\text{‰}$ ;  $\Delta^{199}\text{Hg}$ :  $-0.01 \pm 0.03\text{‰}$ ;  $\Delta^{200}\text{Hg}$ :  $0.00 \pm 0.02\text{‰}$ ) as well as the IAEA SL1 reference sediment ( $\delta^{202}\text{Hg}$ :  $-1.25 \pm 0.04\text{‰}$ ;  $\Delta^{199}\text{Hg}$ :  $-0.10 \pm 0.05\text{‰}$ ;  $\Delta^{200}\text{Hg}$ :  $0.05 \pm 0.02\text{‰}$ ) were acceptable and comparable with previous studies (Biswas et al. 2008; Yin et al. 2016; Janssen et al. 2019).

## RESULTS AND DISCUSSION

### Mercury Profiles

Both sapropel cores featured a sharp rise in Hg in the upper-most layers (Fig. 22). The higher concentrations of Hg in the recent sediment layers are consistent with reports that both airborne Hg concentrations and Hg deposition rates have increased post-industrialization, starting about the mid-19th century (Mason et al. 2012). The mean concentration in the top ~40 cm of the ML1 core corresponding to this period was  $317 \text{ ng g}^{-1}$ , with a high of  $420 \text{ ng g}^{-1}$  (Fig. 22). The Hg profile of ML3 was generally similar, with a mean of  $244 \text{ ng g}^{-1}$  and a high of  $271 \text{ ng g}^{-1}$  in the uppermost layers, but had a slightly lower and more consistent background of  $<50 \text{ ng g}^{-1}$  during the pre-industrial period. Here, we focus on the high resolution ML1 core data because it has

substantially more data points (70 vs. 21 for ML3) and for clarity in the data plots. ML1 also showed some additional features in down core elemental profiles, including a spike in concentration to  $\sim 209 \text{ ng g}^{-1}$  in the early 19th century possibly coinciding with ship and fortress building on the island. The British first colonized the island around 1580 AD. This increase in concentration around 1800 AD was also present for other heavy metals (Figs. 23 and 24), further described below. After the spike in Hg in the early 1800's, the ML1 core averaged  $65 \text{ ng g}^{-1}$  for the remaining 1800's, still elevated above background. Moving downward in the core to before the 1800's, Hg concentration trended lower to  $<50 \text{ ng g}^{-1}$  around 1400 AD. Further down the ML1 core the Hg concentration slowly rose again to a mean of  $148 \text{ ng g}^{-1}$  near the bottom of the core. It should be noted that ML1 core was in closer proximity to the lake shore and ocean front than ML3. To help interpret these trends we measured LOI as a proxy for organic matter and determined the concentration profiles of other trace metals in the sediment core. Because both Hg and other trace metals show similar increases in concentrations in the lowest portion of the ML1 core, despite being measured by independent analytical techniques (DMA and ICP-MS), it suggests the trend is real and not an artifact of the analyses. Rather, variations in the down core elemental concentration profiles may be related to changes in the geochemical environment, seawater intrusion, and climate (prevalence and intensity of hurricanes).

### **Concentration relationships among Hg, LOI (organic matter), and trace metals**

The geochemical behavior of Hg, organic matter, and trace elements in a sapropel is detailed elsewhere (Gehrke et al. 2009). Briefly, sapropels become enriched in trace metals in part because they form under reducing conditions which also results in the accumulation of trace metals in sediments (Gehrke et al. 2009). The trace metals measured in this study include both

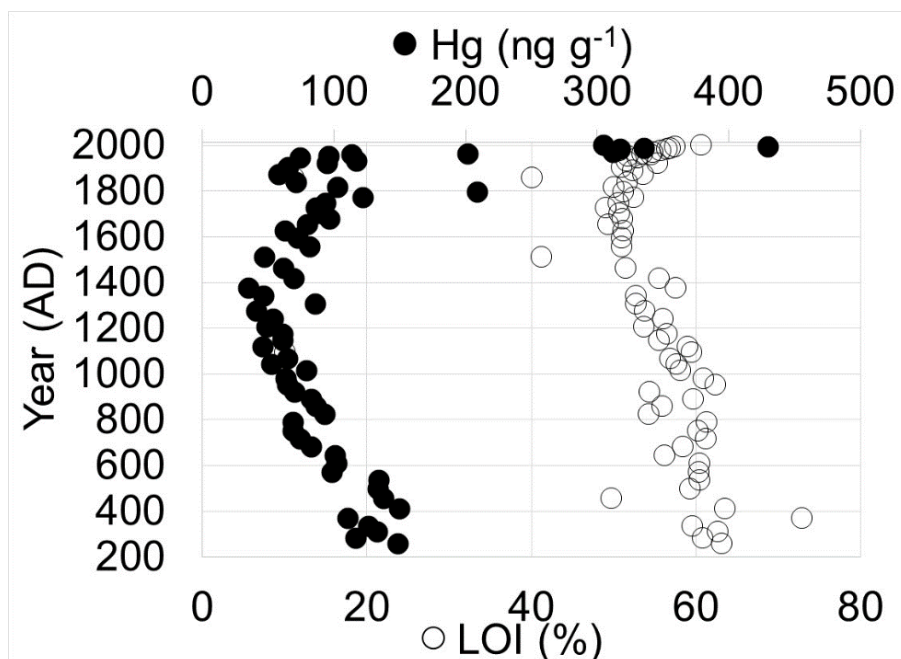


**Figure 22. Mercury distribution in Mangrove Lake sapropel by deposition year, and corresponding weight loss-on-ignition (LOI) data**

productivity sensitive elements (Ni, Cu, Zn, Ba, Cd, and Pb) that are incorporated into plankton at the base of the food chain or into humic and fulvic acids of abiotic organic matter, and redox sensitive elements (V, Cr, U) that tend to precipitate and/or adsorb onto mineral surfaces under reducing conditions (McManus et al. 2005, Boning et al. 2004, Gehrke et al. 2009). As noted earlier, organic matter in sapropel is a significant sink for reduced sulfur species, such as sulfur-containing amino acids that bind and retain many trace elements and Hg species in particular (Hartgers et al. 1997, Passier et al. 1999). Thus, organic matter is an important parameter that can control the distribution of Hg and other trace elements in sediments by affecting physical and chemical processes (Sanei et al. 2006).

Mangrove Lake sediment is primarily composed of phytoplankton (algae) with small amounts of mangrove debris (Orem et al. 1986). It also has low mineral content, generally lacking

solid Fe and Mn minerals. Molecular diffusion dominates solute transport in the sediment below the surficial mixing zone, with the H<sub>2</sub>S-rich pore waters reflecting anoxic conditions associated with decomposition of organic matter (Boudreau et al. 1992). More recently, application of fertilizers to the surrounding golf course may be contributing to continued eutrophication in the lake.

LOI (organic matter) generally increased in the lower half of the ML1 core (between ~1250 AD and the bottom of the core) from ~52% to ~62%. Intense hurricane activity appears to be relatively low in Bermuda during this time interval (Wallace et al. 2017), and thus inorganic sediment delivery was likely low thereby concentrating organic sediment accumulation. Hg concentrations positively correlate with LOI during this period ( $r=0.51$ ;  $p=0.002$ ). Thus, the trend of increasing Hg in the lower portion of the ML1 core may be partly explained by variations in organic matter down core. However, because the ML3 core also shows an increase in LOI with depth toward the bottom of the core but no corresponding increase in Hg, another factor may be at play.

The chronology of other trace metals (Pb, Cu, Zn, Ni, V, Ba, Cr, Cd, and U) in the sediment cores is shown in Figures 23 and 24. The general pattern consisted of three trends: enrichment in the upper third of the core corresponding to a period with increased anthropogenic sources; low levels in the middle portion from around 1000 AD to 1600 AD; and a slow rise in concentration moving to the bottom of the core. Concentrations in the deeper portions of the core are likely more tied to the geochemical environment than the source (emissions) (Like Gehrke et al. 2009). we found that several productivity-sensitive trace metals (Hg, Ni, Cu and Zn) produced similar depth profiles suggesting similar post-depositional behavior to pore water geochemistry. Hg had strong to moderate positive correlations with Zn ( $r^2=0.87$ ), Cu ( $r^2=0.81$ ), Ba ( $r^2=0.71$ ), Pb ( $r^2=0.51$ ), and

U ( $r^2=0.51$ ) in the upper third of the core; Zn ( $r^2=0.71$ ), Ba ( $r^2=0.61$ ), Cr ( $r^2=0.60$ ), Pb ( $r^2=0.56$ ), U ( $r^2=0.48$ ), and Ni ( $r^2=0.45$ ) in the middle of the core; and Zn ( $r^2=0.83$ ), Cu ( $r^2=0.81$ ), and Pb ( $r^2=0.50$ ) in the lower portion of the core. There were poor correlations for Hg with Li and major elements (Al, Fe, Mn, Ca, and Sr). The correlations for these productivity and redox sensitive metals and their lack of correlation with major elements suggest that their presence mainly resulted from high primary productivity and reducing conditions in the water column and sediment.

All the trace metals, except U, were particularly elevated in the first ~40-cm of core, reflecting deposition after ~1950 AD. Several (Cu, Zn, Pb, V, Cr, and Cd) followed the same depth profile as Hg (Figs. 22 and 23), including a spike at ~100-cm (~1800 AD). Moving down core, another possibility for the unusual trend of increasing concentration in the lower third of the core is that the proportion of source water (runoff vs. seawater intrusion) may have changed over time. Indeed, there appears to be a relatively abrupt change in the vertical profiles of some trace metals and major elements (Li, Cs, Cr, Ba, Al, Fe, Mn) at around 1150 AD (Figs. 23 and 24). A fracture (Thomas et al. 1991) may have formed in the surrounding limestone during this period which may have allowed a greater intrusion of seawater than it does today. Isotopic analysis of organic carbon might support or dispel this hypothesis but is beyond the scope of this present work.

Another factor influencing sedimentation in Mangrove Lake is climate. Hurricanes can alter sediment deposition in the lake by introducing material from marine and coastal sources as the storm overwashes in debris and in some cases as ocean water overtops the berm separating the lake and ocean (Fig. 21). Wallace et al. (2017) measured relatively high concentrations of Ca and Sr in these fine (mm-sized) layers by micro-XRF (X-Ray Fluorescence) of the intact core. These data suggest stratigraphically that the frequency of intense hurricanes was high from ~1200 AD to ~1800 AD. Despite using relatively large (1-cm) intervals in the present study, we also observe

more frequent and greater intensity fluctuations in Ca and Sr concentrations after ~1200 AD. Moreover, some of the spikes in Ca and Sr overlap similar spikes in Ca and Sr measured in the earlier study.

### **Enrichment Factors and Degree of Trace Metal Pollution**

Two common approaches to estimating anthropogenic impact on sediments is to calculate either a normalized enrichment factor (EF) or a geoaccumulation index ( $I_{geo}$ ) for metal concentrations above background or baseline concentrations (Müller 1969, Dickinson et al. 1996; Abraham et al. 2008). The EF method normalizes the metal content to Al since it is considered to act as a “proxy” for terrestrial inputs, particularly clay (Abraham et al. 2008). The EF is calculated using Eq. (3):

$$EF = M_x \times Al_b / M_b \times Fe_x \quad (3)$$

Where,  $M_x$  and  $Al_x$  are the sediment sample concentrations of the metal and Al, while  $M_b$  and  $Al_b$  are the concentrations of the pre-industrial baseline concentration.  $I_{geo}$  was also calculated because it minimizes the effect of possible variations in the background values attributed to lithologic variations in the sediments, which are substantial in the upper half of our core.  $I_{geo}$  is calculated using Eq. (4):

$$I_{geo} = \log_2(C_n/1.5/B_n) \quad (4)$$

Where,  $C_n$  is the concentration of the metal in the sample, and  $B_n$  is the pre-industrial background concentration.  $I_{geo}$  assesses the degree of metal pollution with: 0 designated as uncontaminated; 0-1 as uncontaminated to moderately contaminated (enriched); 1-2 moderately enriched; 2-3 as moderately enriched to strongly enriched; and 3-4 strongly enriched.

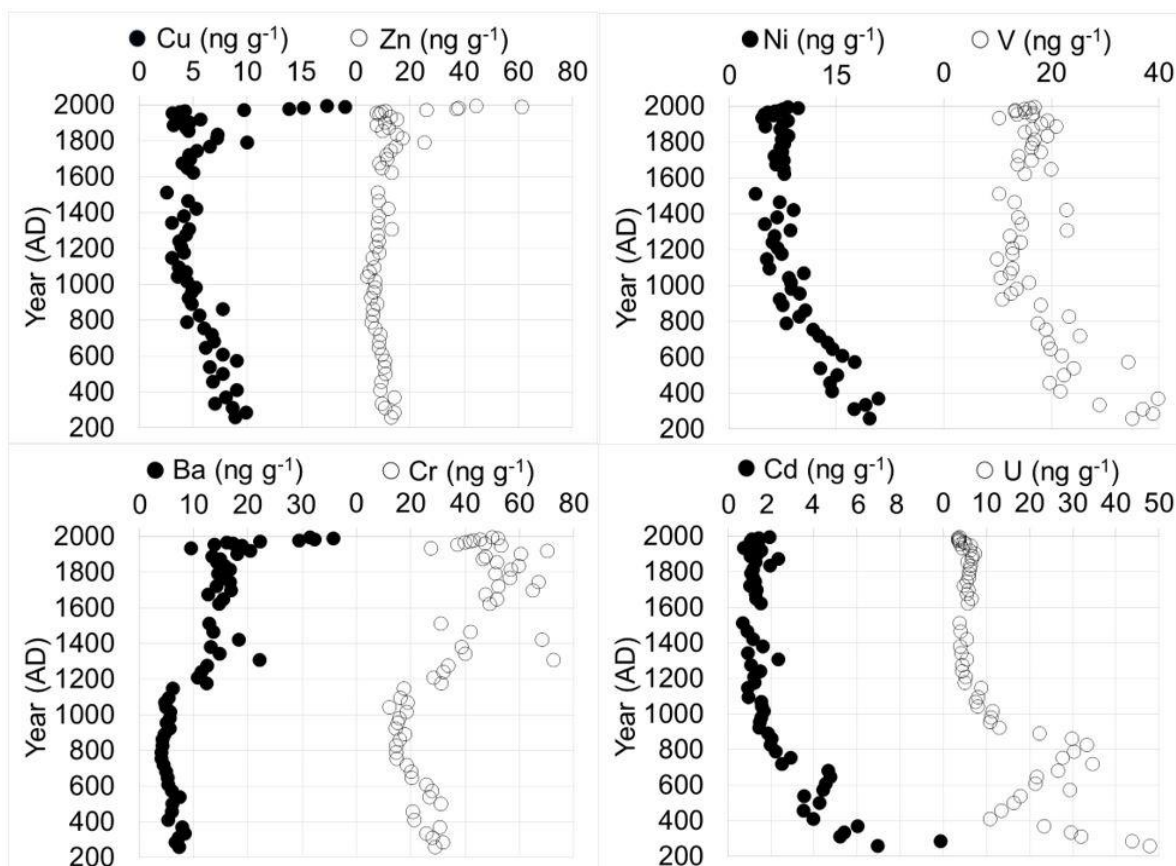


**Figure 23. Down core profiles for productivity and redox sensitive trace elements (Cu, Zn, Ni, V, Ba, Cr, Cd, U) in Mangrove Lake sediments through time**

For background we averaged the concentrations for low concentration samples in the flat baseline area of the core, generally 10 samples between 200 cm and 250 cm (~750 and ~1150 AD).

Enrichment factors and  $I_{\text{geo}}$  values for Hg, Pb, Zn, Cu, Cr, and Ba are given in Table 11. Given some uncertainty of the cause of the general rise in concentration in the lower portion of the ML1 core, and because we are using the index to evaluate the influence of anthropogenic (pollution) sources, we only report values for the upper half of the core from ~1200 AD to present. Ni, V, U, and Cd had EF and  $I_{\text{geo}}$  values that were  $<1$  throughout the core.

For the other metals, maximum EFs ranged between 1.6 and 20.9, all of which occurred in

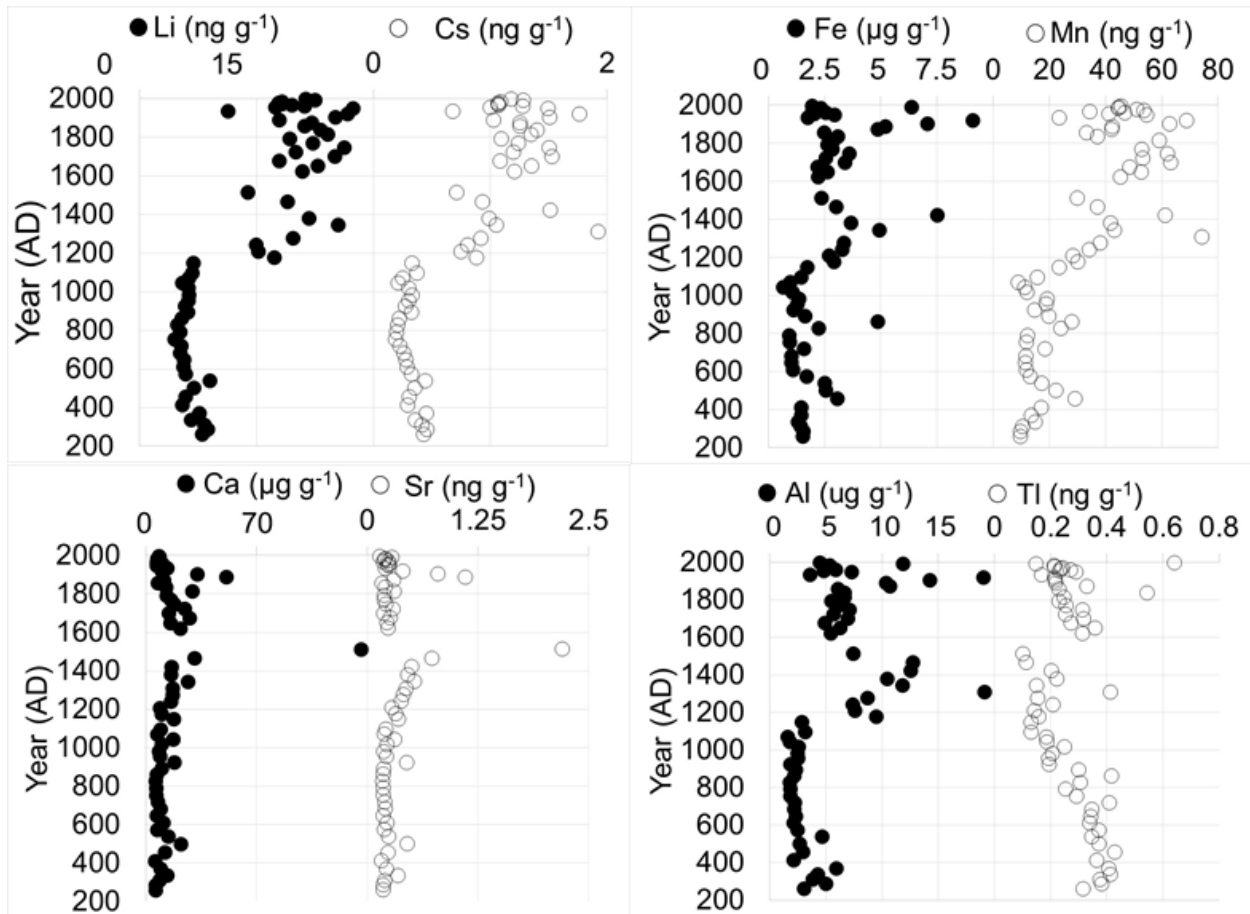


**Figure 24. Down core profiles of Al, Fe, Mn, Ca, Sr, Li, Cs, and Tl in Mangrove Lake sediments through time**

the top layers of the sediment corresponding to the 2nd half of the 20th century. Maximum EFs for Hg and Pb were 3.7 and 20.9, respectively. Similarly,  $I_{geo}$  values peaked in the upper layers, with values of 2.4 for Hg (moderately to strongly enriched) and 5.1 for Pb (extremely enriched). There was also a modest rise in both EFs and the  $I_{geo}$  to values  $>1$  between 1790's and 1850's. It should be noted that a re-evaluation of lake-sediment archives suggests that Hg emissions from pre-industrial gold and silver extraction in the Americas were indeed modest as compared to more recent industrial-era emissions (Engstrom et al. 2014). Overall, these values show that deposition



of metals in sapropel on this geographically remote island varied over time much like other sediment records around the world.

### **Pb isotope ratios**

Profiles of Pb concentration and the  $^{206}\text{Pb}/^{207}\text{Pb}$  isotope ratio is shown in figure 3. The strong-acid leach used should solubilize Pb from both anthropogenic and mineral sources. Prior to ~1100 AD, the concentrations of Pb are low, with variations between  $0.5 \text{ ng g}^{-1}$  and  $\sim 2.5 \text{ ng g}^{-1}$ . During the same period the  $^{206}\text{Pb}/^{207}\text{Pb}$  concentrations varied from about 1.20 to 1.21, representing early natural fluctuations in the influx of material to the lake. The low  $^{206}\text{Pb}/^{207}\text{Pb}$  ratios ( $<1.20$ ) in the upper half of the core from about 1600 AD to present day reflect an increasing proportion of anthropogenic Pb deposited along with the natural geogenic (mineral) Pb. From about the 1600's, total-Pb concentrations rise and there is a spike in the  $^{206}\text{Pb}/^{207}\text{Pb}$  ratio at a depth of ~120 cm (early to mid-1800's), both of which may correspond to increasing Pb ore smelting in the upper Mississippi Valley of the U.S. Others have shown a similar signal with a marked peak in the  $^{206}\text{Pb}/^{207}\text{Pb}$  ratio at about 1840 albeit in Coastal New England, which is in closer proximity to the source, and in a more high-resolution sediment record (Fitzgerald et al. 2018). The authors point out that after about 1840, coal combustion overtook lead-ore smelting as the dominant source of atmospheric Pb, lowering  $^{206}\text{Pb}/^{207}\text{Pb}$  ratios and increasing Pb concentrations further. In the present study, the concentration of Pb is highest in the top ~40 cm (~1950's to ~1990's) reaching a maximum of  $27 \text{ ng g}^{-1}$ . The deposition of Pb from gasoline is the most likely source of Pb in the upper-most layers; sediment isotope ratios on a Pb isotope ratio mixing plot fall closest to European gasoline (Fig. 26), not surprising for this British Dependent Territory.

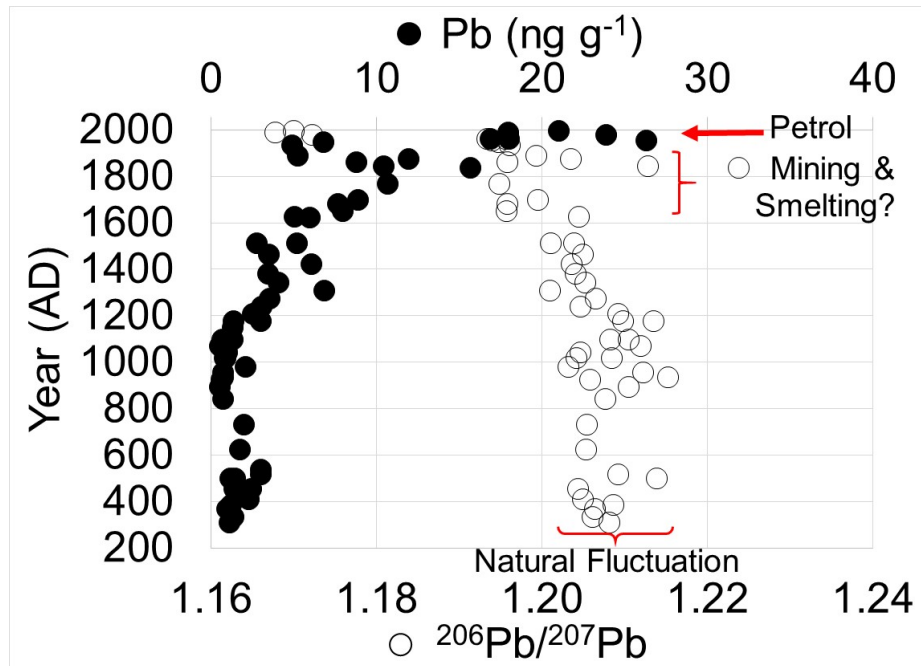


Figure 25. Pb concentration and  $^{206}\text{Pb}/^{207}\text{Pb}$  ratios of Mangrove Lake sediments by deposition year

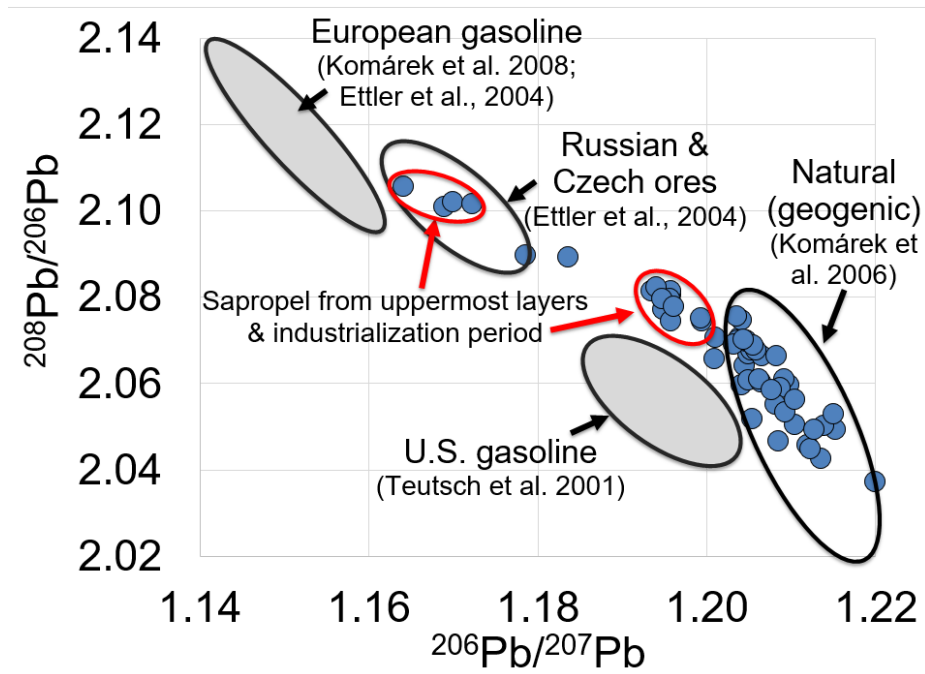


Figure 16. A three-isotope plot showing the isotopic composition of Pb in Mangrove Lake sediments (blue dots) along with different Pb sources

## Sediment Hg Isotopic Composition

Although only eight samples were analyzed for Hg isotopic composition, they are the first such measurements for sapropel from an Island in the North Atlantic, and together with other trace elemental data, help decipher Hg sources and geochemical processes at the site (Table 11; Fig. 27). For pre-1800's samples, the mean  $\delta^{202}\text{Hg}$  value was  $-1.85 \pm 0.17\text{‰}$  ( $n=5$ , 1 SD), representing background Hg. The two samples deposited in the 1800's had relatively high  $\delta^{202}\text{Hg}$  values ( $-0.64 \pm 0.03\text{‰}$  and  $-1.17 \pm 0.05\text{‰}$ ), more representative of industrial-sourced Hg (Blum et al. 2014; Lepak et al. 2015). The most recently deposited sample (~1984) had a  $\delta^{202}\text{Hg}$  value of  $-1.95 \pm 0.02\text{‰}$ . Compared to the Mediterranean sapropel, our down core  $\delta^{202}\text{Hg}$  values are somewhat more negative ( $-1.85 \pm 0.17\text{‰}$  vs.  $-0.91\text{‰} \pm 0.15\text{‰}$ ) (Gehrke et al. 2009); however, there is little in common between these sites, including when the sediments were deposited, sources of Hg (possibly including historic mining activities in Spain and Slovenia at the Mediterranean site), and the concentration of organic carbon (~38% Bermuda sapropel vs. <5% Mediterranean sapropel). Our deep core (background) values better overlap the background values reported by Liu et al. (2011) for sediments from the Pearl River Estuary.

The MIF  $\Delta^{199}\text{Hg}$  positive values during the 1800's ( $0.03 \pm 0.02\text{‰}$  and  $0.14 \pm 0.01\text{‰}$ ) reflect Hg from industrial sources.  $\Delta^{199}\text{Hg}$  values in the lower portions of the core are slightly negative ( $-0.06$  to  $-0.21$ ), suggesting a mix of terrestrial- and atmospherically-delivered Hg. The correlation between  $\Delta^{199}\text{Hg}$  and  $\Delta^{201}\text{Hg}$  ( $r^2 = 0.962$ ) had a slope of 0.926 (not shown), indicating that a portion of the Hg in the sediment could have undergone photo-reduction prior to or during deposition (Liu et al. 2011, Blum et al. 2014). However, photochemical reduction inherently creates positive odd-MIF, yet we observe mostly negative values suggesting that source Hg is even more negative in odd-MIF. These data, together with the relatively low  $\delta^{202}$  values, suggest that

the Hg isotope signature may also be tied to local and regional processes, such as marine scavenging of Hg via sea spray. Odd Hg isotope anomalies have also been linked to photoreduction in droplets (Chen et al. 2012). However, examining the impact of such processes on the isotopic composition of Hg at the site is beyond the scope of this work.

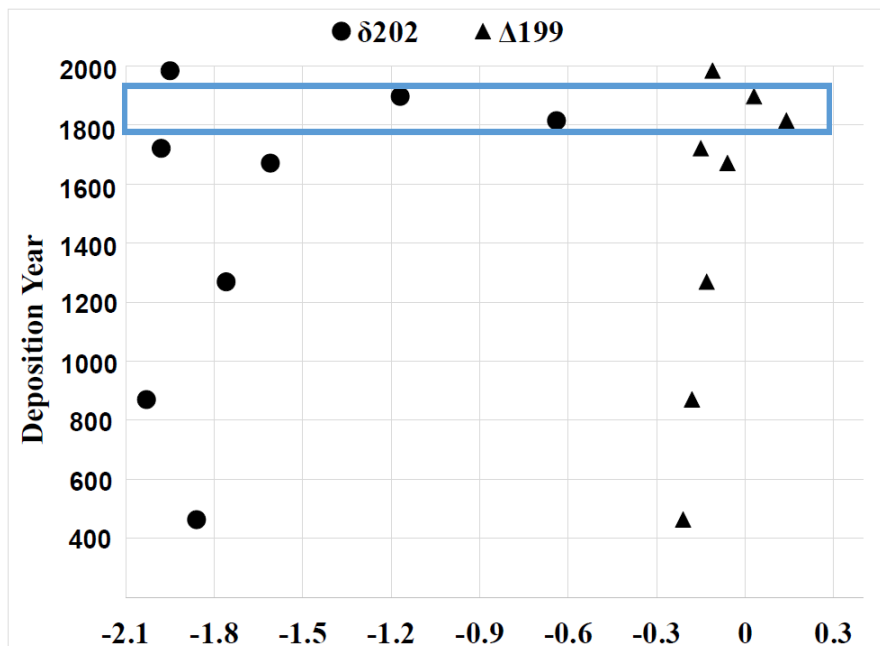


**Figure 27. Variation (‰) in mass dependent ( $\delta^{202}\text{Hg}$ ) and mass independent ( $\Delta^{199}\text{Hg}$ ) stable isotope compositions in sapropel cores from Mangrove Lake, Bermuda. The blue box indicates significant anthropogenic inputs of Hg during the 19th century**

## Conclusions

Sapropel sediment cores provide a unique organic-rich matrix to study the spatial-temporal history of metal pollution. Concentration profiles of Hg, Pb, and other trace metals (Zn, Cu, Cr, Ba) in age-dated Bermuda sapropel cores indicate significant enrichment in the upper-layers compared to the down core pre-anthropogenic background. Variations in down core trace metal concentrations suggest changing conditions and/or metal inputs to the lake. Pb isotope ratios indicate gasoline as a relatively recent and major source of Pb to the sediment. Mercury had moderate to strong correlations with productivity-sensitive trace metals (Zn, Cu, Ba, Pb) and poor correlations with major elements. Elevated levels of Hg and changes in isotopic composition suggest that Hg of industrial origin was deposited to the lake starting in the 1800's. Overall, this study shows that sapropel can be used to trace metal pollution history and that long-range airborne transport as well as historical activities on the island likely contributed to metal contamination in the lake sediment.

**Table 10. ICP-MS Instrumental Settings and Parameters**

Plasma	
Cool gas flow	14 L min <sup>-1</sup>
Aux. gas flow	1.0 L min <sup>-1</sup>
Sample gas flow	1.1 L min <sup>-1</sup>
RF Power	1250 W
Data Acquisition	
Resolution	Isotopes
Low (LR)	<sup>7</sup> Li, <sup>88</sup> Sr, <sup>111</sup> Cd, <sup>133</sup> Cs, <sup>137</sup> Ba, <sup>206</sup> Pb, <sup>207</sup> Pb, <sup>208</sup> Pb, <sup>238</sup> U
Medium (MR)	<sup>27</sup> Al, <sup>44</sup> Ca, <sup>51</sup> V, <sup>53</sup> Cr, <sup>55</sup> Mn, <sup>57</sup> Fe, <sup>62</sup> Ni, <sup>65</sup> Cu, <sup>66</sup> Zn
Mass Window	20% for LR; 150% for MR; 200% for HR
Points per peak	50 for LR; 20 for MR and HR
Scan type	E-scan
Integration time	10 ms for LR; 50 ms MR
Passes & Runs	3 & 2

**Table 11. Hg isotopic composition (‰) for sapropel sediment from Mangrove Lake, Bermuda by depth.**

Core	Depth h (cm)	Hg T (ng g <sup>-1</sup> )	δ199	1SD	δ200	1SD	δ201	1SD	δ202	1SD	δ204	1SD	Δ199	1SD	Δ <sub>0</sub> <sup>20</sup>	1SD	Δ201	1SD	Δ204	1SD
ML3	30	4.32	-0.60	0.04	-0.99	0.02	-1.61	0.02	-1.95	0.02	-2.95	0.04	-0.11	0.04	-	0.01	-0.15	0.02	-0.03	0.04
															0.01					
ML1	74.5	4.10	-0.26	0.03	-0.55	0.02	-0.87	0.03	-1.17	0.05	-1.80	0.01	0.03	0.02	0.04	0.01	0.01	0.02	-0.05	0.06
ML3	90	14.70	-0.02	0.02	-0.30	0.02	-0.40	0.02	-0.64	0.03	-0.99	0.03	0.14	0.01	0.02	0.02	0.08	0.01	-0.03	0.01
ML1	106.5	5.48	-0.65	0.02	-1.02	0.01	-1.65	0.03	-1.98	0.02	-2.95	0.01	-0.15	0.01	-	0.01	-0.16	0.03	0.01	0.02
															0.03					
ML3	115	4.14	-0.46	0.02	-0.79	0.02	-1.32	0.01	-1.61	0.03	-2.46	0.02	-0.06	0.01	0.02	0.01	-0.11	0.02	-0.05	0.03
ML3	180	2.94	-0.58	0.04	-0.88	0.03	-1.51	0.02	-1.76	0.02	-2.68	0.05	-0.13	0.04	0.01	0.02	-0.18	0.02	-0.05	0.05
ML3	240	4.22	-0.69	0.03	-1.02	0.02	-1.77	0.03	-2.03	0.02	-3.02	0.02	-0.18	0.03	0.00	0.01	-0.24	0.03	0.01	0.02
ML3	300	4.36	-0.68	0.02	-0.91	0.02	-1.61	0.03	-1.86	0.03	-2.83	0.01	-0.21	0.01	0.03	0.01	-0.21	0.02	-0.05	0.05
IAEA SL1			-0.41	0.06	-0.58	0.04	-1.09	0.04	-1.25	0.04	-1.95	0.07	-0.10	0.05	0.05	0.02	-0.15	0.01	-0.09	0.03
UM-A			-0.15	0.03	-0.28	0.03	-0.46	0.03	-0.56	0.03	-0.84	0.05	-0.01	0.03	0.00	0.02	-0.04	0.02	-0.01	0.04

## **ACKNOWLEDGMENTS**

This material was also based upon work supported by the National Science Foundation under grant no. 1144869. We would like to thank Drs. Jessica Rodysill and Brian Yellen for fieldwork assistance, Zach Stromer for assistance running  $^{210}\text{Pb}$  samples, and Robert Hollis with ArcGIS assistance. Mercury stable isotope measurements were performed by the USGS Mercury Research Lab in Middleton, WI. We are grateful to Dr. Alfonso Mucci (McGill University) and Dr. Joel Blum (University of Michigan) for helpful comments and suggestions on an early draft of the paper.



## LIST OF REFERENCES

Abraham GM, Parker RJ (2008) Assessment of heavy metal enrichment factors and the degree of contamination in marine sediments from Tamaki Estuary, Auckland, New Zealand. *Environ Monit Assess* 136(1-3):227-238. <https://doi.org/10.1007/s10661-007-9678-2>

Amyot, M.; Mierle, G.; Lean, D. Sunlight-induced Formation of Dissolved Gaseous Mercury in Lake Waters. *Environ. Sci. Technol.* 1994, 28, 2366–237. <https://doi.org/10.1021/es00062a022>  
Angelidis MO, Radakovitch O, Veron A, Aloupi M, Heussner S, Price B (2011) Anthropogenic metal contamination and sapropel imprints in deep Mediterranean sediments. *Mar Pollut Bull* 62 (5):1041-1052. <https://doi.org/10.1016/j.marpolbul.2011.02.030>

Appleby PG (1998) Dating recent sediments by  $^{210}\text{Pb}$ : problems and solutions. In: *Dating of sediments and determination rate*, vol. STUK-A145, Helsinki, pp 7–24

Arnaboldi M, Meyers PA (2007) Trace element indicators of increased primary production and decreased water-column ventilation during deposition of latest Pliocene sapropels at five locations across the Mediterranean Sea. *Palaeogeogr Palaeoclimatol Palaeoecol* 249(3–4):425-443. <https://doi.org/10.1016/j.palaeo.2007.02.016>

Becnel, J.; Falgeust, C.; Cavalier, T.; Gauthreaux, K.; Landry, F.; Blanchard, M.; Beck, M.J.; Beck, J.N. Correlation of mercury concentrations in tree core and lichen samples in southeastern Louisiana. *Microchem. J.* 2004, 78, 205–210. doi:10.1016/j.microc.2004.06.002.

Bindler, R.; Renberg, I.; Klaminder, J.; Emteryd, O. Tree rings as Pb pollution archives? A comparison of  $^{206}\text{Pb}/^{207}\text{Pb}$  isotope ratios in pine and other environmental media. *Sci. Total Environ.* 2004, 319, 173–183. doi:10.1016/S0048-9697(03)00397-8.

Birch L, Hanselmann KW, Bachofen R (1996) Heavy metal conservation in lake Cadagno sediments: Historical records of anthropogenic emissions in a meromictic alpine lake. *Water Res* 30(3):679-687. [https://doi.org/10.1016/0043-1354\(95\)00231-6](https://doi.org/10.1016/0043-1354(95)00231-6)

Biswas A, Blum JD, Bergquist BA, Keeler GJ, Xie Z (2008) Natural mercury isotope variation in coal deposits and organic soils. *Environ Sci Technol* 42(22):8303–8309. <https://doi.org/10.1021/es801444b>

Blaauw M, Christen JA (2011) Flexible Paleoclimate Age-Depth Models Using an Autoregressive Gamma Process. *Bayesian Anal* 6(3):457-474. <https://doi.org/10.1214/11-BA618>

- Blaauw M, Christen JA (2013) Bacon manual – v2.2.  
[http://chrono.qub.ac.uk/blaauw/manualBacon\\_2.2.pdf](http://chrono.qub.ac.uk/blaauw/manualBacon_2.2.pdf) (Last accessed on 22 July 2018)
- Blum JD, Sherman LS, Johnson MW (2014) Mercury isotopes in Earth and Environmental Sciences. *Annual Review of Earth and Planetary Sci.* 42:249-269.  
<https://doi.org/10.1146/annurev-earth-050212-124107>
- Böning P, Brumsack HJ, Böttcher M, Schnetger B, Kriete C, Kallmeyer J, Borchers SL (2004) Geochemistry of Peruvian near-surface sediments. *Geochim Cosmochim Acta* 68(21):4429-4451. <https://doi.org/10.1016/j.gca.2004.04.027>
- Boudreau BP, Canfield DE, Mucci A (1992) Early diagenesis in a marine sapropel, Mangrove Lake, Bermuda. *Limnol Oceanogr* 37(8):1738-1753.  
<http://www.jstor.org.umiss.idm.oclc.org/stable/2838065>
- Bregy JC, Wallace DJ, Minzoni RT, Cruz VJ (2018) 2500-year paleotempestological record of intense storms for the Northern Gulf of Mexico, United States. *Marine Geology* 396:26-42.  
<https://doi.org/10.1016/j.margeo.2017.09.009>
- Brumbaugh, W.G.; Petty, J.D.; May, T.W.; Huckins, J.N. A passive integrative sampler for mercury vapor in air and neutral mercury species in water. *Chemosphere - Glob. Change Sci.* 2000, 2, 1–9. [https://doi.org/10.1016/S1465-9972\(99\)00055-0](https://doi.org/10.1016/S1465-9972(99)00055-0)
- Canfield DE, Boudreau BP, Mucci A, Gundersen JK (1998) The early diagenetic formation of organic sulfur in the sediments of Mangrove Lake, Bermuda. *Geochim Cosmochim Acta* 62(5): 767-781. [https://doi.org/10.1016/S0016-7037\(98\)00032-5](https://doi.org/10.1016/S0016-7037(98)00032-5)
- Chen J, Chakravarty P, Davidson GR, Wren DG, Locke MA, Zhou Y, Brown G, Cizdziel JV (2015) Simultaneous determination of mercury and organic carbon in sediment and soils using a direct mercury analyzer based on thermal decomposition-atomic absorption spectrophotometry. *Anal Chim Acta* 871:9-17. <https://doi.org/10.1016/j.aca.2015.03.011>
- Chen J, Hintelmann H, Feng X, Dimock B (2012) Unusual fractionation of both odd and even isotopes in precipitation from Peterborough, ON, Canada. *Geochim et Cosmochim Acta* 90:33-46. <https://doi.org/10.1016/j.gca.2012.05.005>
- Chen, J.; Chakravarty, P.; Davidson, G.R.; Wren, D.G.; Locke, M.A.; Zhou, Y.; Brown, G.; Cizdziel, J.V. Simultaneous determination of mercury and organic carbon in sediment and soils

using a direct mercury analyzer based on thermal decomposition–atomic absorption spectrophotometry. *Anal. Chim. Acta* 2015, 871, 9–17. <https://doi.org/10.1016/j.aca.2015.03.011>

Cheng, Z.; Buckley, B.M.; Katz, B.; Wright, W.; Bailey, R.; Smith, K.T.; Li, J.; Curtis, A.; Geen, A. van Arsenic in tree rings at a highly contaminated site. *Sci. Total Environ.* 2007, 376, 324–334. doi:10.1016/j.scitotenv.2007.01.074.

Choi, A.L.; Grandjean, P. Methylmercury exposure and health effects in humans. *Environ. Chem.* 2008, 5, 112–120, doi:10.1071/EN08014.

Choi, H.-D.; Holsen, T.M. Gaseous mercury fluxes from the forest floor of the Adirondacks. *Environ. Pollut.* 2009, 157, 592–600. <https://doi.org/10.1016/j.envpol.2008.08.020>

Cizdziel J, Zhou X (2005) Sources and Concentrations of Mercury and Selenium In Compartments within the Las Vegas Wash During A Period of Rapid Change. *Environ Monit Asses* 107:81-99. <https://doi.org/10.1007/s10661-005-2145-z>

Cizdziel, J.V.; Hinnert, T.A.; Heithmar, E.M. Determination of total mercury in fish tissues using combustion atomic absorption spectrometry with gold amalgamation. *Water, Air, Soil Pollut.* 2002, 135, 355–370. <https://DOI.org/10.1023/A:1014798012212>

Cizdziel, J.V.; Zhang, Y.; Nallamothe, D.; Brewer, J.S.; Gao, Z. Air/surface exchange of gaseous elemental mercury at different landscapes in Mississippi, USA. *Atmosphere* 2019, 10(9), 538. <https://doi.org/10.3390/atmos10090538>

Coburn, S.; Dix, B.; Edgerton, E.; Holmes, C.D.; Kinnison, D.; Liang, Q.; ter Schure, A.; Wang, S.; Volkamer, R. Mercury oxidation from bromine chemistry in the free troposphere over the southeastern US. *Atmos. Chem. Phys.* 2016, 16, 3743–3760, doi:10.5194/acp-16-3743-2016.

Cocozza, C.; Ravera, S.; Cherubini, P.; Lombardi, F.; Marchetti, M.; Tognetti, R. Integrated biomonitoring of airborne pollutants over space and time using tree rings, bark, leaves and epiphytic lichens. *Urban For. Urban Green.* 2016, 17, 177–191. doi:10.1016/j.ufug.2016.04.008.

Cutter, B.E.; Guyette, R.P. Anatomical, Chemical, and Ecological Factors Affecting Tree Species Choice in Dendrochemistry Studies. *J. Environ. Qual.* 1993, 22, 611–619. doi:10.2134/jeq1993.00472425002200030028x.

De Vos B, Vandecasteele B, Deckers J, Muys B (2005) Capability of loss-on-ignition as a predictor of total organic carbon in non-calcareous forest soils. *Commun Soil Sci Plant Anal* 36(19-20):2899-2921. <https://doi.org/10.1080/00103620500306080>

Dickinson WW, Dunbar GB, McLeod H (1996) Heavy metal history from cores in Wellington Harbour, New Zealand. *Environ Geol* 27(1):59-69. <https://doi.org/10.1007/BF00770603>

Driscoll, C.T.; Mason, R.P.; Chan, H.M.; Jacob, D.J.; Pirrone, N. Mercury as a Global Pollutant: Sources, Pathways, and Effects. *Environ. Sci. Technol.* 2013, 47, 4967–4983.

Ellison JC (1996) Pollen evidence of Late Holocene mangrove development in Bermuda. *Global Ecol Biogeogr* 5(6):315-326. <https://doi.org/10.2307/2997587>

Engle, M.A.; Tate, M.T.; Krabbenhoft, D.P.; Kolker, A.; Olson, M.L.; Edgerton, E.S.; DeWild, J.F.; McPherson, A.K. Characterization and cycling of atmospheric mercury along the central US Gulf Coast. *Appl. Geochem.* 2008, 23, 419–437, doi:10.1016/j.apgeochem.2007.12.024.

Engstrom DR, Fitzgerald WF, Cooke CA, Lamborg CH, Drevnick PE, Swain EB, Balogh SJ, Balcom PH (2014) Atmospheric Hg emissions from preindustrial gold and silver extraction in the Americas: A reevaluation from lake-sediment archives. *Environ Sci Technol* 48 (12):6533-6543. <https://doi.org/10.1021/es405558e>

Engstrom DR, Swain EB (1997) Recent declines in atmospheric mercury deposition in the upper Midwest. *Environ Sci Technol* 31(4):960-967. <https://doi.org/10.1021/es9600892>

Ericksen, J.; Gustin, M.; Schorran, D.; Johnson, D.; Lindberg, S.; Coleman, J. Accumulation of atmospheric mercury in forest foliage. *Atmos. Environ.* 2003, 37, 1613-1622. [https://doi.org/10.1016/S1352-2310\(03\)00008-6](https://doi.org/10.1016/S1352-2310(03)00008-6)

Ericksen, J.A.; Gustin, M.S.; Xin, M.; Weisberg, P.J.; Fernandez, G.C.J. Air/soil exchange of mercury from background soils in the United States. *Sci. Total Environ.* 2006, 366, 851-863. <https://doi.org/10.1016/j.scitotenv.2005.08.019>

ESRI. USA National Land Cover Database 2011, Based on Data from the Multi-Resolution Land Characteristics Consortium; ESRI ArcGIS Data Server: Redlands, CA, USA, 2019.

Ettler V, Mihaljevič M, Komárek M (2004) ICP-MS measurements of lead isotopic ratios in soils heavily contaminated by lead smelting: tracing the sources of pollution. *Anal Bioanal Chem* 378(2):311-317. <https://doi.org/10.1007/s00216-003-2229-y>

Feigis, M.; Mistry, S.; Snow, M.; Lei, Y.D.; Wania, F. Measuring Vertical Profiles of Gaseous Mercury Concentration using Passive Air Samplers. SETAC North America 39th Annual Meeting, Sacramento, Nov. 4-8, 2018.

Feng, X.; Wang, S.; Qiu, G.; Hou, Y.; Tang, S. Total gaseous mercury emissions from soil in Guiyang, Guizhou, China: Mercury emission from soil in Guiyang. *J. Geophys. Res. Atmospheres* 2005, 110. <https://doi.org/10.1029/2004JD005643>

Fitzgerald WF, Engstrom DR, Hammerschmidt CR, Lamborg CH, Balcom PH, Lima-Braun AA, Bothner MH, Reddy CM (2018) Global and Local Sources of Mercury Deposition in Coastal New England Reconstructed from a Multiproxy, High-Resolution, Estuarine Sediment Record. *Environ Sci Technol* 52(14): 7614-7620.

Fitzgerald, W.F.; Engstrom, D.R.; Mason, R.P.; Nater, E.A. The Case for Atmospheric Mercury Contamination in Remote Areas. *Environ. Sci. Technol.* 1998, 32, 1–7, doi:10.1021/es970284w.

Gay, D.A.; Schmeltz, D.; Prestbo, E.; Olson, M.; Sharac, T.; Tordon, R. The Atmospheric Mercury Network: Measurement and initial examination of an ongoing atmospheric mercury record across North America. *Atmos. Chem. Phys.* 2013, 13, 11339–11349, doi:10.5194/acp-13-11339-2013.

Gehrke GE, Blum JD, Meyers PA (2009) The geochemical behavior and isotopic composition of Hg in a mid-Pleistocene western Mediterranean sapropel. *Geochim Cosmochim Acta* 73(6): 1651-1665. <https://doi.org/10.1016/j.gca.2008.12.012>

Gichuki SW, Mason RP (2014) Wet and dry deposition of mercury in Bermuda. *Atmos Environ* 87:249-257. <https://doi.org/10.1016/j.atmosenv.2014.01.025>

Griggs, T.; Liu, L.; Talbot, R.W.; Torres, A.; Lan, X. Comparison of atmospheric mercury speciation at a coastal and an urban site in Southeastern Texas, USA. *Atmosphere* 2020, 11, 73.

Gustin MS, Amos HM, Huang J, Miller MB, Heidecorn K (2015) Measuring and modeling mercury in the atmosphere: a critical review. *Atmos Chem Phys* 15(10):5697-5713. <https://doi.org/10.5194/acp-15-5697-2015>

Gustin, M.; Ericksen, J.; Schorran, D.; Johnson, D.; Lindberg, S.; Coleman, J. Application of Controlled Mesocosms for Understanding Mercury Air-Soil-Plant Exchange. *Environ. Sci. Technol.* 2004, 38, 6044-6050. <https://doi.org/10.1021/es0487933>

Gustin, M.; Jaffe, D. Reducing the Uncertainty in Measurement and Understanding of Mercury in the Atmosphere. *Environ. Sci. Technol.* 2010, 44, 2222–2227. <https://doi.org/10.1021/es902736k>

Gustin, M.; Kolker, A.; Gardfeld, K. Transport and fate of mercury in the environment. *Appl. Geochem.* 2008, 23, 343-344. <https://doi.org/10.1016/j.apgeochem.2007.12.005>

Gustin, M.S.; Amos, H.M.; Huang, J.; Miller, M.B.; Heidecorn, K. Measuring and modeling mercury in the atmosphere: A critical review. *Atmos. Chem. Phys.* 2015, 15, 5697–5713, doi:10.5194/acp-15-5697-2015.

Gustin, M.S.; Evers, D.C.; Bank, M.S.; Hammerschmidt, C.R.; Pierce, A.; Basu, N.; Blum, J.; Bustamante, P.; Chen, C.; Driscoll, C.T.; et al. Importance of Integration and Implementation of Emerging and Future Mercury Research into the Minamata Convention. *Environ. Sci. Technol.* 2016, 50, 2767–2770. doi:10.1021/acs.est.6b00573.

Gustin, M.S.; Lyman, S.N.; Kilner, P.; Prestbo, E. Development of a passive sampler for gaseous mercury. *Atmos. Environ.* 2011, 45, 5805–5812. <https://doi.org/10.1016/j.atmosenv.2011.07.014>

Gustin, M.S.; Stamenkovic, J. Effect of Watering and Soil Moisture on Mercury Emissions from Soils. *Biogeochemistry* 2005, 76, 215–232. <https://doi.org/10.1007/s10533-005-4566-8>.

Hall, B.D.; Aiken, G.R.; Krabbenhoft, D.P.; Marvin-DiPasquale, M.; Swarzenski, C.M. Wetlands as principal zones of methylmercury production in southern Louisiana and the Gulf of Mexico region. *Environ. Pollut.* 2008, 154, 124–134, doi:10.1016/j.envpol.2007.12.017.

Hartgers WA, Lopez JF, Damste JSS, Reiss C, Maxwell JR, Grimalt JO (1997) Sulfur-binding in recent environments: II. Speciation of sulfur and iron and implications for the occurrence of organo-sulfur compounds. *Geochim Cosmochim Acta* 61(22):4769-4788. [https://doi.org/10.1016/S0016-7037\(97\)00279-2](https://doi.org/10.1016/S0016-7037(97)00279-2)

Hatcher PG, Simoneit BRT, Mackenzie FT, Neumann AC, Thorstenson DC, Gerchakov SM (1982) Organic geochemistry and pore water chemistry of sediments from Mangrove Lake, Bermuda. *Org Geochem* 4(2):93-112. [https://doi.org/10.1016/0146-6380\(82\)90012-2](https://doi.org/10.1016/0146-6380(82)90012-2)

Hedgecock, I.M.; Pirrone, N. Chasing Quicksilver: Modeling the Atmospheric Lifetime of Hg in the Marine Boundary Layer at Various Latitudes. *Environ. Sci. Technol.* 2004, 38, 69–76, doi:10.1021/es034623z.

Heiri O, Lotter AF, Lemcke G (2001) Loss on ignition as a method for estimating organic and carbonate content in sediments: reproducibility and comparability of results. *J Paleolimnol* 25(1): 101-110. <https://doi.org/10.1023/A:1008119611481>

Hojdova M, Rohovec J, Chrastný V, Penížek V, Navrátil T (2015) The Influence of Sample Drying Procedures on Mercury Concentrations Analyzed in Soils. *Bull Environ Contam Toxicol* 94(5):570-576. <https://doi.org/10.1007/s00128-015-1521-9>

Hojdová, M.; Navrátil, T.; Rohovec, J.; Žák, K.; Vaněk, A.; Chrastný, V.; Bače, R.; Svoboda, M. Changes in Mercury Deposition in a Mining and Smelting Region as Recorded in Tree Rings. *Water Air Soil Pollut.* 2011, 216, 73–82. doi:10.1007/s11270-010-0515-9.

Janssen SE, Lepak RF, Tate MT, Ogorek JM, DeWild JF, Babiarz CL, Hurley JP, Krabbenhoft DP (2019) Rapid pre-concentration of mercury in solids and water for isotopic analysis. *Anal Chim Acta* 1054: 95-103. <https://doi.org/10.1016/j.aca.2018.12.026>

Jeon, B.; Cizdziel, J.V. Can the MerPAS Passive Air Sampler Discriminate Landscape, Seasonal, and Elevation Effects on Atmospheric Mercury? A Feasibility Study in Mississippi, USA. *Atmosphere* 2019, 10, 617, doi:10.3390/atmos10100617.

Kainz M, Lucotte M, Parrish CC (2003) Relationships between organic matter composition and methyl mercury content of offshore and carbon-rich littoral sediments in an oligotrophic lake. *Can J Fish Aquat Sci* 60(7):888-896. <https://doi.org/10.1139/F03-075>

Kang S, Huang J, Wang F, Zhang Q, Zhang Y, Li C, Wang L, Chen P, Sharma CM, Li Q, Sillanpää M, Hou J, Xu B, Guo J (2016) Atmospheric Mercury Depositional Chronology Reconstructed from Lake Sediments and Ice Core in the Himalayas and Tibetan Plateau. *Environ Sci Technol* 50(6):2859-2869. <https://doi.org/10.1021/acs.est.5b04172>

Keller, G.; Glinsorn, G.; Pirrone, N. Particulate mercury in the atmosphere: its significance, transport, transformation and sources. *Water Air Soil Pollut.* 1995, 80, 159-168.

Knicker H, Hatcher PG (2001) Sequestration of organic nitrogen in the sapropel from Mangrove Lake, Bermuda. *Org Geochem* 32(5):733-744. [https://doi.org/10.1016/S0146-6380\(01\)00005-5](https://doi.org/10.1016/S0146-6380(01)00005-5)

Knicker H, Scaroni AW, Hatcher PG (1996) <sup>13</sup>C and <sup>15</sup>N NMR spectroscopic investigation on the formation of fossil algal residues. *Org Geochem* 24(6):661-669. [https://doi.org/10.1016/0146-6380\(96\)00057-5](https://doi.org/10.1016/0146-6380(96)00057-5)

Komárek M, Chrastný V, Ettler V, Tlustoš P (2006) Evaluation of extraction/digestion techniques used to determine lead isotopic composition in forest soils. *Anal Bioanal Chem* 385(6):1109-1115. <https://doi.org/10.1007/s00216-006-0543-x>



Komárek M, Vojtěch E, Chrastný V, Mihaljevič M (2008) Lead isotopes in environmental sciences: A review. *Environ Int* 34(4):562-577. <https://doi.org/10.1016/j.envint.2007.10.005>

Kuiken, T.; Gustin, M.; Zhang, H.; Lindberg, S.; Sedinger, B. Mercury emission from terrestrial background surfaces in the eastern USA. II: Air/surface exchange of mercury within forests from South Carolina to New England. *Appl. Geochem.* 2008, 23, 356–368. <https://doi.org/10.1016/j.apgeochem.2007.12.007>

Land LS, Mackenzie FT, Gould SJ (1967) Pleistocene History of Bermuda. *Geol Soc Am Bull* 78(8):993-1006. [https://doi-org.umiss.idm.oclc.org/10.1130/0016-7606\(1967\)78\(993:PHOB\)2.0.CO;2](https://doi-org.umiss.idm.oclc.org/10.1130/0016-7606(1967)78(993:PHOB)2.0.CO;2)

Landis, M.S.; Stevens, R.K.; Schaedlich, F.; Prestbo, E.M. Development and Characterization of an Annular Denuder Methodology for the Measurement of Divalent Inorganic Reactive Gaseous Mercury in Ambient Air. *Environ. Sci. Technol.* 2002, 36, 3000–3009. <https://doi.org/10.1021/es015887t>

Lepak RF, Yin R, Krabbenhoft DP, Ogorek JM, DeWild JF, Holsen TM, Hurley JP (2015) Use of Stable Isotope Signatures to Determine Mercury Sources in the Great Lakes. *Environ Sci Technol Lett* 2(12):335–341. <https://doi.org/10.1021/acs.estlett.5b00277>

Lin, C.-J.; Pehkonen, S.O. The chemistry of atmospheric mercury: a review. *Atmos. Environ.* 1999, 33, 2067–2079. [https://doi.org/10.1016/S1352-2310\(98\)00387-2](https://doi.org/10.1016/S1352-2310(98)00387-2)

Lincoln, R.A.; Shine, J.P.; Chesney, E.J.; Vorhees, D.J.; Grandjean, P.; Senn, D.B. Fish Consumption and Mercury Exposure among Louisiana Recreational Anglers. *Environ. Health Perspect.* 2011, 119, 245–251, doi:10.1289/ehp.1002609.

Lindberg, S.E.; Dong, W.; Meyers, T. Transpiration of gaseous elemental mercury through vegetation in a subtropical wetland in Florida. *Atmos. Environ.* 2002, 36, 5207–5219. [https://doi.org/10.1016/S1352-2310\(02\)00586-1](https://doi.org/10.1016/S1352-2310(02)00586-1)

Lindeberg C, Bindler R, Renberg I, Emteryd O, Karlsson E, Anderson NJ (2006) Natural fluctuations of mercury and lead in Greenland Lake sediments. *Environ Sci Technol* 40(1):90-95. <https://doi.org/10.1021/es051223y>

Liu J, Feng X, Yin R, Zhu W, Li Z (2011) Mercury distributions and mercury isotope signatures in sediments of Dongjiang, the Pearl River Delta, China. *Chem Geol* 287(1–2):81-89. <https://doi.org/10.1016/j.chemgeo.2011.06.001>

Lopez-Anton, M.A.; Yuan, Y.; Perry, R.; Maroto-Valer, M.M. Analysis of mercury species present during coal combustion by thermal desorption. *Fuel* 2010, 89, 629–634.  
<https://doi.org/10.1016/j.fuel.2009.08.034>

Lyman, S.N.; Cheng, I.; Gratz, L.E.; Weiss-Penzias, P.; Zhang, L. An updated review of atmospheric mercury. *Sci. Total Environ.* 2020, 707, 135575,  
doi:10.1016/j.scitotenv.2019.135575.

Lyman, S.N.; Gustin, M.S.; Prestbo, E.M. A passive sampler for ambient gaseous oxidized mercury concentrations. *Atmos. Environ.* 2010, 44, 246–252,  
doi.org/10.1016/j.atmosenv.2009.10.008.

Madejón, P.; Marañón, T.; Murillo, J.M.; Robinson, B. White poplar (*Populus alba*) as a biomonitor of trace elements in contaminated riparian forests. *Environ. Pollut.* 2004, 132, 145–155. doi:10.1016/j.envpol.2004.03.015.

Mason RP, Choi AL, Fitzgerald WF, Hammerschmidt CR, Lamborg CH, Soerensen AL, Sunderland EM (2012) Mercury biogeochemical cycling in the ocean and policy implications. *Environ Res* 119:101-117. <https://doi.org/10.1016/j.envres.2012.03.013>

Mazur, M.; Mitchell, C.; Eckley, C.; Eggert, S.; Kolka, R.; Sebestyen, S.; Swain, E. Gaseous mercury fluxes from forest soils in response to forest harvesting intensity: A field manipulation experiment. *Sci. Total Environ.* 2014, 496, 678–687.  
<https://doi.org/10.1016/j.scitotenv.2014.06.058>

McCarroll, D.; Loader, N.J. Stable isotopes in tree rings. *Quat. Sci. Rev.* 2004, 23, 771–801.  
doi:10.1016/j.quascirev.2003.06.017.

McLagan, D.S.; Huang, H.; Lei, Y.D.; Wania, F.; Mitchell, C.P.J. Application of sodium carbonate prevents sulphur poisoning of catalysts in automated total mercury analysis. *Spectrochim. Acta Part B At. Spectrosc.* 2017, 133, 60–62.  
<https://doi.org/10.1016/j.sab.2017.04.014>

McLagan, D.S.; Mazur, M.E.E.; Mitchell, C.P.J.; Wania, F. Passive air sampling of gaseous elemental mercury: a critical review. *Atmospheric Chem. Phys.* 2016, 16, 3061–3076.  
<https://doi.org/10.5194/acp-16-3061-2016>

McLagan, D.S.; Mitchell, C.P.J.; Huang, H.; Abdul Hussain, B.; Lei, Y.D.; Wania, F. The effects of meteorological parameters and diffusive barrier reuse on the sampling rate of a passive air

sampler for gaseous mercury. *Atmospheric Meas. Tech.* 2017, 10, 3651–3660.  
<https://doi.org/10.5194/amt-10-3651-2017>

McLagan, D.S.; Mitchell, C.P.J.; Huang, H.; Lei, Y.D.; Cole, A.S.; Steffen, A.; Hung, H.; Wania, F. A High-Precision Passive Air Sampler for Gaseous Mercury. *Environ. Sci. Technol. Lett.* 2016, 3, 24–29, doi:10.1021/acs.estlett.5b00319.

McLagan, D.S.; Mitchell, C.P.J.; Steffen, A.; Hung, H.; Shin, C.; Stupple, G.W.; Olson, M.L.; Luke, W.T.; Kelley, P.; Howard, D.; et al. Global evaluation and calibration of a passive air sampler for gaseous mercury. *Atmospheric Chem. Phys.* 2018, 18, 5905–5919.  
<https://doi.org/10.5194/acp-18-5905-2018>

McLagan, D.S.; Monaci, F.; Huang, H.; Lei, Y.D.; Mitchell, C.P.J.; Wania, F. Characterization and Quantification of Atmospheric Mercury Sources Using Passive Air Samplers. *J. Geophys. Res. Atmos.* 2019, 124, 2351–2362, doi:10.1029/2018JD02937327.

McManus J, Berelson W, Klinkhammer GP, Hammond DE, Holm C (2005) Authigenic uranium: Relationship to oxygen penetration depth and organic carbon rain. *Geochim Cosmochim Acta* 69(1):95-108. <https://doi.org/10.1016/j.gca.2004.06.023>

Merritt, K.A.; Amirbahman, A. Mercury methylation dynamics in estuarine and coastal marine environments—A critical review. *Earth Sci. Rev.* 2009, 96, 54–66, doi:10.1016/j.earscirev.2009.06.002.

Monticelli, D.; Di Iorio, A.; Ciceri, E.; Castelletti, A.; Dossi, C. Tree ring microanalysis by LA-ICP-MS for environmental monitoring: Validation or refutation? Two case histories. *Microchim. Acta* 2009, 164, 139–148. doi:10.1007/s00604-008-0049-7.

Muhaya BBM, Leermakers M, Baeyens W (1998) Influence of sediment preservation on total mercury and methylmercury analyses. *Water Air Soil Pollut* 107(1-4):277-288.  
<https://doi.org/10.1023/A:1019886606856>

Müller G (1969) Index of Geoaccumulation in Sediments of the Rhine River. *GeoJournal* 2(3):108-118

Nair, U.S.; Wu, Y.; Walters, J.; Jansen, J.; Edgerton, E.S. Diurnal and seasonal variation of mercury species at coastal-suburban, urban, and rural sites in the southeastern United States. *Atmos. Environ.* 2012, 47, 499–508, doi:10.1016/j.atmosenv.2011.09.056.

National Atmospheric Deposition Program/Mercury Deposition Network. Available online: <http://nadp.slh.wisc.edu> (accessed on 24/9/2020).

Navrátil, T.; Šimeček, M.; Shanley, J.B.; Rohovec, J.; Hojdová, M.; Houška, J. The history of mercury pollution near the Spolana chlor-alkali plant (Neratovice, Czech Republic) as recorded by Scots pine tree rings and other bioindicators. *Sci. Total Environ.* 2017, 586, 1182–1192. doi:10.1016/j.scitotenv.2017.02.112.

NOAA (2018) Bermuda 1 arc-second Coastal Digital Elevation Model. <https://www.ngdc.noaa.gov/metadata/page?xml=NOAA/NESDIS/NGDC/MGG/DEM/iso/xml/5010.xml&view=getDataView&header=none> (Last accessed on 18 July 2018)

Nriagu, J.O. Mechanistic steps in the photoreduction of mercury in natural waters. *Sci. Total Environ.* 1994, 154, 1–8. [https://doi.org/10.1016/0048-9697\(94\)90608-4](https://doi.org/10.1016/0048-9697(94)90608-4)

Obrist, D.; Johnson, D.W.; Edmonds, R.L. Effects of vegetation type on mercury concentrations and pools in two adjacent coniferous and deciduous forests. *J. Plant Nutr. Soil Sci.* 2012, 175, 68–77. doi:10.1002/jpln.201000415.

Orem WH, Hatcher PG, Spiker EC, Szeverenyi NM, Maciel GE (1986) Dissolved organic matter in anoxic pore waters from Mangrove Lake, Bermuda. *Geochim Cosmochim Acta* 50(4):609-618. [https://doi.org/10.1016/0016-7037\(86\)90109-2](https://doi.org/10.1016/0016-7037(86)90109-2)

Osterwalder, S.; Eugster, W.; Feigenwinter, I.; Jiskra, M. First eddy covariance flux measurements of gaseous elemental mercury (Hg<sup>0</sup>) over a grassland. *Atmos. Meas. Tech. Discuss*, in review, 2019. <https://doi.org/10.5194/amt-2019-278>

Padilla, K.L.; Anderson, K.A. Trace element concentration in tree-rings biomonitoring centuries of environmental change. *Chemosphere* 2002, 49, 575–585. doi:10.1016/S0045-6535(02)00402-2.

Pandey, S.K.; Kim, K.-H.; Brown, R.J.C. Measurement techniques for mercury species in ambient air. *TrAC Trends Anal. Chem.* 2011, 30, 899–917. <https://doi.org/10.1016/j.trac.2011.01.017>

Park J, Presley BJ (1997) Trace metals contamination of sediments and organisms from the Swan Lake area of Galveston Bay. *Environ Pollut* 98(2):209-221. [https://doi.org/10.1016/S0269-7491\(97\)00137-1](https://doi.org/10.1016/S0269-7491(97)00137-1)

Passier HF, Böttcher ME, De Lange GJ (1999) Sulphur enrichment in organic matter of eastern Mediterranean sapropels: A study of sulphur isotope partitioning. *Aquat Geochem* 5(1):99-118. <https://doi.org/10.1023/A:1009676107330>

Peckham, M.A.; Gustin, M.S.; Weisber, P.J. Assessment of the Suitability of Tree Rings as Archives of Global and Regional Atmospheric Mercury Pollution. *Environ. Sci. Technol.* 2019, 53, 3663–3671. doi:10.1021/acs.est.8b06786.

Peterson, C.; Alishahi, M.; Gustin, M.S. Testing the use of passive sampling systems for understanding air mercury concentrations and dry deposition across Florida, USA. *Sci. Total Environ.* 2012, 424, 297–307. <https://doi.org/10.1016/j.scitotenv.2012.02.031>

Poissant, L.; Casimir, A. Water-air and soil-air exchange rate of total gaseous mercury measured at background sites. *Atmos. Environ.* 1998, 32, 883–893. [https://doi.org/10.1016/S1352-2310\(97\)00132-5](https://doi.org/10.1016/S1352-2310(97)00132-5)

Reimer PJ, Bard E, Bayliss A, Beck JW, Blackwell PG, Bronk C, Caitlin R, Hai EB, Edwards RL (2013) IntCal13 and Marine13 radiocarbon age calibration curves 0–50,000 years cal BP. *Radiocarbon* 55(4):1869–1887. [https://doi.org/10.2458/azu\\_js\\_rc.55.16947](https://doi.org/10.2458/azu_js_rc.55.16947)

Ren, X.; Luke, W.; Kelley, P.; Cohen, M.; Ngan, F.; Artz, R.; Walker, J.; Brooks, S.; Moore, C.; Swartzendruber, P.; et al. Mercury Speciation at a Coastal Site in the Northern Gulf of Mexico: Results from the Grand Bay Intensive Studies in Summer 2010 and Spring 2011. *Atmosphere* 2014, 5, 230–251, doi:10.3390/atmos5020230.

Ren, X.; Luke, W.T.; Kelley, P.; Cohen, M.D.; Artz, R.; Olson, M.L.; Schmeltz, D.; Puchalski, M.; Goldberg, D.L.; Ring, A.; et al. Atmospheric mercury measurements at a suburban site in the Mid-Atlantic United States: Inter-annual, seasonal and diurnal variations and source-receptor relationships. *Atmos. Environ.* 2016, 146, 141–152, doi:10.1016/j.atmosenv.2016.08.028.

Ren, X.; Luke, W.T.; Kelley, P.; Cohen, M.D.; Olson, M.L.; Walker, J.; Cole, R.; Archer, M.; Artz, R.; Stein, A.A. Long-Term Observations of Atmospheric Speciated Mercury at a Coastal Site in the Northern Gulf of Mexico during 2007–2018. *Atmosphere* 2020, 11, 268, doi:10.3390/atmos11030268.

Rezende PS, Silva NC, Moura WD, Windmüller CC (2018) Quantification and speciation of mercury in streams and rivers sediment samples from Paracatu, MG, Brazil, using a direct mercury analyser®. *Microchem. J.* 140:199-206. <https://doi.org/10.1016/j.microc.2018.04.006>

Rolison, J.M.; Landing, W.M.; Luke, W.; Cohen, M.; Salters, V.J.M. Isotopic composition of species-specific atmospheric Hg in a coastal environment. *Chem. Geol.* 2013, 336, 37–49, doi:10.1016/j.chemgeo.2012.10.007.

Sanei H, Goodarzi F (2006) Relationship between organic matter and mercury in recent lake sediment: The physical-geochemical aspects. *Appl Geochem* 21(11):1900-1912.  
<https://doi.org/10.1016/j.apgeochem.2006.08.015>

Schneider, L; Allen, K.; Walker, M.; Morgan, C. Haberle Using Tree Rings to Track Atmospheric Mercury Pollution in Australia: The Legacy of Mining in Tasmania. *Environ. Sci. Technol.* 2019, 53, 5697–5706. doi:10.1021/acs.est.8b06712.

Schroeder, W.H.; Munthe, J. Atmospheric mercury—An overview. *Atmos. Environ.* 1998, 32, 809–822. [https://doi.org/10.1016/S1352-2310\(97\)00293-8](https://doi.org/10.1016/S1352-2310(97)00293-8)

Sexauer Gustin, M.; Weiss-Penzias, P.S.; Peterson, C. Investigating sources of gaseous oxidized mercury in dry deposition at three sites across Florida, USA. *Atmos. Chem. Phys.* 2012, 12, 9201–9219, doi:10.5194/acp-12-9201-2012.

Sigler, J.M.; Mao, H.; Sive, B.C.; Talbot, R. Oceanic influence on atmospheric mercury at coastal and inland sites: A springtime noreaster in New England. *Atmos Chem Phys* 2009, 9, 4023–4030.

Siwik, E.I.H.; Campbell, L.M.; Mierle, G. Distribution and trends of mercury in deciduous tree cores. *Environ. Pollut.* 2010, 158, 2067–2073. doi:10.1016/j.envpol.2010.03.002.

Skov, H.; Christensen, J.H.; Goodsite, M.E.; Heidam, N.Z.; Jensen, B.; Wåhlin, P.; Geernaert, G. Fate of Elemental Mercury in the Arctic during Atmospheric Mercury Depletion Episodes and the Load of Atmospheric Mercury to the Arctic. *Environ. Sci. Technol.* 2004, 38, 2373–2382.  
<https://doi.org/10.1021/es030080h>

Skov, H.; Sørensen, B.T.; Landis, M.S.; Johnson, M.S.; Sacco, P.; Goodsite, M.E.; Lohse, C.; Christiansen, K.S. Performance of a new diffusive sampler for Hg<sub>0</sub> determination in the troposphere. *Environ. Chem.* 2007, 4, 75–80, doi:10.1071/EN06082.

Sommar, J.; Zhu, W.; Lin, C.-J.; Feng, X. Field Approaches to Measure Hg Exchange Between Natural Surfaces and the Atmosphere—A Review. *Crit. Rev. Environ. Sci. Technol.* 2013, 43, 1657–1739. <https://doi.org/10.1080/10643389.2012.671733>

Sprovieri, F.; Pirrone, N.; Bencardino, M.; D'Amore, F.; Carbone, F.; Cinnirella, S.; Mannarino, V.; Landis, M.; Ebinghaus, R.; Weigelt, A.; et al. Atmospheric mercury concentrations observed at ground-based monitoring sites globally distributed in the framework of the GMOS network. *Atmos. Chem. Phys.* 2016, 16, 11915–11935, doi:10.5194/acp-16-11915-2016.

Stamenkovic, J.; Gustin, M.S. Nonstomatal versus Stomatal Uptake of Atmospheric Mercury. *Environ. Sci. Technol.* 2009, 43, 1367–1372. <https://doi.org/10.1021/es801583a>

Stratford K, Williams RG, Myers PG (2000) Impact of the circulation on sapropel formation in the eastern Mediterranean. *Global Biogeochem Cycles* 14(2):683-695.

<https://doi.org/10.1029/1999GB001157>

Stuppel, G.; McLagan, D.; Steffen, A. In situ reactive gaseous mercury uptake on radiello diffusive barrier, cation exchange membrane and teflon filter membranes during atmospheric mercury depletion events. In Proceedings of the 14th International Conference on Mercury as a Global Pollutant (ICMGP), Krakow, Poland, 8–13 September 2019.

Stuppel, G.W.; McLagan, D.S.; Steffen, A. In situ reactive gaseous mercury uptake on Radiello diffusive barrier, cation exchange membrane and teflon filter membranes during atmospheric depletion events. International Conference on Mercury as a Global Pollutant, Krakow, Poland, Sept. 8-13, 2019.

Szponar, N.; McLagan, D.S.; Kaplan, R.J.; Mitchell, C.P.J.; Wania, F.; Steffen, A.; Stuppel, G.W.; Monaci, F.; Bergquist, B.A. Isotopic Characterization of Atmospheric Gaseous Elemental Mercury by Passive Air Sampling. *Environ. Sci. Technol.* 2020, 54, 10533–10543, doi:10.1021/acs.est.0c02251.

Tchounwou P.B., Yedjou C.G., Patlolla A.K., Sutton D.J. (2012) Heavy Metal Toxicity and the Environment. In: Luch A. (eds) *Molecular, Clinical and Environmental Toxicology. Experientia Supplementum*, vol 101. Springer, Basel. [https://doi.org/10.1007/978-3-7643-8340-4\\_6](https://doi.org/10.1007/978-3-7643-8340-4_6)

Teutsch N., Erel Y, Halicz L, Banin A (2001) Distribution of natural and anthropogenic lead in Mediterranean soils. *Geochim Cosmochim Acta* 65(17):2853-2864.

[https://doi.org/10.1016/S0016-7037\(01\)00607-X](https://doi.org/10.1016/S0016-7037(01)00607-X)

Thomas M.L.H., Eakins K.E., Logan A. (1991) Physical characteristics of the anchialine ponds of Bermuda. *Bulletin of Marine Science* 48:125-136.

USEPA. Toxic Release Inventory. 2020. Available online: <https://www.epa.gov/toxics-release-inventory-triprogram/tri-basic-data-files-calendar-years-1987-2018> (accessed on 13 January 2020).



Valente, R.J.; Shea, C.; Lynn Humes, K.; Tanner, R.L. Atmospheric mercury in the Great Smoky Mountains compared to regional and global levels. *Atmos. Environ.* 2007, 41, 1861–1873. <https://doi.org/10.1016/j.atmosenv.2006.10.054>

Wallace D, Donnelly J, Woodruff J, van Hengstum P, Rosenheim B (2017) Late Holocene Reconstruction of Hurricane Strikes from Mangrove Lake, Bermuda. 6th International Summit on Hurricanes and Climate Change: From Hazard to Impact. *Aegean Conference Series* 106: 66.

Wallace DJ, Rosenheim BE, Roberts ML, Burton JR, Donnelly JP, Woodruff JD (2014) Paleotempestological chronology developed from gas ion source AMS analysis of carbonates determined through real-time Bayesian statistical approach. AGU Fall Meeting abstract id PP41D-1429.

Watmough, S.A.; Hutchinson, T.C. Analysis of tree rings using inductively coupled plasma mass spectrometry to record fluctuations in a metal pollution episode. *Environ. Pollut.* 1996, 93, 93–102. doi:10.1016/0269-7491(95)00107-7.

Watts WA, Hansen, BCS (1986) Holocene climate and vegetation of Bermuda. *Pollen Et Spores* 28, 355-364.

Woodruff JD, Donnelly JP, Okusu A (2009) Exploring typhoon variability over the mid-to-late Holocene: evidence of extreme coastal flooding from Kamikoshiki, Japan. *Quat Sci Rev* 28(17-18):1774-1785. <https://doi.org/10.1016/j.quascirev.2009.02.005>

Woodruff JD, Kanamaru K, Kundu S, Cook TL (2015) Depositional evidence for the Kamikaze typhoons and links to changes in typhoon climatology. *Geol* 43(1):91-94. <https://doi.org/10.1130/G36209.1>

Wright, G.; Woodward, C.; Peri, L.; Weisberg, P.J.; Gustin, M.S. Application of tree rings (dendrochemistry) for detecting historical trends in air Hg concentrations across multiple scales. *Biogeochemistry* 2014, 120, 149–162. doi:10.1007/s10533-014-9987-9.

Yang H, Rose N (2003) Distribution of mercury in six lake sediment cores across the UK. *Sci Total Environ* 304(1-3):391-404. [https://doi.org/10.1016/S0048-9697\(02\)00584-3](https://doi.org/10.1016/S0048-9697(02)00584-3)

Yang, Y.; Yanai, R.D.; Driscoll, C.T.; Montesdeoca, M.; Smith, K.T. Concentrations and content of mercury in bark, wood, and leaves in hardwoods and conifers in four forested sites in the northeastern USA. *PLOS ONE* 2018, 13, e0196293. doi:10.1371/journal.pone.0196293.



Yang, Y.; Yanai, R.D.; Montesdeoca, M.; Driscoll, C.T. Measuring mercury in wood: challenging but important. *Int. J. Environ. Anal. Chem.* 2017, 97, 456–467. doi:10.1080/03067319.2017.1324852.

Yi, J.; Cizdziel, J.; Lu, D. Temporal patterns of atmospheric mercury species in northern Mississippi during 2011–2012: Influence of sudden population swings. *Chemosphere* 2013, 93, 1694–1700, doi:10.1016/j.chemosphere.2013.05.039.

Yin R, Feng X, Hurley JP, Krabbenhoft DP, Lepak RF, Kang S, Yang H, Li X (2016) Historical records of mercury stable isotopes in sediments of Tibetan Lakes. *Sci Rep* 6:23332. <https://doi.org/10.1038/srep23332>

Zhang, Y.; Jacob, D.J.; Horowitz, H.M.; Chen, L.; Amos, H.M.; Krabbenhoft, D.P.; Slemr, F.; St. Louis, V.L.; Sunderland, E.M. Observed decrease in atmospheric mercury explained by global decline in anthropogenic emissions. *Proc. Natl. Acad. Sci. USA* 2016, 113, 526–531, doi:10.1073/pnas.1516312113.

Zhu, J.; Wang, D.; Ma, M. Mercury release flux and its influencing factors at the air-water interface in paddy field in Chongqing, China. *Chin. Sci. Bull.* 2013, 58, 266–274. <https://doi.org/doi:10.1007/s11434-012-5412-8>

## **CURRICULUM VITAE 2021**

### **BYUNGGWON JEON**

#### **Education**

- 2017 – 2021 Ph.D. Environmental Analytical Chemistry, The University of Mississippi.
- 2012 – 2014 M.S. Analytical Chemistry, Chungnam National University.
- 2006 – 2012 B.S. Chemistry, Chungnam National University.

#### **Scholarships and Grants**

- Jan. 2021 - May 2021 Dissertation Fellowship Program, Graduate School, University of Mississippi
- Jan. 2019 - Sep. 2019 Seed Grant Program, Emergent Polymer Sensing Technologies for Gulf Coast Water Quality Monitoring, University of Southern Mississippi
- Sep. 2010 - Dec. 2011 Scholarships during each of the three semesters for good grades and for experiment projects for the Medical-Bio Project at Chungnam National University

#### **Research Experience**

- Sources, cycling and distribution of mercury in the environment
- Development and application of passive air samplers for atmospheric mercury studies
- Development a new method to analyze heavy metals in tree rings using DMA and ICP-MS
- Trace and heavy metal analyses using ICP-MS
- Determination of sodium content of various Kimchi products using Flame Atomic Absorption Spectrophotometry, Ministry of Food and Drug Safety, South Korea

- Analysis of toxic metals in food and drug products by ICP-OES, Ministry of Food and Drug Safety, South Korea
- Development a new method for arsenic speciation using Ion Chromatography-ICP-MS (Masters Thesis)
- Development of a modified QuEChERS method for multi-class pesticide in agricultural products by GC-MS and HPLC-MS/MS

### **Skills**

Instrumental UV-VIS, IR, Raman, GC-MS, GC-FID, LC-PDA, LC-RID, HPLC-MS/MS, ICP-OES, ICP-MS, FI-AAS, DMA, XRF, SEM

Software Origin, MS Office applications, Chemdraw, SPSS

### **Conferences and Meetings**

Mar. 2020 Pittcon Conference, Chicago, Oral presentation.

Feb. 2020 Mississippi Academy of Sciences 84<sup>th</sup> annual meeting, Oral and poster presentation.

Apr. 2019 The University of Mississippi Center for Water and Wetland Resources Science Conference, Oral Presentation

Oct. 2013 112<sup>th</sup> General Meeting of the Korean Chemical Society, Poster presentation

Nov. 2012 49<sup>th</sup> Meeting of the Korean Society of Analytical Sciences, Poster presentation

Oct. 2012 110<sup>th</sup> General Meeting of the Korean Chemical Society, Poster presentation

### **Teaching Assistant Experience**

2018 – present Instrumental Analysis and Advanced Instrumental Analysis

2017 – 2020 General Chemistry Laboratory

2010 spring Analytical Chemistry Laboratory

2010 fall General Chemistry Laboratory

## Certificates

2012 Engineer Chemical Analysis (Korea, of Republic)

## Publications

Jeon B., Cizdziel J. (2020) Gaseous elemental mercury concentrations along the Northern Gulf of Mexico using passive air sampling, with a comparison to active sampling, *atmosphere*, 11, 1034, DOI:10.3390/atmos11101034 (Featured on the cover of a journal)

Jeon B., Cizdziel J. (2020) Determination of metals in tree rings by ICP-MS using ash from a Direct Mercury Analyzer, *molecules*, 25, 2126, DOI:10.3390/molecules25092126

Jeon B., Scircle A., Cizdziel J., Chen J., Black O., Wallace D., Zhou Y., Lepak R., Hurley J. (2020) Historical deposition of trace metals in a marine sapropel from Mangrove Lake, Bermuda with emphasis on mercury, lead, and their isotopic composition, *J. Soils Sediments*, DOI:10.1007/s11368-020-02567-6

Jeon, B., Cizdziel, J. (2019) Can the MerPAS Passive Air Sampler Discriminate Landscape, Seasonal, and Elevation Effects on Atmospheric Mercury? A Feasibility Study in Mississippi, USA. *Atmosphere*, 10, 617, DOI: 10.3390/atmos10100617

Orr, W.E., Barnes, M.C., George, H.S., Joshee, L., Jeon, B., Scircle, A., Black, O., Cizdziel, J.V., Smith, B.E., and Bridges, C.C. (2018) Exposure to mixtures of mercury, cadmium, lead, and arsenic alters the disposition of single metals in tissues of Wistar rats, *Journal of Toxicology and Environmental Health, Part A*, 81:24, 1246-1256, DOI: 10.1080/15287394.2018.1551164

Lee, k., Jeon, B., Seo, M., Cho, M., Yoon, H., Kim, D., Park, K., Kim, K., Yang, J., Yang, J., and Lee, G. (2016) Speciation Analysis of 6 Arsenic Species in Sea Mustard using IC-ICP-MS, *Journal of the Korean Chemical Society*, 60, 6, DOI: 10.5012/jkcs.2016.60.6.452